



HAL
open science

Synthèse et caractérisation d'hydrures d'éléments légers sous haute pression

Charles Pépin

► **To cite this version:**

Charles Pépin. Synthèse et caractérisation d'hydrures d'éléments légers sous haute pression. Physique [physics]. Ecole polytechnique, 2015. Français. NNT : . tel-01204564

HAL Id: tel-01204564

<https://pastel.hal.science/tel-01204564>

Submitted on 24 Sep 2015

HAL is a multi-disciplinary open access archive for the deposit and dissemination of scientific research documents, whether they are published or not. The documents may come from teaching and research institutions in France or abroad, or from public or private research centers.

L'archive ouverte pluridisciplinaire **HAL**, est destinée au dépôt et à la diffusion de documents scientifiques de niveau recherche, publiés ou non, émanant des établissements d'enseignement et de recherche français ou étrangers, des laboratoires publics ou privés.



THESE DE DOCTORAT DE L'ÉCOLE POLYTECHNIQUE (ED447)

pour obtenir le grade de

Docteur de l'École Polytechnique

Spécialité doctorale "Physique des solides"

présentée et soutenue publiquement par

Charles PEPIN

le 11 Septembre 2015

Synthesis and Characterization of Light Elements Hydrides

Directeur de thèse : **Paul LOUBEYRE**

Jury

| | | |
|----------------------------|--|------------|
| Yaroslav FILINCHUK, | Professeur, Université Catholique de Louvain | Rapporteur |
| Alfonso SAN MIGUEL, | Professeur, Université Lyon 1 | Rapporteur |
| Matteo CALANDRA, | Directeur de recherche, UPMC | Examineur |
| Didier DALMAZZONE, | Enseignant-Chercheur, ENSTA Paris-Tech | Examineur |
| Paul LOUBEYRE, | Directeur de recherche, CEA | Examineur |

*"Where must we go, we who wander in this wasteland,
in search of our better selves?"*

- The First History Man

Remerciements

Si ces trois années de thèse m'ont paru passer rapidement, cela est sûrement dû au fait qu'elles ont été ponctuées d'échanges et de rencontres avec des personnes talentueuses, qui ont su me communiquer leur enthousiasme pour leur travail, répondre à mes questions ou encore m'apporter leur soutien. Je tiens donc à les remercier dans cette section.

Tout d'abord, je tiens à remercier très respectueusement Paul Loubeyre de m'avoir accueilli au sein de son laboratoire et d'avoir dirigé cette thèse. Je le remercie d'avoir été aussi disponible pour partager son expérience et m'offrir de précieux conseils mais aussi (et surtout!) pour m'avoir enseigné une certaine vision de la science, qui sans aucun doute influencera mes futurs projets.

C'est un grand honneur que Messieurs Y. Filinchuk, A. San Miguel, M. Calandra, et D. Dalmazzone aient accepté d'être membre du jury et je remercie Messieurs Y. Filinchuk et A. San Miguel pour leurs commentaires et leurs corrections.

Merci ensuite à Florent Occelli, Agnès Dewaele, Ramesh André et Gunnar Weck d'avoir pris du temps pour partager avec moi leurs connaissances et me prodiguer des conseils toujours très pertinents. Mon arrivée dans le laboratoire a coïncidé avec celle de Thomas Plisson avec qui j'ai également pu partager des souvenirs marquants que ce soit au laboratoire, au synchrotron ou en conférences (le thai pot!). Cela a été un plaisir de faire partie d'une telle équipe et de pouvoir bénéficier de l'expérience de chacun. Je remercie Grégory Géneste pour sa volonté de travailler avec des expérimentateurs ainsi que pour sa patience pour répondre à mes questions naïves sur les simulations. J'en profite également pour remercier Raffaella Torchio, Captain D. Spaulding et Lieutenant S. Anzellini pour leur accueil dans le laboratoire à mon arrivée.

Je remercie également les personnes qui ont permis que cette thèse se déroule sans problèmes, aussi bien d'un point de vue administratif que d'un point de vue expérimentale, et en particulier Sandra Boul-lier, Brigitte Flouret, Martine Millerioux et Olivier Mary. De même, je remercie tout particulièrement les beamline scientists Paul Dumas, de SOLEIL, Mohamed Mezouar, Gaston Garbarino, Volodimir et Michael Hanfland, de l'ESRF, qui ont largement contribué à la bonne réalisation de ces travaux.

Un remerciement particulier va à mes parents et à ma famille, qui m'ont toujours soutenu et incité à aller de l'avant en ayant la chance de toujours pouvoir compter sur eux, ainsi qu'à mes amis (qui ne liront probablement jamais ces lignes!) qui ont su me sortir la tête de ces problèmes d'hydruration pour mieux m'y replonger avec plus de légèreté ensuite.

Résumé de la thèse en français

Il existe une vaste littérature sur les changements de propriétés des matériaux en fonction de la concentration d'hydrogène qu'il peut absorber, formant ainsi un hydrure. De nombreuses prédictions théoriques s'intéressent actuellement à l'influence du paramètre pression sur ces hydrures. En effet, il a été remarqué que les hydrures covalents devraient être des analogues de l'hydrogène métallique. Ils offrent ainsi une alternative pour étudier ce système quantique qui devrait posséder des propriétés exceptionnelles et pourrait permettre de concevoir une nouvelle classe de supraconducteurs conventionnels à haute-température critique ou de nouveaux matériaux énergétiques. De fait, la recherche de l'hydrogène métallique est un problème phare de la physique des hautes pressions. La fermeture du gap électronique de l'hydrogène en dessous de 1.5 eV ayant été observée à 320 GPa, l'obtention de l'hydrogène métallique a pu être extrapolée comme se trouvant aux alentours de 450 GPa, une pression à la limite des possibilités expérimentales actuelles. L'hydrogène métallique qui pourrait être ramené de manière métastable à pression ambiante présenterait alors des propriétés physiques exceptionnelles, telles qu'un stockage d'hydrogène optimum (100% en masse), un pouvoir énergétique de 215 kJ/g (*i.e.* 13 fois supérieur à celui du couple O_2/H_2) et une supraconductivité à température ambiante. Un chemin alternatif à l'obtention d'hydrogène métallique a donc été proposé par l'étude sous haute pression des hydrures covalents. En effet, dans ces hydrures covalents l'hydrogène est sujet à une "pré-compression chimique" si bien qu'une augmentation supplémentaire de la pression devrait conduire à un chevauchement des bandes électroniques et à la métallisation de l'hydrure à des pressions cette fois-ci atteignables expérimentalement. Les propriétés physiques d'un tel hydrure métallique devraient être dominées par celle de l'hydrogène donnant ainsi lieu, entre autres, à une supraconductivité à haute température. Dans ces hydrures covalents la molécule d'hydrogène est dissociée et les atomes d'hydrogène forment des liaisons covalentes avec les atomes de la maille hôte. Il a récemment été prédit qu'une nouvelle classe d'hydrures avec des stœchiométries inédites, et contenant de l'hydrogène sous forme moléculaire, devrait devenir énergétiquement favorable sous haute pression. L'hydrure de lithium est un cas d'école illustrant ces prédictions théoriques sur la stabilisation de nouvelles stœchiométries sous pression : à pression ambiante la stœchiométrie respectant la règle de la valence est LiH, tandis que sous pression de nouvelles stœchiométries comme LiH_2 ou LiH_6 , contenant des unités H_2 , sont prédites comme étant plus stables que LiH. La présence d'un atome donneur d'électrons (Li dans ce cas) va permettre de peupler l'orbitale anti-liante de H_2 , ce qui conduira à la métallisation du composé grâce à l'élargissement des bandes électroniques sous pression. La présence d'un réseau étendu d'hydrogène dans ces nouveaux hydrures devrait ainsi lui conférer des propriétés physiques similaires à celle de l'hydrogène métallique et ce à des pressions abordables expérimentalement. De nombreux systèmes présentent théoriquement une stabilisation sous pression de nouvelles stœchiométries et une règle empirique émerge de ces abondantes prédictions théoriques : la concentration en hydrogène dans les hydrures devraient augmenter fortement sous pression.

Le but de cette thèse est donc d'exploiter expérimentalement l'utilisation du paramètre pression pour progresser dans la compréhension et la synthèse d'hydrures d'éléments légers avec un double objectif :

- Étudier le comportement des hydrures covalents sous pression et confirmer l'influence des propriétés du sous-réseau d'hydrogène sur les propriétés physiques de l'hydrure;
- Synthétiser et étudier de nouveaux hydrures avec des stœchiométries inhabituelles.

Dans ce contexte une étude expérimentale systématique sur les hydrures obtenus sous pression à partir des éléments Li, Be, Al et Fe a été réalisée. Les expériences sous pression se sont faites à l'aide de cellules à enclumes de diamant, équipées de membrane. La caractérisation *in situ* des échantillons synthétisés a

été faite d'une part en laboratoire par spectroscopie Raman, permettant ainsi de remonter aux propriétés vibrationnelles des composés, et d'autre part devant les synchrotrons (SOLEIL et ESRF) pour réaliser des expériences d'absorption infra-rouge et de diffraction X et ainsi obtenir des informations sur les propriétés électroniques et les structures cristallographiques des hydrures formés. Des calculs *ab initio* sont venus compléter les résultats des expériences afin de remonter à des informations microscopiques inaccessibles à l'expérience.

Une première partie de cette thèse a porté sur le développement d'une méthode de synthèse des hydrures sous pression, en cellule à enclumes de diamant. Une feuille de l'élément hôte (Be, Al ou Fe) d'une épaisseur de $\sim 2\text{-}5\ \mu\text{m}$ est déposée dans la cavité expérimentale sur une couche isolante faite de NaCl, LiF ou de grains c-BN se trouvant à la surface du diamant. L'isolation est thermique mais permet également d'éviter les réactions parasites qui pourraient avoir lieu entre le diamant et l'échantillon ou entre le diamant et l'hydrogène. Une fois l'échantillon mis en place, l'hydrogène est chargé dans la cavité expérimentale et servira de milieu transmetteur de pression. Une technique de cristallisation rapide de l'hydrogène consistant à augmenter brusquement la pression dans la cavité expérimentale est ensuite utilisée : cela permet de solidifier l'hydrogène en une fine poudre, assurant la stabilité de notre échantillon sur la couche isolante qui risquerait sinon de bouger lors d'une cristallisation lente de l'hydrogène en mono-cristaux. La feuille de métal en contact avec le milieu d'hydrogène est ensuite portée à haute température de manière contrôlée grâce à un four externe (pour des températures $< 800\ \text{K}$) ou grâce à un laser YAG infra-rouge (permettant d'atteindre des températures comprises entre 1000 et 2000 K).

Cette méthode a été appliquée pour la synthèse d'hydrures cristallins de très bonne qualité possédant une grande pureté : les hydrures d'aluminium, de béryllium et de fer. L'hydrure de lithium est quant à lui disponible dans le commerce. Les résultats obtenus sur ces différents systèmes sont décrits dans les lignes suivantes.

Hydrure d'aluminium :

Les propriétés vibrationnelles, électroniques et structurales de l'hydrure d'aluminium (ou alane), AlH_3 , ont été mesurées jusqu'à 120 GPa. En plus de la phase pression ambiante, deux nouvelles phases ont été identifiées sous pression, à 67 GPa et 107 GPa respectivement. Une détermination de la structure des nouvelles phases a pu être réalisée grâce aux données de diffraction X et comparée aux précédents résultats expérimentaux qui avaient été obtenus sur cet hydrure par une autre équipe. Les résultats des mesures d'absorption infra-rouge ont montré que la seconde transition de phase à 107 GPa induit une transition isolant-métal. La phase métallique se caractérise par la présence d'un plasmon de basse énergie autour de $\sim 1\ \text{eV}$ qui avait été prédit théoriquement en décrivant cette phase comme un réseau d'hydrogène légèrement perturbé par un fond continu simulant les atomes d'aluminium. La détermination expérimentale d'un tel plasmon confirme ainsi l'influence prédominante de l'hydrogène sur les propriétés physiques des hydrures. Enfin il a été montré que la phase métallique peut être ramenée de manière métastable jusqu'à 40 GPa. A hautes pressions, d'importants effets d'anharmonicité inhibent la supraconductivité dans cet hydrure. La décompression de cette phase pourrait permettre de réduire ces effets anharmoniques, et ainsi conduire à la réapparition d'une supraconductivité à haute température critique.

Hydrure de béryllium

L'hydrure de béryllium, BeH_2 , a pu être synthétisé pour la première fois sans impuretés sous forme cristalline, ce qui a permis de réaliser une première étude expérimentale de son comportement sous haute pression. Celle-ci a montré l'existence d'un polymorphisme important à basse pression, plusieurs phases

coexistant jusqu'à 27 GPa et un parallèle avec le comportement sous pression de SiO_2 a été proposé. Au-dessus de 27 GPa, l'hydrure se dissocie pour former du béryllium et de l'hydrogène pur, ce qui n'avait été prédit par aucune étude théorique. Aucune synthèse d'un hydrure de béryllium n'a été possible entre 27 et 75 GPa. Au-dessus de 80 GPa l'hydrure a pu être reformé en utilisant la méthode de chauffage par laser YAG, et une nouvelle phase a pu être déterminée et identifiée comme correspondant une phase de structure 1-T prédite par certaines études théoriques. Les expériences, réalisées jusqu'à 100 GPa, ont montré que l'hydrure reste isolant au-moins jusqu'à la pression maximal atteinte.

Hydrures de fer

L'hydrure de fer connu, FeH, se forme de manière spontanée sous pression à 3.5 GPa. L'équation d'état (évolution du volume de l'échantillon en fonction de la pression) de cet hydrure était connue jusqu'à 80 GPa, toutefois un doute subsistait sur une possible augmentation de son bulk modulus au-dessus de 50 GPa, laissant supposer une possible augmentation légère de la stœchiométrie sous pression. La compression à température ambiante d'un échantillon de FeH jusqu'à 136 GPa n'a révélé aucun changement de stœchiométrie sous pression. En revanche le chauffage par laser YAG de l'hydrure en milieu d'hydrogène a permis la synthèse de deux nouvelles phases dont la détermination structurale couplée aux calculs *ab initio* a permis de montrer qu'il s'agissait de phases de nouvelles stœchiométries FeH_2 et FeH_3 . La détermination expérimentale de la séquence $\text{FeH} \rightarrow \text{FeH}_2 \rightarrow \text{FeH}_3$ confirme ainsi la règle empirique énoncée par les prédictions théoriques selon laquelle la stœchiométrie des hydrures devraient augmenter fortement sous pression. De plus la structure de FeH_2 est constituée de plans denses d'hydrogène atomiques, ce qui en fait un excellent candidat pour une possible supraconductivité à haute température critique.

Hydrures de lithium

L'hydrure de lithium, réagissant extrêmement facilement avec l'oxygène ou l'eau, a été manipulé exclusivement en boîte à gants et a été étudié par spectroscopie d'absorption infra-rouge uniquement, cette technique est non-invasive et extrêmement sensible aux changements chimiques et électroniques. La compression à température ambiante de LiH montre l'apparition de nouvelles bandes d'absorption sous pression à 130 GPa et 160 GPa, identifiées comme correspondant respectivement à l'apparition de LiH_6 et de LiH_2 . Ces bandes d'absorption sont la signature infra-rouge de la présence d'hydrogène moléculaire dans ces nouvelles phases et confirment ainsi la stabilité à haute pression de nouvelles stœchiométries inhabituelles.

En conclusion, l'étude systématique de différents systèmes d'hydrures réalisée au cours de cette thèse a permis de développer une nouvelle technique de synthèse d'hydrures sous pression et a apporté la première confirmation expérimentale de la prédiction d'une très forte augmentation de la solubilité de l'hydrogène dans les métaux sous pression, offrant ainsi la possibilité de stabiliser de nouvelles phases avec des stœchiométries inhabituelles. Les travaux réalisés sur les hydrures covalents ont en outre montré que les propriétés physiques de l'hydrure sont dominés par les propriétés issues du sous-réseau d'hydrogène et ainsi confirment l'existence d'une analogie forte entre les hydrures et l'hydrogène pur. Enfin les résultats présentés identifient certains points faisant actuellement défaut dans les modèles théoriques utilisés pour décrire le comportement des hydrures sous pression, montrant ainsi qu'une confrontation calculs-expérience plus poussée est nécessaire. Ces travaux constituent une première étape très encourageante avant l'étude d'une possible supraconductivité dans les hydrures étudiés.

Contents

| | |
|--|-----------|
| Résumé de la thèse en français | 4 |
| General introduction | 7 |
| I Experimental techniques | 13 |
| 1 Generating high pressure | 15 |
| 1.1 Principle of the diamond anvil cell | 15 |
| 1.2 The membrane diamond anvil cell | 16 |
| 1.3 Gasket | 18 |
| 1.4 High pressure gauges | 20 |
| A. X-ray gauges | 21 |
| B. Luminescence gauges | 21 |
| C. Raman gauges | 23 |
| 2 Generating high temperature | 25 |
| 2.1 Resistive heating | 25 |
| 2.2 Laser Heated Diamond Anvil Cell | 26 |
| 3 Sample preparation | 31 |
| II High pressure characterization of the sample | 35 |
| 4 Raman spectroscopy | 37 |
| 4.1 Background of the Raman spectroscopy | 37 |
| 4.2 Theory of Raman spectroscopy | 37 |
| 4.3 High-pressure Raman instrumentation | 38 |
| 5 Infra-red spectroscopy | 41 |
| 5.1 Theory of the infra-red spectroscopy | 41 |
| 5.2 Infra-red spectroscopy combined with high pressure experiments | 42 |
| 6 X-ray diffraction | 45 |
| 6.1 Crystal diffraction | 45 |
| 6.2 Data analysis | 48 |

| | | |
|------------|---|------------|
| III | Structural changes in hydrides under pressure: AlH₃ and BeH₂ | 51 |
| 7 | Motivations | 53 |
| 8 | Aluminum Hydride AlH₃ under Pressure | 55 |
| 8.1 | Introduction | 55 |
| 8.2 | Article: "Structural, vibrational and electronic properties of AlH ₃ up to 120 GPa" | 58 |
| 9 | Beryllium Hydride BeH₂ | 69 |
| 9.1 | Introduction | 69 |
| 9.2 | Article: "High pressure study of Crystalline Beryllium Hydride: New Structures and Re-entrant Disproportionation" | 72 |
| IV | Changing the stoichiometry of hydrides: iron hydrides and lithium hydrides | 79 |
| 10 | Motivations | 81 |
| 11 | Lithium Hydrides | 83 |
| 11.1 | Introduction | 83 |
| 11.2 | Article: "Synthesis of Lithium polyhydrides above 130 GPa at 300 K" | 86 |
| 12 | Iron hydrides | 91 |
| 12.1 | Introduction | 91 |
| 12.2 | Article: "New Iron Hydrides under High Pressure" | 95 |
| V | Discussion and conclusion | 101 |
| 13 | Discussion | 103 |
| A. | Improving the crystal quality of hydrides under pressure | 103 |
| B. | Overcoming energetic barriers | 103 |
| C. | Metallic state of hydrides under pressure: a universal volume increase | 104 |
| D. | Candidates for a high-T _c superconductivity and analogy with pure hydrogen | 104 |
| E. | Predictability of the DFT calculations | 106 |
| F. | The next step | 107 |
| | General conclusion | 109 |

General Introduction

Pressure is of fundamental interest for physics and chemistry to explore the various thermodynamic states of a chemical system. The recent technical developments in high-pressure physics now allow physicists to routinely achieve pressures exceeding 100 GPa (1 GPa=10000 bar=9869 atm). In this (multi-)megabar range the free-energy change of a system (coming from the pV term of the Gibbs free-energy $G = E + pV - TS$) can be greater than 2 eV per two atoms, which can be compared to the bond energy of the strongest chemical bond [1]. Consequently, this pressure range is the place of drastic modifications of the chemical bonds and unexpected chemical re-arrangements may happen under such extreme conditions with emergence of new materials possessing intriguing properties. To cite a few:

- Pressure usually breaks the molecular bonds and new associations can be formed: a famous illustration of this phenomenon is the sp^2 - sp^3 hybridization transition in carbon between graphite and diamond. Recently oxygen, O_2 , has been shown to become a reddish O_8 solid above 10 GPa [2] and becomes metallic around 100 GPa [3];
- It was long thought that all materials should transform into metals at sufficiently high pressure: a very simple picture consists in considering the simple picture of the free electron theory for which the total energy is formed by the addition of a Coulombic potential that scales as $\frac{-1}{r}$ where r is a lattice constant and of the Fermi kinetic energy for free electrons that scales as $\frac{1}{r^2}$. This gives a minimum in energy for a particular r which eventually can be reached under pressure. Such an insulator-metal transition is observed in xenon for instance, this van der Waals solid becomes metallic at 138 GPa [4];
- Recently the reverse, *i.e.* metal-insulator transitions, has also been obtained under pressure, evidencing the influence of core electrons: sodium exhibits such metal-insulator transition at 200 GPa [5], and so does lithium at 80 GPa [6];
- With another order of compression, aluminum is expected to become an electride [7], an host-guest structure consisting of positive ions and interstitial electrons 'blobs', showing again that the model expecting a free electron delocalization at very high density is too simple;
- New unusual stoichiometries can be stabilized under pressure: for instance new phases of sodium chlorides, $NaCl_3$ and Na_3Cl , appear above 60 GPa [8];
- Under ambient pressure, mixtures of simple molecules do not form stoichiometric compounds in cryogenic solids, but such compounds are stable and ubiquitous in molecular mixtures under pressure as demonstrated in the case of $Ne(He)_2$ [9], $Ar(H_2)_2$ [10] or $(N_2)_6Ne_7$ [11].

The simplest and most abundant element, hydrogen, is no exception to this phenomenon of progressive complexity under pressure and can be considered as a textbook case to illustrate this exceptional novel

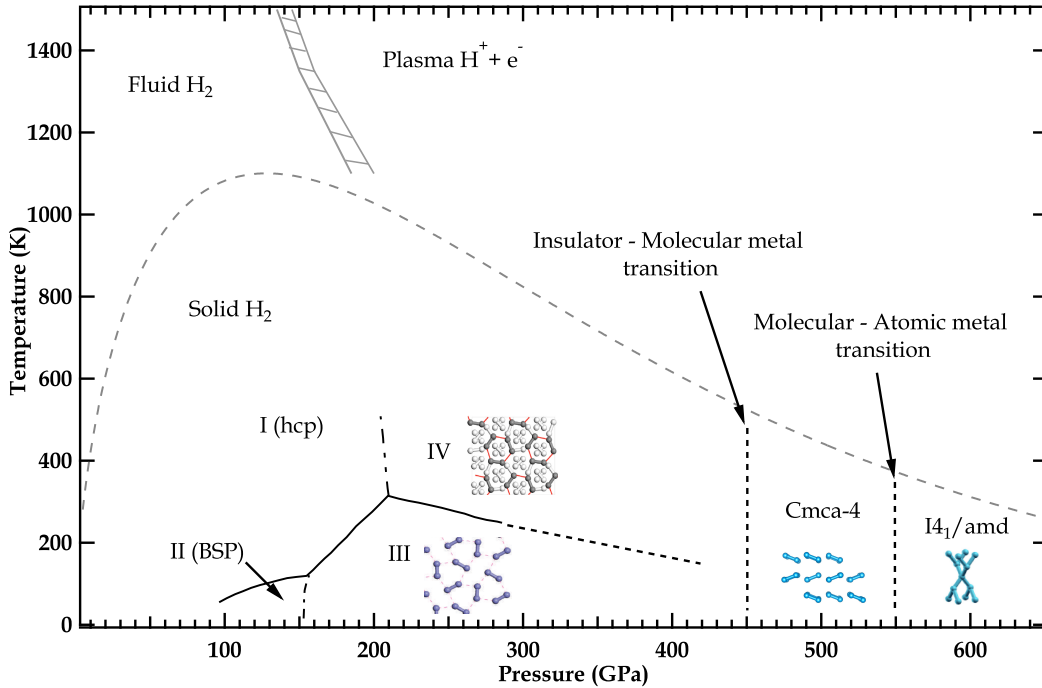


Figure 1: High pressure phase diagram of hydrogen.

physico-chemistry under pressure and the formation of new intriguing compounds - the hydrides - and new energetic materials. As early as 1935, Wigner and Huntington studied the effect of density on an assembly of protons and electrons and suggested that above 25 GPa hydrogen would become an atomic metal with protons embedded in an electron sea [12]. 80 years later using modern calculation techniques and after tremendous efforts of the high pressure community, our knowledge of the phase diagram of hydrogen has been greatly improved and extended up to much higher pressure as shown in figure 1. Although hydrogen is the simplest element it can be seen that it does not form the simplest solids. As a consequence from the low proton mass, quantum effects in the different phases are substantial and largely influence their physical properties, characterized for instance at low pressures by large zero point motions, rotational disorder or the distinguishability of molecules into even and odd parity nuclear spin states. At high pressures, experimental measurements, using Raman spectroscopy and synchrotron infrared spectroscopy, have shown that hydrogen undergoes a series of phase transitions (referred to as phases I, II, III and IV) and remains an insulating molecular solid up to 330 GPa [13]. Metallization of molecular hydrogen is now expected around 450 GPa and the atomic phase predicted by Wigner and Huntington should appear at even higher pressures, above 550 GPa. At even higher pressures, given the slope of the melting curve, compressed hydrogen should adopt a liquid state and is predicted to exhibit a new state of matter: a near ground state liquid metal with superconductive and superfluid properties [14].

Within the framework of the Bardeen-Cooper-Schrieffer (BCS) theory [15], the McMillan-Dynes equation to estimate the temperature of superconductivity, T_c , can be written as [16]:

$$T_c = \frac{\langle \omega \rangle}{1.2} \exp \left[-\frac{1.04(1 + \lambda)}{\lambda - \mu^*(1 + 0.62\lambda)} \right]$$

| System | Pressure (GPa) | $\langle\omega\rangle$ (cm ⁻¹) | λ | μ^* | T _c (K) | Reference |
|--------------------|----------------|--|-----------|---------|--------------------|-----------|
| MgB ₂ | 0 | 504 | 0.87 | 0.1 | 39 | [21] |
| Molecular Hydrogen | 445 | 664 | 2 | ~0.1 | 225 | [22] |
| Atomic Hydrogen | 500 | 1430 | 1.81 | 0.089 | 356 | [23] |
| AlH ₃ | 70 | 573 | 0.89 | 0.14 | 37 | [24] |
| CaH ₆ | 150 | 954 | 2.69 | 0.1 | 235 | [25] |

Table 1: Parameters used in the McMillan-Dynes equation to calculate the T_c of different systems.

where λ is the electron-phonon interaction, μ^* is the renormalized Coulomb repulsion and $\langle\omega\rangle$ is the average phonon frequency. This formula straightforwardly shows why metallic hydrogen should be a high-T_c superconductor: first, its light proton mass gives rise to a very high phonon frequency. Second, in this case the electron-ion interaction only results from the Coulomb interaction so that the electron-phonon coupling should be strong. Third, the Coulomb repulsion between electrons in high-density systems is expected to be low. It is then easy to deduce that if both $\langle\omega\rangle$ and λ are high and μ^* is low then hydrogen should be a high-temperature superconductor, which was predicted by N. W. Ashcroft in 1968 [17]. Recent calculations for atomic metallic hydrogen predict a T_c of ~300 K, *i.e.* superconductivity at room temperature.

In the field of astrophysics hydrogen also holds a central position as it is the most abundant element in the Universe and one of the principle component of most of the recently discovered exoplanets. There are further motivations for studying dense hydrogen, such as technological applications, like inertial confinement fusion where hydrogen is compressed with a laser-driven shock. Metallic hydrogen, if calculated metastable, is also considered to be the best potential energy storage material and used as rocket fuel it could provide four times more propellant power than conventional liquid hydrogen rocket fuel [18]. Such intriguing properties predicted for dense hydrogen, the test of quantum effects of density by comparing theory and experiments and the need to accurately model the new exoplanets greatly motivate a large number of recent studies.

The latest developments in high pressure generation techniques now allow physicist to achieve pressures around 5 Mbar on transition metals [19]. However, achieving pressures beyond 350 GPa on hydrogen remains very challenging due to different factors: it is highly compressible (its bulk modulus in phase I is B₀=0.16 GPa while typical bulk moduli for transition metals are greater than 100 GPa [20]), its reactivity greatly increases under pressure and it diffuses relatively easily in the diamond anvils used to generate pressure thus resulting in their premature failure. If one were still able to overcome these issues, getting convincing signal (X-ray diffraction, Raman or Infra-red spectroscopy) coming from dense hydrogen would constitute a second major challenge, even when using third-generation synchrotron light sources.

In view of the extreme difficulties to reach the metallic state of hydrogen, can we find systems in which a similar physics is occurring?

While technical developments are still undergoing to be able to achieve the metallization of pure hydrogen, an alternative pathway to obtain a dense hydrogen metallic lattice has been recently proposed by N. W. Ashcroft in 2004: the study of covalent hydrides [26] of formula MH_x. The key argument supporting this suggestion is that in such covalent hydrides hydrogen is subjected to a "chemical precompression". Further compression should result in a wide overlap of electronic bands from both the hydrogen and the associated host element and the hydrides could become metallic at pressures well within the range of our current high-pressure devices. Just like in pure hydrogen, such covalent hydrides should still exhibit high phonon frequencies, a strong electron-phonon coupling and a low Coulomb repulsion, so that they could

be high-temperature superconductors.

In these covalent hydrides hydrogen is dissociated and hydrogen atoms are forming covalent bonds with the host element. Recently it has been predicted that a new class of hydrides with unusual high stoichiometries, hence in which hydrogen is found in its molecular form, should also become stable under high pressure [27]. The first prediction was made for lithium hydride. While the known stoichiometry respecting the valence rule is LiH, pressure should promote the stabilization of new stoichiometries like LiH₂ or LiH₆ containing H₂ units. In such hydrides, the Li atom will act as an electron donor filling the σ_u^* electronic bands of the H₂ units and hence leading to metallization through the pressure-induced band broadening but at lower pressure than for pure hydrogen. Assuming that in the high-pressure metallic phase hydrogen units form an extended network, one would expect to obtain a hydrogen-dominant state having properties similar to metallic hydrogen. Subsequently, various new H-stoichiometries were predicted for other elements than lithium, most of them predicted to have a high-temperature superconductivity within the framework of the BCS theory, $\langle\omega\rangle$ and λ being very high and μ^* being low. These parameters are compared in table 1 for the highest known conventional superconductor, MgB₂, molecular and atomic hydrogen and for two hydrides: AlH₃, an hydride having a conventional stoichiometry, and CaH₆, one of the so-called high-hydrides. From these selected examples, it clearly appears that the electron-phonon interaction λ and the average phonon frequency $\langle\omega\rangle$ are the key ingredients for the high-T_c. However, these two parameters are highly sensitive to the crystal structure and could be strongly influenced by anharmonic effects. Consequently, an experimental confirmation of the predicted structures and their associated high-T_c is therefore highly needed, making the predictability and the design of high-T_c superconductivity into test beds for theory and simulations.

An overview of the various predictions found in the literature is summarized in figures 2 and 3. The very extensive literature found on hydrides of transition metals (see for example [46]) is not reported here. In these transition metals hydrides, the initial host structure is conserved with hydrogen atoms occupying interstitial sites. We focus here on covalent/ionic hydrogen-rich systems becoming metallic under pressure and on stoichiometry greater than 2 for transition metals. As it can be seen from figures 2 and 3, high pressure appears as a privileged pathway to a stable novel hydrides with high-T_c properties. The schematic periodic table of figure 2 also allows to draw the following conclusions:

- The predictions of new polyhydrides with unusual stoichiometries abound. When starting this PhD-thesis the only observed changes of stoichiometry under pressure were the molecular compound SiH₄(H₂)₂ [37] and the rhodium dihydride RhH₂ [47]. Therefore, clear experimental confirmations of high stoichiometry hydrides were needed.
- From these numerous first-principles calculations a rough rule emerges: the hydrogen content in hydrides should significantly increase with pressure. This rule also holds for heavier elements as reported in Refs. [48], [49], [50], [51] and [52].

The aim of this work was then to bring an experimental confirmation or invalidation for these two points.

In this context the first step has been to study two compounds, aluminum hydride and beryllium hydride, for which no changes of stoichiometry were expected. Their study is presented in the first part of this dissertation. Studying these low-Z hydrides allowed us:

1. to develop an *in situ* synthesis technique from the elements under pressure at high temperature using either a resistive heater or an infrared YAG-laser;
2. to develop a set of measuring techniques to characterize the hydrogen arrangement in these compounds, which involves the use of X-ray diffraction to detect the structural changes under pressure

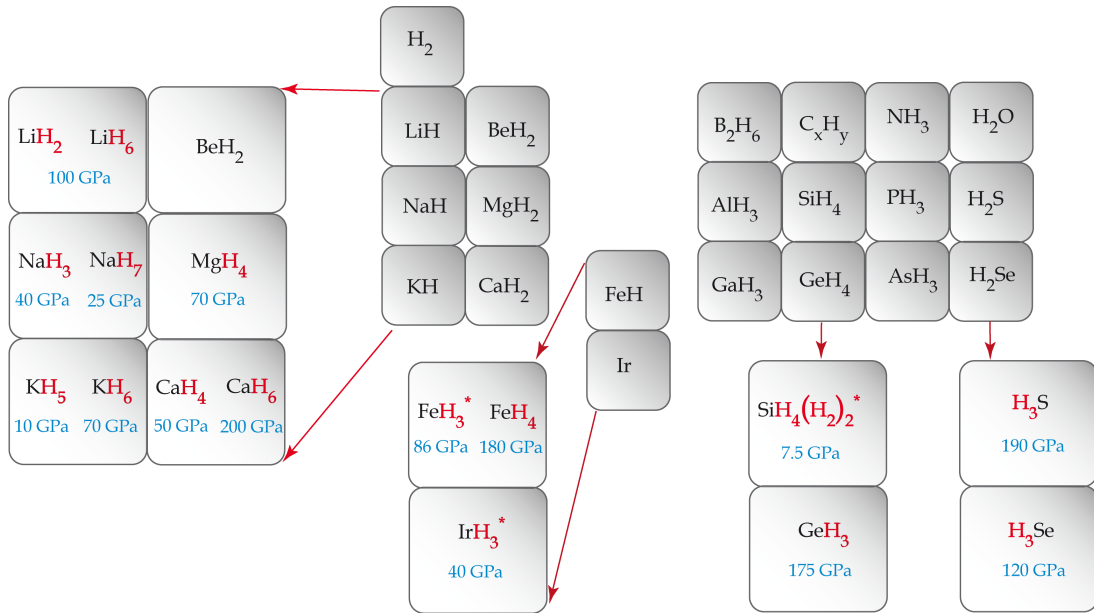


Figure 2: Schematic periodic table showing the predicted changes of stoichiometry for selected various "light" elements adapted from Refs. [27],[28],[29],[30], [31],[25],[32], [33], [34], [35], [36], [37], [38] and [39]. For each element the unusual stoichiometries appear in red with their stabilization pressure. Red asterisks identify the surtoichiometric hydrides that have been experimentally observed. Noble gases hydrides have been omitted as they can be viewed as a special case: they form van der Waals compounds under pressure which would become metallic at very high pressures.

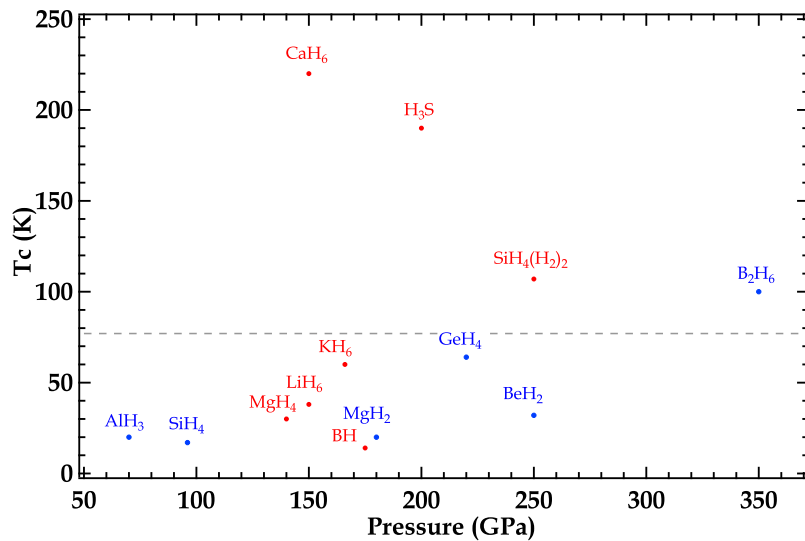


Figure 3: Critical temperatures of superconductivity for various hydrides, adapted from Refs. [24], [40], [36],[32], [25], [28],[29], [31], [41], [42], [43], [44] and [45]. Usual stoichiometries appear in blue and unusual stoichiometries in red.

and the use of Raman and infrared spectroscopy to probe bonding changes, coupled with *ab initio* calculations;

3. to get a first understanding of their high-pressure behaviour (high compressibility, poor recrystallization / amorphization occurring after phase transitions, dissociation into the elements under pressure...);
4. to show the contribution of the hydrogen sublattice on the physical properties of metallic hydrides;

The second step was to induce changes of H-stoichiometry under pressure, as exposed in the second part of this manuscript. In the first case, lithium hydrides, it was obtained only using pure compression of the sample. In the second case, iron hydrides, laser heating in hydrogen medium under pressure was mandatory to overcome kinetic barriers. In this instance, care in sample preparation proved to be of high importance as chemical reactions between iron/hydrogen and the diamond anvils were easily induced.

The present manuscript is structured as follows. In the first two parts the experimental techniques of high pressure research, the specific development made to study hydrides at elevated pressures and the background for the sample characterization under pressure are described. In a third part the structural changes observed in AlH_3 and BeH_2 are presented. This part is followed by a fourth one presenting the changes of stoichiometry induced in two hydrides: iron hydride and lithium hydride. Finally a discussion of the results and some indications on possible future studies on hydrides are given in the last part.

Part I

Experimental techniques

Chapter 1

Generating high pressure

1.1 Principle of the diamond anvil cell

In the early 1900's Percy W. Bridgman used opposed carbide tungsten anvils to generate high pressures, which lead to the modern version of the Paris-Edinburgh press. Nowadays the opposed anvils principle is still used except that flawless single crystal diamonds are now used as anvils, as represented in figure 1.1. Such device is called a diamond anvil cell (DAC) and was first made by Weir *et al.* in 1959 [53]. Its principle is the following: the two diamonds face each other, a sample being squeezed between the

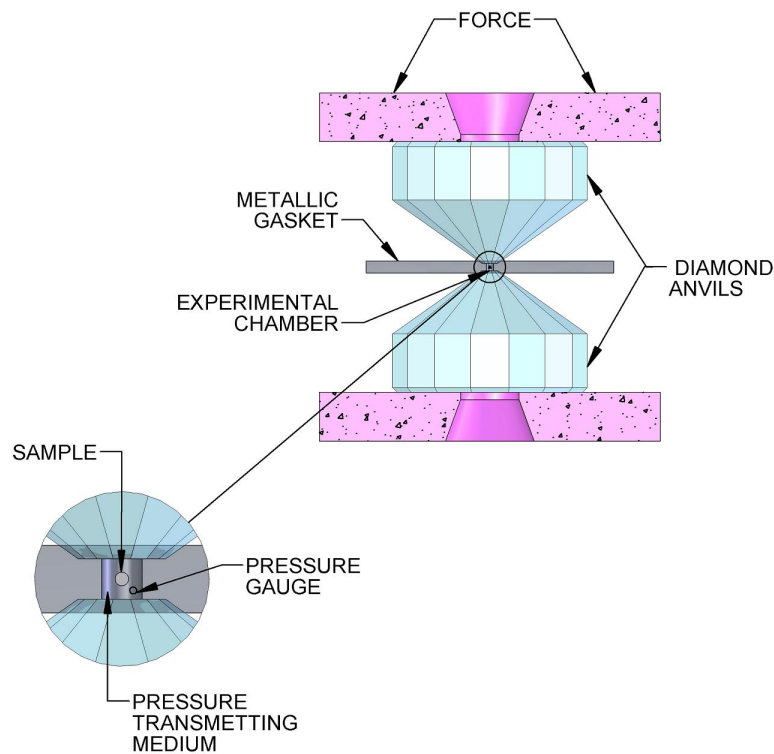


Figure 1.1: Standard diamond anvil cell schematics.

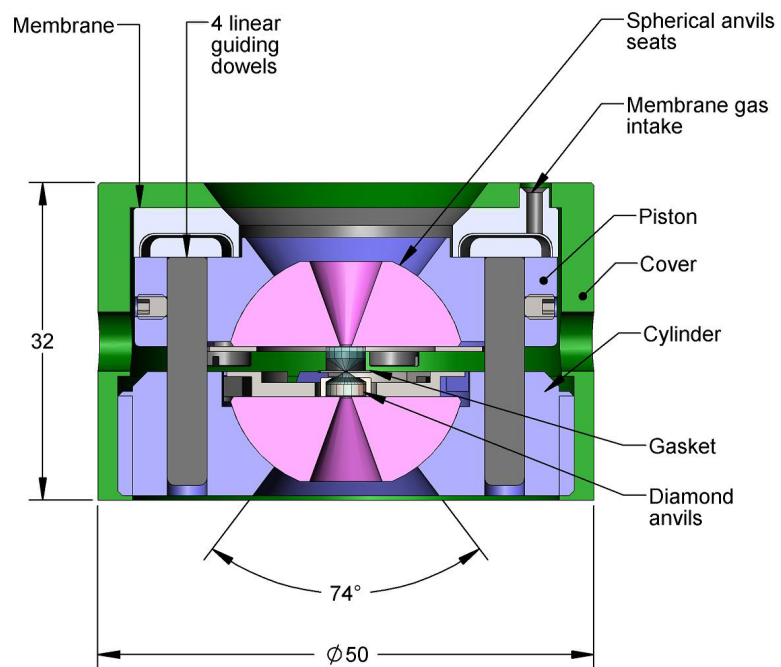
anvil tips (culets), and while one anvil is stationary on a cylinder, the other one is mounted on a sliding piston. By applying a large load on anvils with small culets (ranging from 700 to 20 μm) high pressures can be achieved. Since pressure is roughly defined by $P = \frac{F}{A}$, reducing the surface area A will result in significantly higher achievable pressures. To apply pressure to a confined sample it can be seen in figure 1.1 that a metallic foil called gasket is used. This gasket is typically a high bulk modulus material like rhenium or tungsten. The gasket is pre-indented to a given thickness and so perfectly matches to the shape of the anvils culets. A cavity, the experimental chamber, is then drilled in its center and filled with the sample immersed in a pressure-transmitting medium used to achieve quasi-hydrostatic conditions. A small pressure gauge is also added if the pressure-transmitting medium itself can not be used as a pressure gauge. As pressure is exerted the gasket deforms plastically and the volume of the cavity becomes smaller thereby increasing the pressure in the experimental chamber.

The extreme hardness of the diamond allows to generate static pressures greater than 300 GPa. Conveniently, the diamond is transparent to a wide range of electromagnetic radiation from high energy x-rays to low-energy infrared radiations, except for a narrow region between 3.5 eV and 8 keV corresponding to the ultraviolet radiation and the soft x-rays. Therefore a large number of *in situ* experimental probes can be used under pressure, such as infrared absorption, Brillouin scattering, Raman scattering, EXAFS, x-ray diffraction, x-ray inelastic scattering, etc... However it has to be noted that these techniques can be limited by the thickness of the samples (typically $\sim 5 \mu\text{m}$ in our studies), the thickness of the diamond anvils and the angular opening of the DAC as we will see in the following section. While Brillouin and Raman scattering and Infra-red spectroscopy can be performed in laboratory, a lot of the experimental probes are related to the use of the synchrotron radiation. It was first used in the 1980's [54] and nowadays the beam-lines of the third-generation facilities (currently state-of-the-art) are massively used by the high-pressure community.

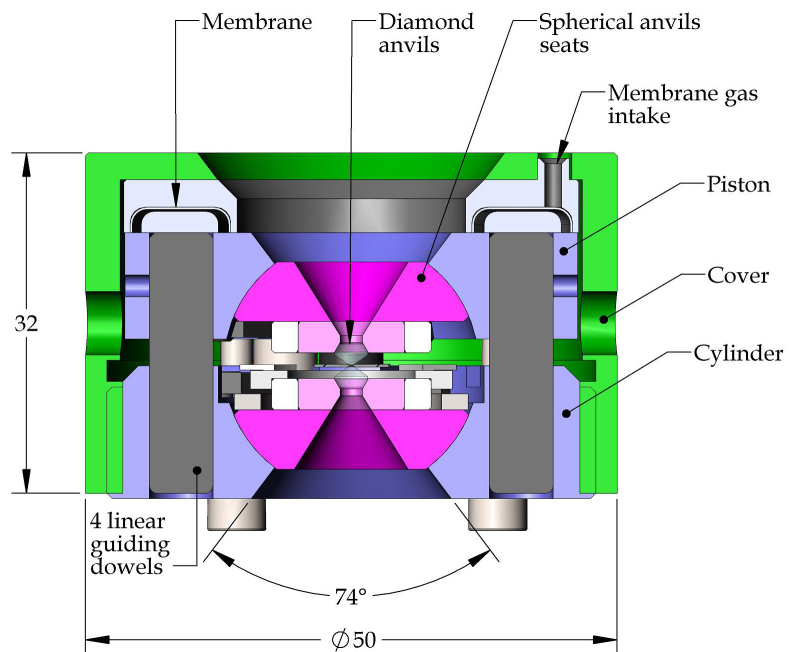
1.2 The membrane diamond anvil cell

The thrust required on a DAC to achieve high pressures is in the order of a few kN. Various mechanisms have been developed over time such as a nutcracker mechanism [55] or a 3-4 bolts mechanism [56]. In our group membrane diamond anvil cells are used [57], as displayed on figure 1.2. The thrust mechanism in this case is a metallic toroidal membrane that will be inflated with helium supplied by an external bottle, thereby exerting a finely tuned pressure on the piston. The applied uniaxial compression is then transformed in an (quasi-)isotropic pressure on the sample via the deformation of the gasket. The use of a membrane DAC, with the pressure being externally tuned by a pressure controller, is very successful for high and low-temperature measurements where the cell has to be located in a vacuum chamber and for x-ray measurements as the time needed to realign the cell and the x-ray beam is minimal since the cell itself doesn't move. Another advantage of the membrane is that very large single crystal can be very easily grown in the experimental chamber by very slowly increasing the pressure in the membrane, or on the contrary a very rapid crystallization in a fine powder can be achieved by quickly releasing pressure in the membrane. This later point proved to be a key element in our experiments as it will be seen in the following chapters.

As it can be seen in figure 1.2 two different membrane DACs are used, the first one using diamonds with the conventional "Drukker design" and the second one using the recently developed "Boelher-Almax" design [58]. In both cases the diamonds can be classified in two types called type I and II. Type I diamonds contain a small amount of nitrogen causing a strong absorption between 1100 and 1500 cm^{-1} . Types II contain no nitrogen and only show the intrinsic absorption band at 2000 cm^{-1} . The type of experiment that



(a) Membrane diamond anvil cell schematics, using a conventional design.



(b) Membrane diamond anvil cell schematics, using the Boehler-Almax design.

Figure 1.2: Membrane diamond anvil cells. Distances are in mm. Image courtesy of F. Occelli.

needs to be conducted dictate the choice and the quality of gem. As pressure increases these gems will undergo a progressive elastic deformation (cupping) near the sample region, hence greatly attenuating the force transmitted to the sample and consequently representing a limitation to the highest pressure achievable. In order to postpone this phenomenon and to reach pressures greater than 1 Mbar double- and triple-beveled anvils (with respect to single-beveled anvils) are used. Drukker type diamonds have a 4 mm diameter base and are 2.8 mm thick. Boelher-Almax type diamonds have a 3.10 mm diameter base and are 1.72 mm thick. The gems with the Boelher-Almax design are therefore usually cheaper and its smaller thickness allows to slightly reduce the signal coming from the anvils. Moreover this design offers the possibility to have a much wider angular aperture as seen on figure 1.2, up to 74° with respect to the 35° aperture available when using the conventional design. This appears to be very advantageous when performing X-ray diffraction to attain large diffraction angles.

In both designs the gems are mounted on spherical backing seats that are necessary to transfer the typical load of a few kN. Hard material is required and traditionally tungsten carbide (WC) is used. Tungsten carbide seats are ideally suited when performing Raman or infrared spectroscopy but not for diffraction studies as WC is opaque to x-rays. Consequently backing seats made of cubic boron nitride (c-BN) are used in this case.

The use of spherical seats combined with translational movements available on the diamond mounted on the piston allow to very precisely center and align in parallel the culets of the anvils. A great care has to be taken when aligning the culets (typically within 1 micron precision) as it will be an influential parameter on the success of the experiment.

1.3 Gasket

Another key factor for the success of an experiment is the selection of the gasket material and the way in which it is prepared. In our case it is meant to contain our hydride sample in pure hydrogen, the pressure-transmitting medium, which is highly reactive at megabar conditions. The hydrogen embrittlement of the gasket material has then to be prevented. Therefore two criteria guided the choice of the gasket material:

- a high hardness and ductility
- the absence or at least the limitation of chemical reaction with hydrogen

A relevant candidate is rhenium (Re) as it fulfills the first condition¹. However this gasket material is far from being chemically inert with hydrogen. It is known to form rhenium hydride above 5 GPa and the hydrogen solubility in this hydride increases both with time and pressure to reach the stoichiometric composition Re_2H [59]. The formation of this hydride greatly affects the bulk properties of the gasket and has a non-negligible impact on the maximum pressure that can be reached. To prevent this chemical reaction, or at least reduce it, a thin gold coating is deposited on the edges on the experimental chamber. This gold coating deposited by a plasma deposition method or laser-drilled is typically $\sim 1\text{-}2\ \mu\text{m}$ thick and confines hydrogen under pressure up to $\sim 550\ \text{K}$, and is presented on figure 1.3a. At the end of this thesis our laboratory has been equipped with a new femtosecond laser, allowing us to test new coating materials to confine hydrogen under pressure. A successful candidate has been dehydrated sodium chloride (NaCl) which was tested up to 40 GPa and 850 K and is seen on figure 1.3b.

¹Other possible candidates are tungsten (W) and a copper-beryllium mixture (CuBe). However the brittleness of the first one causes difficulties in the gasket preparation and the second one, although chemically inert in presence of hydrogen, presents a significantly lower hardness, hence limiting its use at pressures below 20 GPa.

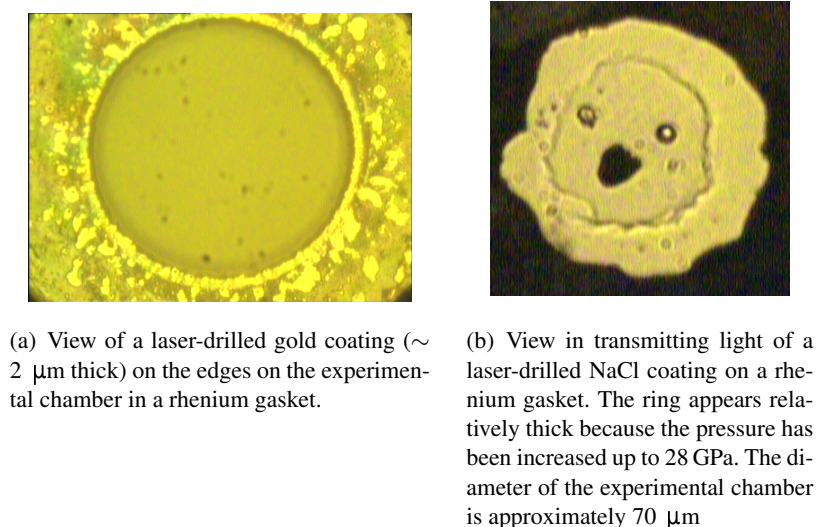


Figure 1.3: Coatings on the edges on the experimental chamber

The experimental chamber is made by drilling a hole in the gasket, with a diameter adapted to the culets size. Usually the hole is laser-drilled. In the major part of this work a 8 ns pulsed doubled YAG laser (532 nm) has been used. As it can be seen in figure 1.4 this technique is far from optimal as the edges of the experimental chamber have been annealed and are irregular, which can affect the stability of the chamber under pressure.

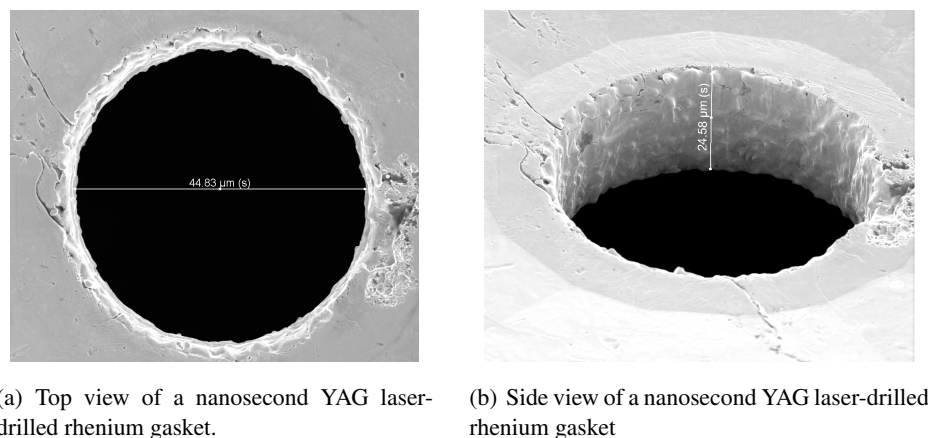
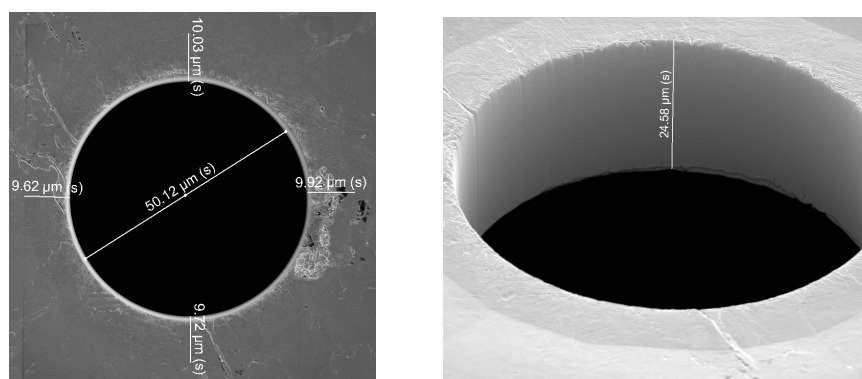


Figure 1.4: Aspect of the experimental chamber when using a 8 ns pulsed doubled YAG laser.

For culets size $\leq 70 \mu\text{m}$ the use of a focused ion beam (FIB) greatly improves the aspect of the edges of the chamber, as seen on figure 1.5. However drilling a hole using a FIB is both time and money consuming. In order to reduce the time needed to drill a hole, for culets size ranging from 70 to $40 \mu\text{m}$, a first hole was laser-drilled and then a remaining $\sim 3 \mu\text{m}$ thick part was FIB-drilled to remove the infrared damaged part on the edge. For culets size $< 40 \mu\text{m}$ the whole hole was FIB-drilled, assuring a sub-micron precision to center the hole.

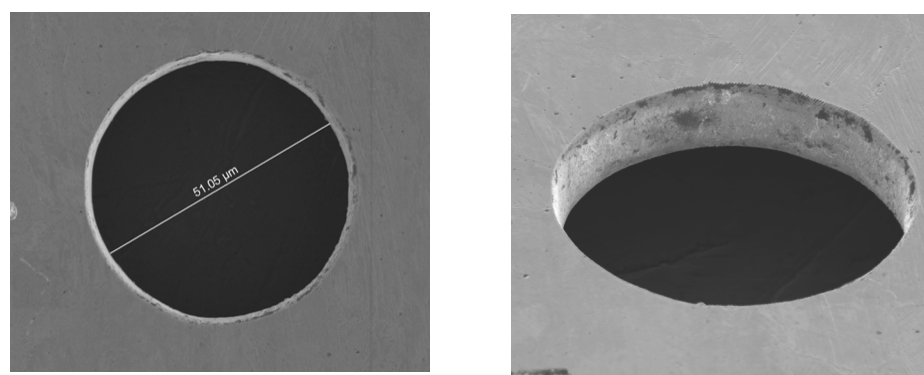


(a) Top view of a FIB-drilled rhenium gasket.

(b) Top view of a FIB-drilled rhenium gasket.

Figure 1.5: Aspect of the experimental chamber when using a focused ion beam.

The very recent acquisition of a femtosecond laser opens up for new efficient drilling possibilities. It is much faster than the use of a FIB but shows comparable results, as shown in figure 1.6. However the sub-micron precision of the FIB still remains very advantageous for the smallest culets size ($<40 \mu\text{m}$).



(a) Top view of a femtosecond laser-drilled rhenium foil.

(b) Top view of a femtosecond laser-drilled rhenium foil.

Figure 1.6: Aspect of the experimental chamber when using a femtosecond laser.

1.4 High pressure gauges

To measure high pressure in a diamond anvil cell a calibrated pressure gauge is placed close to the sample inside the experimental chamber. This gauge can either be:

- A small crystal of a transition metal for which equation of state (*i.e.* the relation between volume and pressure $P(V, T)$) is known. Such gauges require the use of x-ray diffraction.
- A small luminescence gauge exhibiting a calibrated pressure-dependent fluorescence line.
- A Raman gauge. In this case the evolution of a Raman mode is measured under pressure.

A. X-ray gauges

The evolution of the lattice parameters as a function of pressure of a standard material for which the equation of state (EoS) is known can be used to determine the pressure inside the experimental chamber, when using x-ray diffraction. At ambient temperatures, the EoS reduced from shock-waves measurements are used to calibrate the X-ray gauge (e.g. [60]). The accuracy of these EoS are cross-checked by compressing several standards in a diamond anvil cell and by comparing the corresponding pressure obtained from the volumes measured by X-ray diffraction, see for example [61]. In our case the choice of an x-ray gauge is dictated by three criteria:

- The compound is compressible enough as to allow a precise determination of pressure
- The gauge must be chemically inert to avoid any chemical reaction with the sample or with the transmitting pressure medium
- No phase transition must take place in the studied (P, T) range.
- The effect of the deviatoric stress should be minimum

A widely used x-ray gauge respecting these three criteria is gold (Au): it is relatively compressible (bulk modulus $K_0 = 167$ GPa [62]), it is chemically inert (it doesn't react with hydrogen under pressure [63], although under high pressure and high temperature the question of the formation of a gold hydride still remains [64]) and experimentally no phase transition at room temperature has been observed up to 640 GPa [19]. Moreover gold has a high atomic number ($Z=79$, which has to be compared with the heaviest element we studied, iron (Fe), $Z=26$) so that even a very small piece of gold inside the experimental will produce a strong x-ray diffraction pattern. The downside of using gold is that it seems to be extremely sensitive to non-hydrostatic conditions [62]. Other x-ray gauges used by the high-pressure community are tungsten (W) and platinum (Pt). However in our case both metals form hydrides under pressure in presence of hydrogen and therefore could not be used.

B. Luminescence gauges

An effective way to measure pressure in the experimental chamber without using x-ray diffraction is to put a luminescent compound next to the sample. In 1972 it was proposed to use a ruby crystal (Al_2O_3 doped with Cr^{3+}) [65]. Cr^{3+} -doped aluminum oxide exhibit two very intense luminescence peaks labeled R_1 and R_2 , at 6942.48 and 6927.0 Å respectively at ambient conditions. A typical luminescence spectrum of a ruby chip under pressure is shown in figure 1.7. The shift of the R_1 luminescence peak has been the subject of several calibrations. From 1986 to 2007 the calibration from Mao and Bell has been used [66]. The pressure as a function of the isothermal shift of the wavelength of the R_1 peak in quasi-hydrostatic conditions is given by:

$$P = \frac{A}{B} \left[\left(\frac{\lambda_{R_1}(P)}{\lambda_{R_1}(P=0)} \right)^B - 1 \right] \quad (1.1)$$

with $A = 0.224\lambda_{R_1}(P=0)$ GPa and $B = 7.665$. However it has been shown that this calibration tends to underestimate the pressure: ~ 6 GPa at 100 GPa and ~ 17 GPa at 200 GPa. Therefore a reworked calibration has been proposed with the same formula, with the value $B=9.5$ instead of 7.665 [67]. Another formula was later proposed [68]:

$$P = A \frac{\lambda_{R_1}(P) - \lambda_{R_1}(P=0)}{\lambda_{R_1}(P=0)} \left[1 + B \frac{\lambda_{R_1}(P) - \lambda_{R_1}(P=0)}{\lambda_{R_1}(P=0)} \right] \quad (1.2)$$

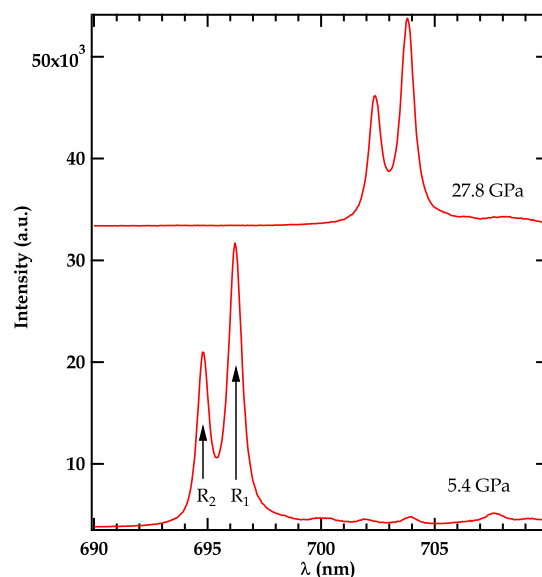


Figure 1.7: Typical luminescence spectra of a ruby chip at pressures of 5.4 GPa and 27.8 GPa.

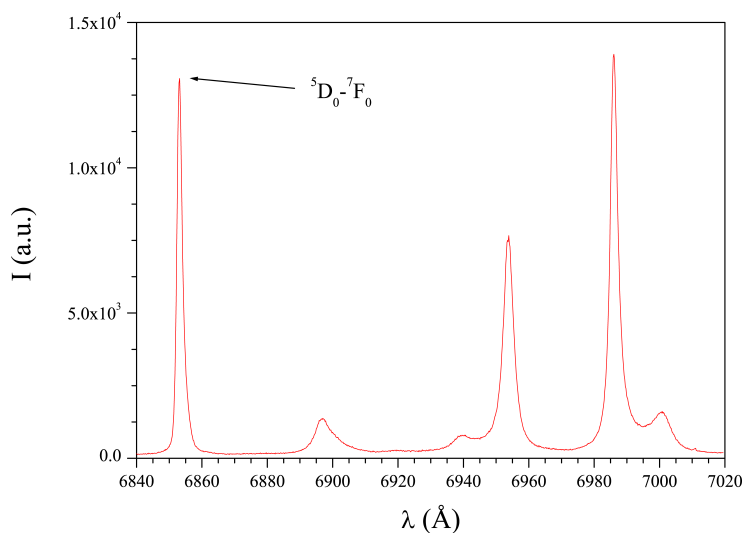


Figure 1.8: Typical luminescence spectra of a $\text{SrB}_4\text{O}_7:\text{Sm}^{2+}$ sample.

with $A = 1884$ GPa and $B = 5.5$.

Using a ruby chip as a pressure gauge is very effective when working at room temperature. Under high temperature conditions the R_1 and R_2 both drastically broaden and overlap which makes the precise calibration of the pressure more difficult. Therefore when high temperature was also required another luminescence gauge has been: strontium borate doped with samarium Sm^{2+} , $\text{SrB}_4\text{O}_7:\text{Sm}^{2+}$. In this case the shift under pressure of the ${}^5\text{D}_0-{}^7\text{F}_0$ luminescence peak (at 685.41 nm under ambient conditions) is measured, see figure 1.8. The pressure $P(\lambda)$ for temperatures below 500 K is given by:

$$P = A\Delta\lambda \left(\frac{1 + B\Delta\lambda}{1 + C\Delta\lambda} \right) \quad (1.3)$$

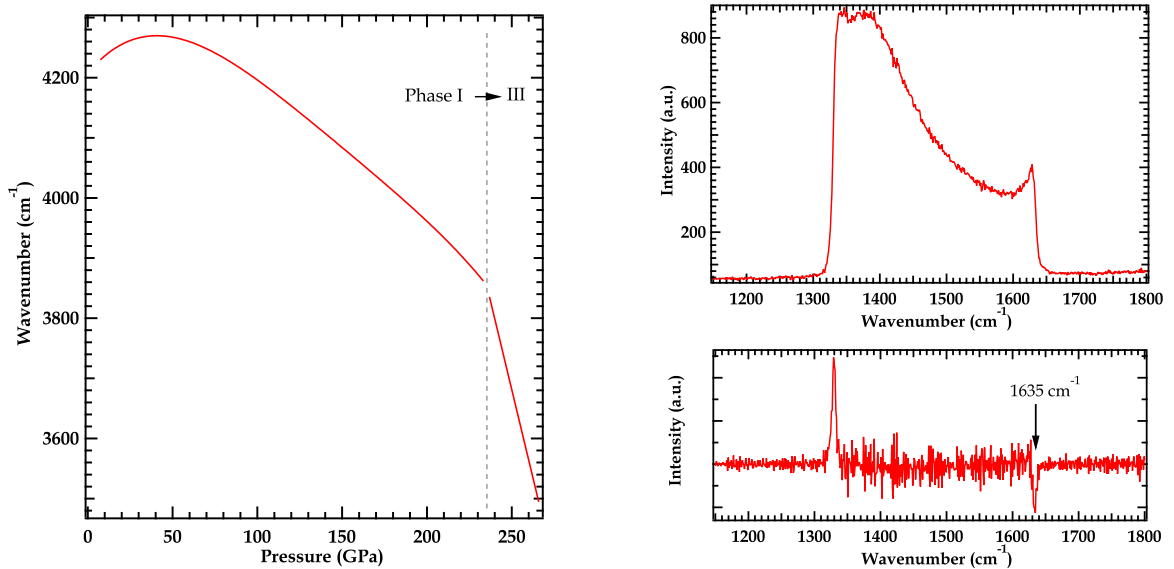
with $\Delta\lambda = \lambda(P) - \lambda(P = 0)$ $A = 4.032 \text{ GPa/nm}$, $B = 9.26 \cdot 10^{-3} \text{ nm}^{-1}$ and $C = 2.32 \cdot 10^{-2} \text{ nm}^{-1}$ in the precedent calibration [69] and with $A = 4.003 \text{ GPa/nm}$, $B = 7.71 \cdot 10^{-3} \text{ nm}^{-1}$ and $C = 1.78 \cdot 10^{-2} \text{ nm}^{-1}$ in the reworked calibration [68]. Above 500 K the effect of the temperature on the shift of the luminescence peak can not be neglected anymore and is given by [69]:

$$\Delta\lambda(500 < T < 900) = 1.06 \times 10^{-4}(T - 500) + 1.5 \times 10^{-7}(T - 500)^2 \quad (1.4)$$

While these two pressure gauges are very useful at low pressures (<140 GPa), under very high pressures they can not be used anymore because of the small size of the experimental chamber ($\sim 10\text{-}15 \text{ }\mu\text{m}$ in diameter at 200 GPa) and because of the drastic decrease of the signal intensity at high pressure. In this case Raman gauges can be employed.

C. Raman gauges

During this thesis a very convenient Raman gauge has been the high frequency vibron of the H_2 molecule since hydrogen has often been used as a pressure-transmitting medium to study hydrides. The evolution as a function of pressure of this vibron is represented in figure 1.9.



(a) Evolution of the H_2 vibron under pressure, measured by Raman spectroscopy at room temperature. Adapted from Ref. [70].

(b) Up: Raman spectrum of a diamond anvil. Bottom: Derivative of Raman signal showing the high-frequency edge at 1635 cm^{-1} used to determine the pressure, 163 GPa in this case.

Figure 1.9: Possible Raman gauges to be used under pressure: H_2 and diamond.

This vibron being very sensitive to pressure above 60 GPa it becomes very useful when other gauges are not available.

Another possible Raman gauge is the diamond anvil itself, as shown in figure 1.9. A calibration of the high-frequency edge of the T_{2g} Raman mode has been proposed by Akahama *et al.* [71]:

$$P = A \frac{\Delta\omega}{\omega_0} \left[1 + \frac{1}{2}(B - 1) \frac{\Delta\omega}{\omega_0} \right] \quad (1.5)$$

with $\omega_0 = 1333 \text{ cm}^{-1}$, $A = 547 \text{ GPa}$ and $B = 3.75 \text{ GPa}$. However, the samples used in the study by Akahama *et al.* were Mo and Pt, *i.e.* materials with much lower compressibility than the samples studied in this thesis (H_2 as a pressure-transmitting medium, LiH...). Due to this large difference in the compressibility, one may think that exact dependence under pressure of the frequency shift might be slightly different. Experiments performed by our laboratory on hydrogen, helium and xenon showed that this pressure scale is relevant at least up to 200 GPa, and leads to an uncertainty of $\pm 20 \text{ GPa}$ above 250 GPa.

Chapter 2

Generating high temperature

High pressures can be coupled with high temperatures in diamond anvil cells. Varying the temperature on the sample is of great interest to explore their structural and thermodynamic behavior and to initiate chemical reactions.

Two different techniques have been used in this thesis in order to explore different $[P, T]$ regions: resistive heating for pressures below 35 GPa and temperatures below 900 K, and laser heating for pressures greater than 10 GPa and temperatures greater than 900 K. These two techniques will be briefly described in this chapter.

2.1 Resistive heating

Resistive heaters can be easily implemented on diamond anvil cells to perform a mild heating of a sample. For temperatures below 500 K a very simple resistive cylinder, fitting the dimensions of the DAC, can be used. It consists of a resistive wire wound around a metallic tube. A K-type thermocouple controls the temperature of the ring via an external electronic controller. Another K-type thermocouple is placed inside the DAC and touches a diamond and in this case we assume that our sample and the diamond are at the same temperature. The losses by thermal conduction induce a temperature difference between the resistive ring and the sample of $\sim 10\%$.

When resistive heating at temperatures above 500 K oxidation phenomena can occur and in particular will greatly damage the backing seats and the diamond anvils of the DAC. To prevent this oxidation the home-made resistive heater presented in figure 2.1 is used. This device, specifically adapted for a membrane-DAC, allows the injection a continuous flux of a reductive mixture (95% Ar - 5% H₂) around the DAC, thus protecting it. Moreover the air stream combined with the chilling system prevent damaging the parts supporting the heater and damaging the lenses used for Raman spectroscopy. This device combined with the use of a NaCl ring on the edges of the experimental chamber to confine hydrogen presented in section 1.3, allowed us to heat our samples up to 800 K below 30 GPa in hydrogen medium.

Resistive devices allow to perform a very mild and prolonged¹ heating of the sample. The temperature increase and decrease are both very slow and can take up to several hours.

¹In order to form crystalline BeH₂, beryllium was heated uninterruptedly at 550 K during 70 hours.

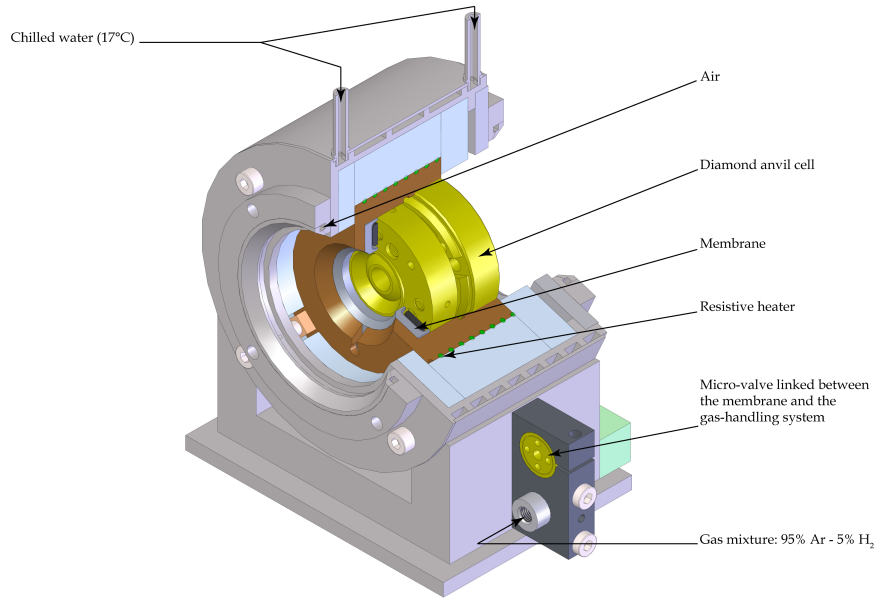


Figure 2.1: Home-made external heater. Image courtesy of F. Occelli.

2.2 Laser Heated Diamond Anvil Cell

The laser heating technique is performed by directing a focused laser beam through the diamond windows onto the sample placed inside the experimental chamber. This is the method of choice to achieve static high- P, T conditions with $[P, T] \leq [360 \text{ GPa}, 5700 \text{ K}]$ and it is extensively used to study planetary interiors, synthesize new materials or determine melting curves. By using a continuous wave (CW) near-infrared laser ($\lambda \sim 1 \mu\text{m}$) metals and dark samples can be easily heated in a DAC. Other materials that do not absorb near-infrared light can generally be heated using a CO_2 laser ($\lambda \approx 10.6 \mu\text{m}$). For hydrides a near-infrared light source (Nd:YAG laser, $\lambda = 1.076 \mu\text{m}$) has been used as our samples were either metals or dark. The infrared beam is focused on the sample surface by lenses to form a heated spot of $\sim 10 \mu\text{m}$ in diameter. A recent study has shown that the temperature distribution inside the heated sample decays rapidly within a few microns [72]. Thus, infrared laser-heating is usually carried out using a double-sided heating with two beams directed simultaneously at opposing sides of the sample.

Laser-heating can be coupled with both Raman spectroscopy, which was realized in our laboratory and is presented in figure 2.2, and with X-ray diffraction, in this case performed on ID27 beamline at the synchrotron ESRF.

Pyrometry is used to measure the temperature of a laser-heated sample in a DAC: the emitted radiation from the sample is collected by a Schwarzschild objective (the reflective objectives appearing on figure 2.2), is directed in a spectrometer and its intensity profile is fitted by the Planck radiation function, usually over the spectral range [400–950 nm], given by ²:

$$I(\lambda, T) = \epsilon \frac{2\pi hc^2}{\lambda^5} \frac{1}{\exp \frac{hc}{\lambda kT} - 1} \quad (2.1)$$

²if $\frac{hc}{\lambda kT} \gg 0$, i.e. for $T \leq 5000 \text{ K}$, the Wien approximation can be used $I(\lambda, T) \simeq \epsilon \frac{2\pi hc^2}{\lambda^5} \exp \frac{-hc}{\lambda kT}$

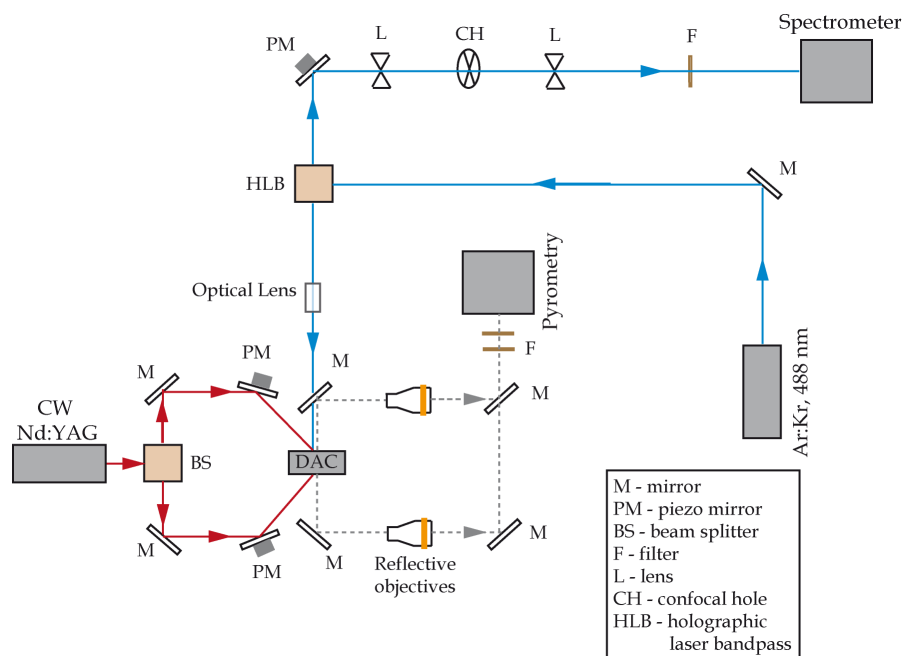


Figure 2.2: Schematic layout of the laser-heating system coupled with Raman spectroscopy. The sample can be laser-heated on both sides and the emitted radiation can be collected by two Schwarzschild reflective objectives to measure the temperature using the Planck radiation function. A similar laser-heating system is available at the ESRF on beamline ID27, coupled with X-rays.

where c is the speed of light in vacuum, h is the Planck's constant, k is the Boltzmann's constant and ϵ is the emissivity of the material. For a black body $\epsilon = 1$ at all wavelengths. In a grey-body approximation, used in our case, $\epsilon < 1$ at all wavelengths and is fitted to the experimental results.

In our case, determining the temperature from a laser-heated sample was particularly difficult and most of the time it was not possible at all. These difficulties were the consequences of two effects:

- The time's collection of the emitted radiation is in the order of 1 second during which the temperature of the sample must stay relatively stable. In our case the laser-induced chemical reaction in hydrogen medium could result in a very drastic increase of the temperature, creating very intense bright flashes. When such flashes were observed the laser-heating was immediately turned off to prevent damaging the diamond anvils and to prevent any chemical contamination of the sample, meaning that the temperature could not be determined.
- The second difficulty is inherent to the first one. In order to avoid these very bright flashes the laser-heating needed to be finely controlled and the temperature was kept relatively low, below 1500 K and most of the time it was estimated around 1000 K. Looking at the figure 2.3 showing the Planck distribution for different temperatures over the range [400-1000 nm], it can be clearly seen that detecting temperatures at 1400 K is at the very limit of what can be measured. Note that in this figure the spectral range has been extended for clarity purpose, we normally have access to the spectral range [400-950 nm]. To measure temperatures with a significant accuracy below 1400 K a detector working in the infra-red spectrum, *i.e.* >1000 nm, would be required.

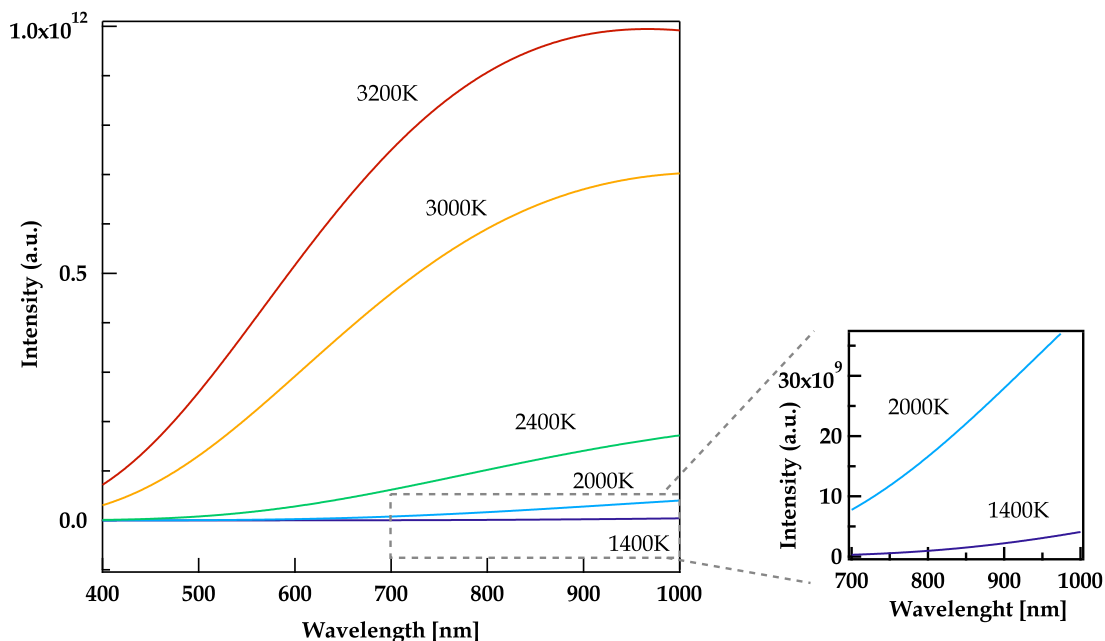
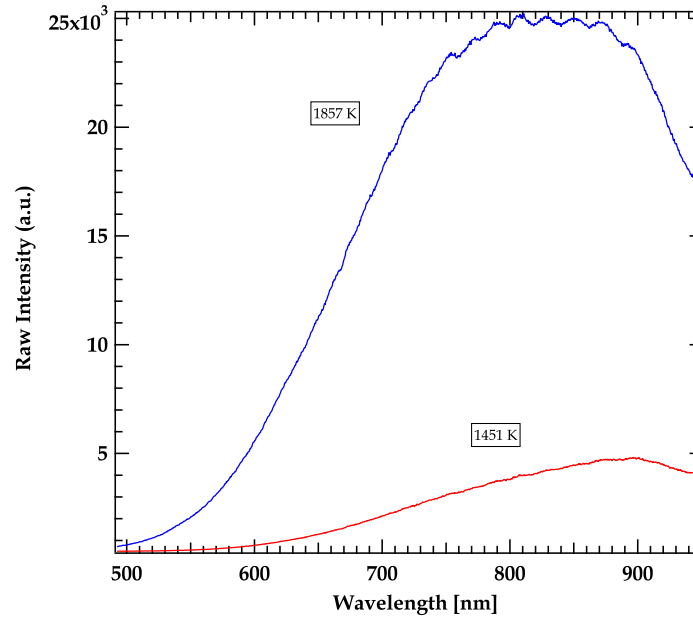


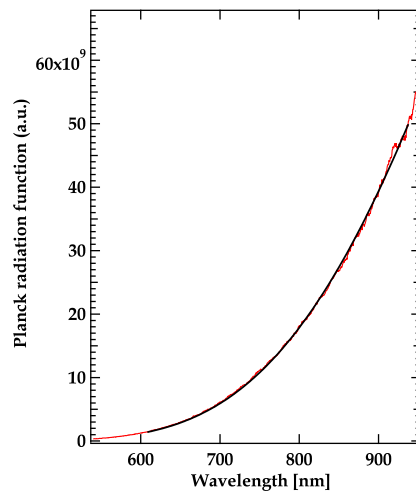
Figure 2.3: Intensity as a function of the wavelength calculated from the Planck's formula for different temperatures.

In some (rare) cases however the system was stable enough to realize temperature measurements. An example is shown in figure 2.4: the intensity of the emitted light was measured over 5 seconds at 1857 K and 1451 K, evidencing the difficulties to measure temperatures below 1400 K over this spectral range. The fits of the Planck radiation function and of the Wien function, used to determine the temperature of 1451 K, are also represented in figure 2.4b and 2.4c.

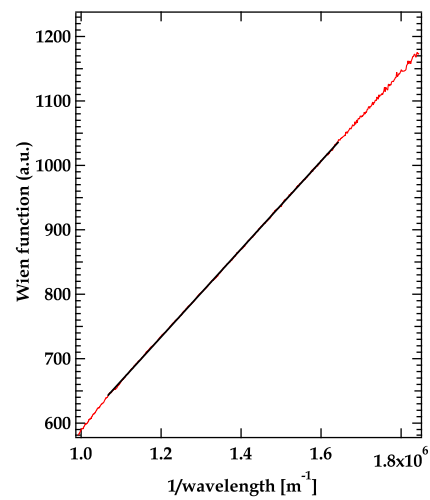
The two different techniques used to heat our samples, resistive and laser-heating, are both complementary and very different. Complementary because they allow heating in two distinct ranges: at low temperature in the case of the resistive technique, above 900 K when using lasers. It would be impossible to use resistive heating above 1200 K as it would irretrievably damage the cell and it would be very ineffective to laser heat a sample below 900 K. On the other side these two techniques are very different: in the first case, resistive heating provides a very slow, progressive and homogenous heating of the sample, while using lasers will allow to heat and cool the sample almost instantaneously but with large temperature gradients. It is thus understandable why the choice of a technique can have consequences in material synthesis.



(a) Raw intensity of the emitted light coming from the sample at two different temperatures.



(b) Planck radiation function and its fit, corresponding to a temperature of 1451 K.



(c) Wien function and its fits, corresponding to a temperature of 1451 K.

Figure 2.4: Measured black body radiations at 1857 K and 1451 K. The fits for the Planck function and for the Wien function are shown for the measurement at 1451 K.

Chapter 3

Sample preparation

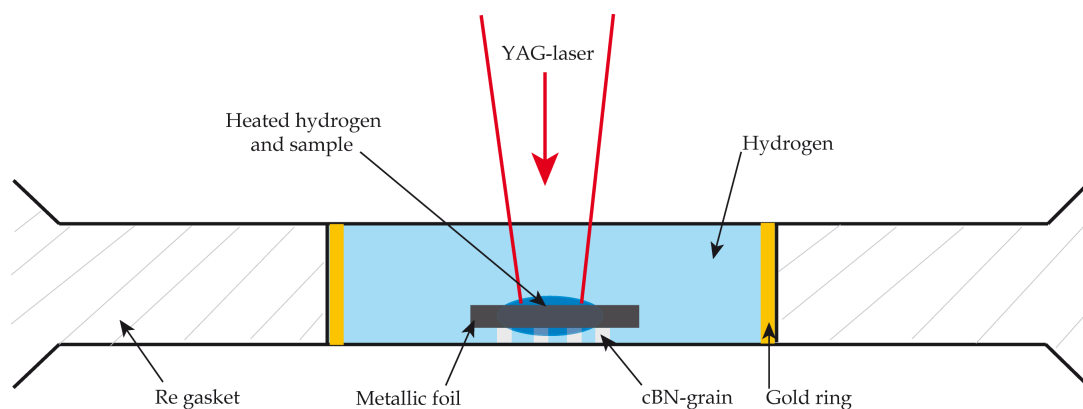
Laser heating techniques require to pay particular attention to perfectly insulate the sample from the diamond for two main reasons:

- If the sample were to be placed in contact with a diamond, the extremely high thermal conductivity of diamond would induce an important heat loss and it would be very difficult to heat up the sample, if not impossible.
- If a part of the sample were to be in contact with the diamond, chemical reactions between the diamond and the sample or between the diamond and the pressure-transmitting medium, hydrogen in our case, would be very easily induced.

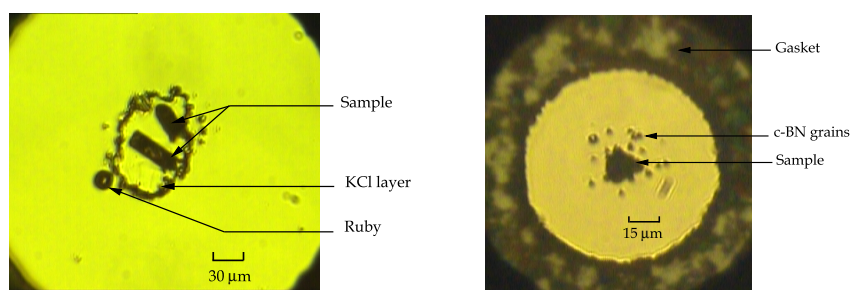
Therefore our samples were thermally and chemically insulated from the anvils using thin layers ($\sim 1-2 \mu\text{m}$) of LiF or KCl, or small single crystals of c-BN ($\sim 2-4 \mu\text{m}$) as presented on figure 3.1. Using different insulating materials also allowed us to check for possible chemical contaminations between the insulator and the sample. The salt layers were prepared by compressing a small grain between two diamonds. A small part was then left on a diamond and the sample was carefully deposited on top of the remaining layer. The c-BN grains were deposited on the diamond using a micro-manipulator with a precision of $\sim 1 \mu\text{m}$. In both cases the metallic foil had been slightly pre-compressed using very large diamonds (culet sizes of 1 mm) in order to make it flat to facilitate the coupling with the YAG-laser. In each arrangement the sample was placed at the center of the experimental chamber: above 30 GPa the volume of the experimental chamber has been reduced by 2 when using hydrogen as pressure-transmitting medium, since it is highly compressible, and the edges of the chamber should not touch the sample as it could:

- destabilize the sample configuration and the sample will most likely enter in contact with the diamond which has to be avoided
- induce a local heating of the gasket when laser heating the sample which would inevitably lead to the diffusion of hydrogen in the gasket and thus to the complete closure of the experimental chamber.

Once the sample has been placed on top of the c-BN grains or the salt layer, hydrogen is loaded in the experimental chamber using a gas loading system. The pressure in the experimental chamber at this moment is approximately ~ 0.14 GPa which means that hydrogen is still liquid. Hydrogen solidifies at 5.5 GPa and usually large monocrystals are easily grown in the experimental chamber if the pressure



(a) Schematic cross-section of the sample arrangement. The heating thick metallic foil rests on cBN grains that thermally insulate the foil from the bottom anvil.



(b) Sample arrangement with a KCl layer. (c) Sample arrangement with cBN-grains.

Figure 3.1: Sample arrangement when laser heating a metallic foil in hydrogen medium.

is increased slowly. The growth of such crystals is incompatible with our sample arrangement as the crystallization front will push the metallic foil from the cBN-grains or from the insulating layer, hence destroying the insulating configuration. To avoid this phenomenon we used the possibility offered by the membrane-DAC to quickly increase the pressure in the chamber by instantaneously increasing the membrane pressure: usually the pressure increased in few 10 ms from 4.5 GPa up to 8-10 GPa. In turn hydrogen instantaneously solidified into a fine powder and the sample did not move.

The stability of this sample configuration is mandatory to avoid any chemical reaction or the formation of parasitic compounds. If the insulation of the sample fails it can mislead the interpretation of the results.

When studying the mixture iron+hydrogen we heated an iron foil in hydrogen at 160 GPa: both Raman and infrared spectroscopy revealed the appearance of new high-frequency vibrations that could not be attributed to pure hydrogen, as shown in figure 3.2, and these vibrations could be monitored down to 89 GPa. Most of the theoretical calculations on hydrides with unusual stoichiometry predict the appearance of H_3^- entities and of H_2 molecules inside these hydrides, with vibrations in the $[3000 - 3500 \text{ cm}^{-1}]$ range and above 4000 cm^{-1} respectively. Thus our first guess was that we had synthesized a new iron hydride containing H_3^- entities and/or H_2 molecules. The careful reproduction of the experiment combined with X-ray diffraction measurements revealed that these vibrations in fact resulted from a parasitic reaction and

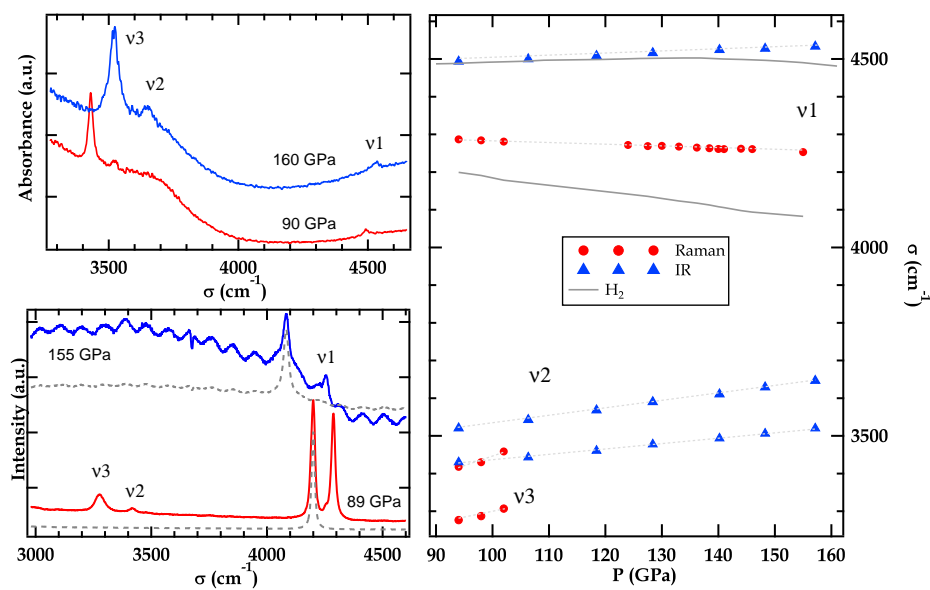


Figure 3.2: Parasitic infra-red and Raman signals most likely due to the chemical reaction of hydrogen with the diamond anvil. Upper left: Absorbance spectra at 160 and 90 GPa, showing three new absorption bands labelled ν_1 , ν_2 and ν_3 . Bottom left: Raman spectra at 155 GPa and 89 GPa. At 155 GPa a fluorescence signal coming from the sample masked the vibrations below 4000 cm^{-1} . The grey dashed lines correspond to signal from pure hydrogen at the same pressure measured near the sample. Right: Pressure dependence of the observed vibrations upon decompression.

they could not be reproduced. These vibrations are in fact the evidence of a chemical reaction between H_2 and $\text{C}_{diamond}$: the same peaks were also observed with the systems $\text{B}+\text{H}_2$ and $\text{Be}+\text{H}_2$ and were also most likely observed by another group working on the system $\text{Na}+\text{H}_2$.

Part II

High pressure characterization of the sample

Chapter 4

Raman spectroscopy

4.1 Background of the Raman spectroscopy

At the beginning of the 20th century, in 1928, Sir Chandrasekhra Venkata Raman observed for the time the phenomenon that would bare his name. Using sunlight as the source, a telescope as the optics and his eyes as the detector he was able to detect Raman shifts in a liquid. Since then, large improvements in the various components of the Raman instrumentation have been made (invention of the laser, improvement of the detection instrumentation) and this phenomenon is well understood and documented for all three normal phases of the matter. What Sir C.V. Raman observed in 1928 is an inelastic scattering process: when matter (gas, liquid, solid) is illuminated with a monochromatic beam (usually visible light) of frequency ν_i most of the radiation is scattered elastically (Rayleigh scattering) and a small component is scattered inelastically (Raman scattering). Experimentally it is observed in the spectrum by the appearance of additional pairs of spectral lines, at symmetrical frequencies either side of the Rayleigh line: with a positive frequency shift this process is called Raman anti-Stokes scattering, and with a negative frequency shift it is called Raman Stokes scattering.

4.2 Theory of Raman spectroscopy

Raman scattering can be described by two different approaches: a classical one or by quantum mechanics.

In a classical description we consider the electric field strength, \mathbf{E} , of the time dependent electromagnetic wave illuminating a molecule as given by:

$$\mathbf{E} = \mathbf{E}_0 \cos \omega_i t \quad (4.1)$$

It induces an electric dipole moment \mathbf{P} :

$$\mathbf{P} = \alpha \mathbf{E} = \alpha \mathbf{E}_0 \cos 2\pi \omega_i t \quad (4.2)$$

where α is the polarizability. If the molecule is vibrating with a pulsation ω_m the nuclear displacement q is given by:

$$q = q_0 \cos \omega_m t \quad (4.3)$$

where q_0 is the vibrational amplitude. For a small amplitude of vibration, we can write:

$$\alpha = \alpha_0 + \left(\frac{\partial \alpha}{\partial q} \right)_0 q \quad (4.4)$$

α_0 is the polarizability at the equilibrium position, *i.e.* if α does not vary the scattered wave has the same frequency as the incident wave, and this corresponds to the Rayleigh scattering. When combining equations 4.2 and 4.4 we then get:

$$\begin{aligned} \mathbf{P} &= \alpha_0 \mathbf{E}_0 \cos \omega_i t + \left(\frac{\partial \alpha}{\partial q} \right)_0 q_0 \cos \omega_m t \mathbf{E}_0 \cos \omega_i t \\ &= \alpha_0 \mathbf{E} + \frac{1}{2} \left(\frac{\partial \alpha}{\partial q} \right)_0 q_0 \mathbf{E}_0 [\cos((\omega_i + \omega_m)t) + \cos((\omega_i - \omega_m)t)] \end{aligned}$$

The first term of this equation is the Rayleigh scattering which has the same frequency as the incident wave, the second term shows that two new waves with different pulsations can be observed: the first one with a pulsation $\omega_i + \omega_m$ corresponds to a anti-Stokes Raman band, and the second one with a pulsation $\omega_i - \omega_m$ to a Stokes Raman band.

This classical model, while explaining the observation of the Stokes and anti-Stokes Raman bands, does not explain the observed difference between the relative intensities of these two bands as the intensity ratio in this classical calculation gives:

$$\frac{I_{anti-Stokes}}{I_{Stokes}} = \frac{(\omega_i + \omega_m)^4}{(\omega_i - \omega_m)^4} \quad (4.5)$$

which is not corresponding to the observation. The quantum mechanical treatment of Raman scattering explains this difference. In this model the intensity depends on the occupation of the initial state determined by the Boltzmann distribution. The intensity is then given by:

$$\frac{I_{anti-Stokes}}{I_{Stokes}} = \frac{(\omega_i + \omega_m)^4}{(\omega_i - \omega_m)^4} \exp \frac{-\hbar\omega_m}{k_B T} \quad (4.6)$$

This ratio is dependent of the temperature, *i.e.* Raman spectroscopy can be used to measure temperatures by measuring this intensity ratio.

The quantum mechanical description brings another interesting information. In this description an incident photon (pulsation ω_i , wave vector \vec{q}_i) can induce the creation (Stokes Raman scattering) or the annihilation (anti-Stokes Raman scattering) of a phonon (ω_p , \vec{q}_p) during the scattering of a photon (ω_s , \vec{q}_s). The law of momentum conservation then imposes:

$$\begin{aligned} \hbar\omega_i &= \hbar\omega_d \pm \hbar\omega_{phon} \\ \hbar\vec{k}_i &= \hbar\vec{k}_d \pm \hbar\vec{k}_{phon} \end{aligned}$$

With an exciting light in the visible spectrum the modules of \vec{k}_i and \vec{k}_d are in the order of $\sim \frac{1}{\lambda} \sim 10^6 m^{-1}$ which is far smaller than the dimension of the first Brillouin zone $\sim \frac{\pi}{a} \sim 10^{10} m^{-1}$ (with a a characteristic cell parameter), meaning that the created or annihilated photon is at the center of the Brillouin zone and that Raman spectroscopy is used to probe optical phonons at the Γ point.

4.3 High-pressure Raman instrumentation

The typical sample dimensions when working with a diamond anvil cell range in general from 10 to 100 μm in diameter and a few micrometers in thickness. These dimensions can be even smaller for experiments at ultra-high pressure, *i.e.* >200 GPa. Moreover the presence of a diamond window in the optical path will induce geometric and chromatic aberrations which will lower the image quality and affect the signal collection. Some home-made adaptation are therefore required to interface this Raman bench with

the diamond anvil cell, as the commercial microscopes often do not meet the level of specificity required in this case.

As the distance between the sample and the back of the cell is approximately 15 mm (diamond+cylinder), objective lenses with a large working distance are necessary: usually specific objective lenses with a 20 times magnification offering a working distance of 30.5 mm. The counter-part of such long working distance is that the numerical aperture (N.A.) is lowered which leads to a larger depth of focus, 3.5 μm in this case, meaning that a Raman 3D-mapping of a sample will not be possible. Nowadays optical lenses with a 50 times magnification offering a working distance of 20.5 mm are available and lower the depth of focus down to 1.6 μm . However such lenses will not be suitable for the use of a cryostat or an external heater similar to the one presented in figure 2.1. An alternative way to reduce the depth of focus while working with a 20 times magnification lens is to place in the optical path a confocal field aperture (or spatial filter) with a diameter corresponding to the one of the focused laser spot. Such confocal hole also helps reducing the spurious elastically scattered laser radiation.

Finally high-pressure Raman set-ups often offer the possibility to change the excitation wavelength: sample fluorescence can occur under pressure and can be easily decreased by varying the excitation wavelength.

A schematic description of a Raman set-up used during this thesis is shown in figure 2.2.

Chapter 5

Infra-red spectroscopy

5.1 Theory of the infra-red spectroscopy

Molecular vibrational frequencies are found in the infra-red (IR) region of the electromagnetic spectrum and can be measured using infrared absorption techniques: a polychromatic infra-red light is passed through a sample and the intensity of the transmitted light is measured over a wide range of frequencies (typically [650 cm^{-1} - 8000 cm^{-1}]). When molecules absorb IR radiation, transitions occur from a vibrational energy level n to the vibrational level m , typically corresponding to the vibrational ground and excited states respectively. The $n \rightarrow m$ transition results from the absorption of a photon. This process is controlled by the electrical dipole moment operator $\hat{\mu}_q$ defined by:

$$\hat{\mu}_q = \sum_{\alpha} e_{\alpha} \cdot q_{\alpha} \quad (5.1)$$

where e_{α} is the effective charge of the atom α and q_{α} is the distance to the center of gravity of the molecule in Cartesian coordinates ($q = x, y, z$). The IR intensity for this $n \rightarrow m$ transition is then given by:

$$I_{nm} \propto [\mu_x]_{nm}^2 + [\mu_y]_{nm}^2 + [\mu_z]_{nm}^2 \quad (5.2)$$

where $[\mu_q]_{nm}$ is the integral

$$[\mu_q]_{nm} = \langle \psi_m^* \hat{\mu}_q \psi_n \rangle \quad (5.3)$$

where ψ_n and ψ_m are the wavefunctions for the vibrational states n and m . The square of the integral will then give information about the probability of a transition occurring. Expanding $\hat{\mu}_q$ in Taylor series with respect to the normal coordinates Q_k in the harmonic approximation, the transition probability of Eq. 5.3 is then given by:

$$[\hat{\mu}_q] = \langle \psi_m^* \hat{\mu}_q \psi_n \rangle = \mu_q^0 \langle \psi_m^* \psi_n \rangle + \sum_{k=1}^{3N-6} \left(\frac{\partial \mu_q}{\partial Q_k} \right)_0 \langle \psi_m^* Q_k \psi_n \rangle \quad (5.4)$$

The first term of the right hand-side of Eq. 5.4 is zero as ψ_n and ψ_m are orthogonal. The transition probability will then be non-zero (*i.e.* IR active) if:

- the derivative of the dipole moment in Eq. 5.4 is non-zero, which requires that the normal mode is associated with a change in the dipole moment
- the integral $\langle \psi_m^* Q_k \psi_n \rangle$ must be non-zero, which is the case if the vibrational number n and m differ by one, *i.e.* only fundamentals are IR active in the harmonic approximation.

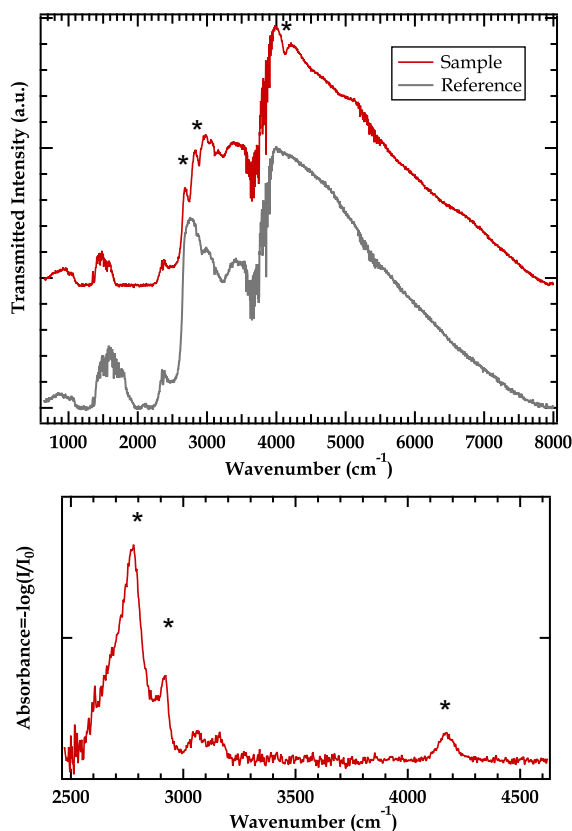


Figure 5.1: Top: Infra-red transmitted intensity through an empty used as a reference, and through a sample. Bottom: Corresponding measured absorbance over a selected spectral range. Absorption bands are denoted by the black asterisks.

5.2 Infra-red spectroscopy combined with high pressure experiments

Depending on the material, the same or different vibrational transitions can be probed by IR absorption and Raman spectroscopy and both techniques are usually referred as complementary. Hence both IR and Raman spectra are usually plotted in an analogous way with the abscissa referring to the energies of the vibrational transitions, expressed in wavenumbers (cm^{-1}) usually over the range [400 cm^{-1} - 4500 cm^{-1}]. In IR spectroscopy the ordinate refers to the amount of absorbed light and is expressed in term of absorbance: $abs = -\log\left(\frac{I}{I_0}\right)$ where I is the intensity of the transmitted light through the sample and I_0 the intensity of a reference, usually corresponding to the transmitted light in an empty diamond anvil cell before loading the sample in experimental chamber. An example of data analysis is shown in figure 5.1.

Compared to Raman spectroscopy, infra-red absorption offers several advantages for high-pressure studies:

- The energy used in IR spectroscopy is in the order of 0.5 to 0.012 eV so that this probing technique can be called non-invasive and prevents inducing chemical reactions, between the pressure transmitting medium and the sample for instance, or to avoid any deterioration/decomposition of our sample.

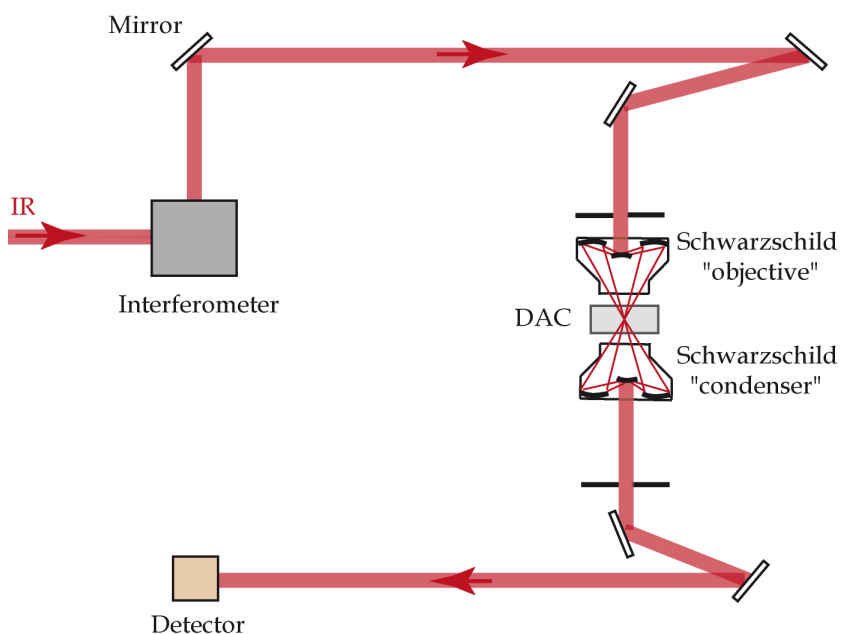


Figure 5.2: Schematic of the infra-red microscope used on the SMIS beamline at the synchrotron SOLEIL.

- Any parasitic fluorescence which may come from the diamond anvils or from the sample when performing Raman spectroscopy, will be avoided or at least greatly reduced when performing IR absorption.
- Above 280 GPa the diamonds start to absorb the visible light because of the progressive closure of its band gap, which can lead to its premature failure. This is not the case with IR light.
- IR absorption of light can be used to detect the progressive band gap closure of a compound and hence to precisely determine the pressure at which the sample will become metallic.

However the major disadvantage of this technique is that most of the time it requires the use of a synchrotron light source. Even though some sources are suitable for the use in a laboratory, like Globar sources usually consisting of silicon carbide heated between 1000 and 1800 K that use the black body radiation as an IR source, the intensity of the collected signal will be very weak if the experimental chamber is inferior to 100 μm , which was the case in most of our experiments (for instance the we worked with an experimental chamber of ~ 20 μm diameter when compressing LiH). This is why in our case infra-red spectroscopy experiments were performed on the SMIS beamline at the synchrotron SOLEIL to benefit from the great brilliance of the synchrotron source. A home-made horizontal microscope equipped with two Schwarzschild objectives that produce a 22 μm IR spot has been used and is schematically represented on figure 5.2. Such horizontal microscope allows us to quickly and easily perform IR absorption experiments combined with DACs or even with DACs mounted in a cryostat.

In our case IR spectroscopy also proved to be very useful to detect any chemical contamination of our LiH sample: LiH can react with oxygen or water to form LiOH which exhibits a very strong and characteristic absorption band around 3500 cm^{-1} at low pressure. Such contamination could then be easily detected and a new sample was then loaded in the experimental chamber.

Chapter 6

X-ray diffraction

6.1 Crystal diffraction

The wavelength of an x-ray photon is in the order of $\sim 1 \text{ \AA}$ which is comparable with the interatomic spacing in a crystal. Thus a diffraction phenomena can occur when such waves interact with the planes of atoms in a crystal. The resulting diffraction pattern will allow us to determine the space group, the size of the unit cell and the position of the atoms within the cell. The angle through which an x-ray beam will be diffracted depends both on the crystal structure and on the wavelength of this beam. The diffracted beam will be found when the reflections from parallel planes interact constructively. Such constructive interferences occur when the path difference is an integral number n of the radiation wavelength λ , which gives the following condition for constructive reflections, called the Bragg law:

$$2d_{hkl} \sin(\theta) = n\lambda \quad (6.1)$$

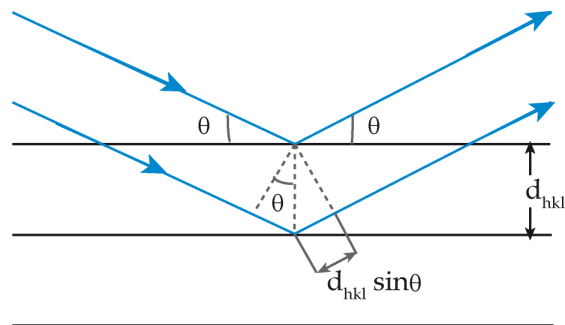


Figure 6.1: Illustration of the Bragg formalism: the incident x-ray beam scatters elastically off a set of parallel interreticular planes separated by a distance d_{hkl} , with h, k, l the Miller indices.

Experimentally we know the value of λ and θ so that using Eq. 6.1 we can have access to the value of d_{hkl} . This value is then related to cell parameters $a, b, c, \alpha, \beta, \gamma$ by the relation [73]:

$$\begin{aligned} \frac{1}{d_{hkl}^2} &= \frac{1}{V^2} (S_{11}h^2 + S_{22}k^2 + S_{33}l^2 + 2S_{12}hk + 2S_{23}kl + 2S_{13}hl) \\ \text{with} \\ S_{11} &= b^2c^2 \sin^2 \alpha \\ S_{22} &= a^2c^2 \sin^2 \beta \\ S_{33} &= a^2b^2 \sin^2 \gamma \\ S_{12} &= abc^2 \cos \alpha \cos \beta - \cos \gamma \\ S_{23} &= a^2bc \cos \beta \cos \gamma - \cos \alpha \\ S_{13} &= ab^2c \cos \alpha \cos \gamma - \cos \beta \\ V &= abc \sqrt{1 - \cos^2 \alpha - \cos^2 \beta - \cos^2 \gamma + 2 \cos \alpha \cos \beta \cos \gamma} \end{aligned}$$

These relations allow us to determine the structural parameters of the studied sample. However at this point the position of the nuclei within the cell still remain unknown. This information is found in the relative intensities of the Bragg's reflections. For an atom i with the position $\vec{r}_i = \vec{a}x_i + \vec{b}y_i + \vec{c}z_i$, $x, y, z \in [0, 1]$ the structure factor can be expressed as [73]:

$$\vec{F}_{hkl} = \sum_{j=1}^n f_j(hkl) e^{-2\pi i(hx_i + ky_i + lz_i)} \quad (6.2)$$

with f_j the atomic form factor given by

$$f_j(\theta) = \int_0^\infty r \rho(r) G(\theta, r) dr \quad (6.3)$$

where $G(\theta, r) = (2 \sin(4\pi r \sin \theta)) / (\sin \theta / \lambda)$ represents the scattering efficiency of atom j , and $\rho(r)$ the electron density. The intensity I of a reflection is then given by $I \propto |F|^2$, which means that it will be highly dependent of the atomic scattering factor. This factor can be computed for a given wavelength and selected examples, H, Be, Al and Fe, have been plotted on figure 6.2 for $\lambda=0.3738 \text{ \AA}$, which corresponds to the wavelength used in our experiments on beamline ID27 at the synchrotron ESRF. At low angle we see that $f_j(s) \sim Z$, the atomic number, which means that light elements will produce reflections with weak intensities. This is why it is often said that hydrogen atoms can not be seen in x-ray diffraction: their contribution to the reflection intensities is the weakest of all elements.

Our x-ray diffraction experiments were performed at the European Synchrotron Light Source, ESRF, on the high-pressure beamlines ID09a and ID27 with wavelengths around 33 keV and a focalized spot on the sample varying from $20 \times 20 \text{ \mu m}$ to $3 \times 2 \text{ \mu m}$, depending on the requirements of the experiment. Both beamlines perform angular-dispersive x-ray diffraction: the detector is placed behind the sample that can rotate around an axis perpendicular to the x-ray beam, in a plane perpendicular to the monochromatic beam. The data are collected using an image plate 2D detector (Mar555) or a large area Charged Coupled Device (CCD). The sample-to-detector distance is precisely determined using the calibration pattern of a LaB_6 or CeO_2 powder.

When working with diamond anvil cells specific issues need to be taken into account:

- As seen in section 1.2 the angular aperture of cell is very limited. The recent use of the Almax-Boelher design partially solved this problem, offering a much larger aperture, up to $2\theta \sim 70 \text{ deg}$.

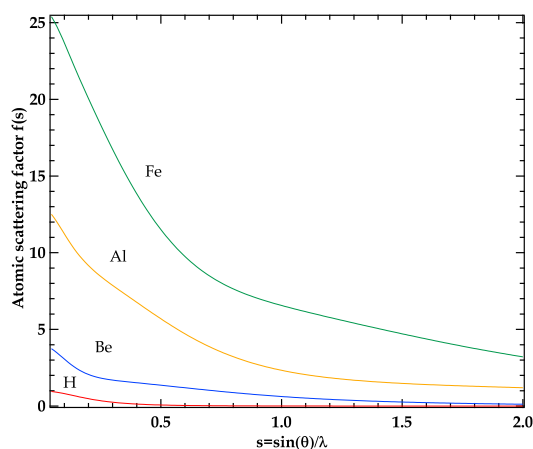


Figure 6.2: Plot of the atomic scattering factors for hydrogen, beryllium, aluminum and iron, at $\lambda=0.3738 \text{ \AA}$.

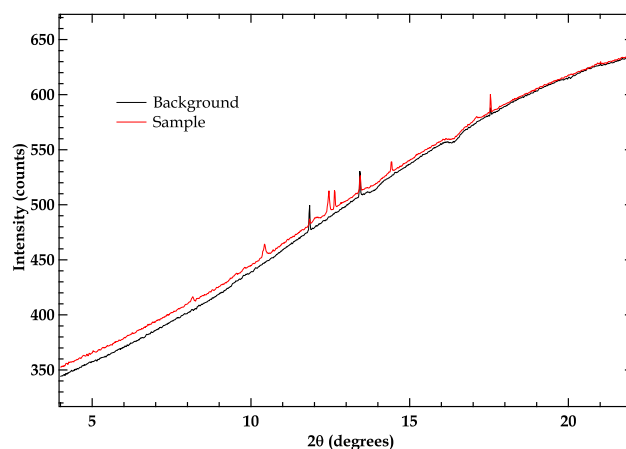


Figure 6.3: Diffractogram of a BeH_2 sample in hydrogen pressure transmitting medium. The background has been taken by performing diffraction a few microns near the sample in hydrogen medium, showing the importance of the Compton scattering.

- Parasitic diffraction signal will come from the different parts of the cells: the diamonds, that are very thick compared to the sample, will produce very intense Bragg's spots that will locally saturate the detector; the rhenium gasket and the gold ring around the experimental chamber will produce intense¹ diffraction powder pattern that can overlap with diffraction signal from the sample.
- A large background signal will be produced when the x-ray beam goes through the diamond anvils as due to the Compton scattering from the diamond. As it can be seen on figure 6.3 for low-Z elements this effect can make the data analysis difficult.

¹intensive relatively to the signal coming from our sample, as $Z_{\text{Re}}=75$, $Z_{\text{Au}}=79$ and for the heaviest element studied $Z_{\text{Fe}}=26$

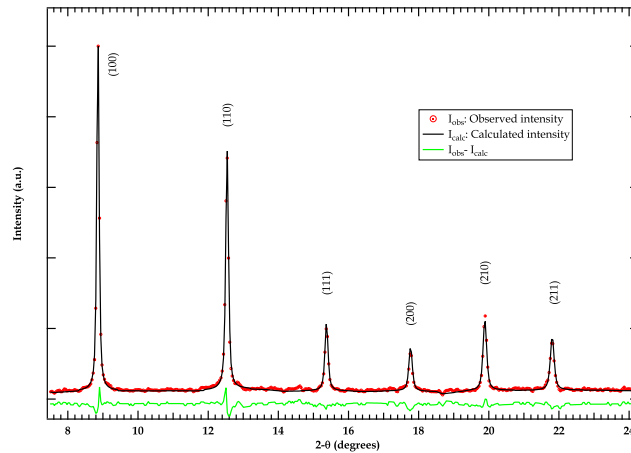


Figure 6.4: Example of Rietveld refinement performed on a powder of FeH_3 at 87 GPa, with a R-Bragg factor $R_B = 8.4\%$.

6.2 Data analysis

Throughout this thesis the data collected on the ESRF beamlines were either powder² diffraction or poorly crystallized samples, meaning that only powder diffraction analysis techniques were used.

Diffraction from such polycrystalline and powder samples will form Debye-Scherrer rings. This 2D-data is integrated azimuthally using the software Fit2D [74], producing a 1D-diffractogram. This 1D-diffraction profile then contains the necessary information to refine the data. Different cases are to be distinguished. First, if the spacegroup of the studied phases are already known - which is often the case for ambient/low-pressure phases - only the cell parameters need to be refined. In this case the data were treated using the Le Bail method, using the software suite FULLPROF. In the Le Bail method, individual integrated peak intensities and shapes are treated as free least squares parameters. The peak shapes are modelled as Pseudo-Voigt profiles, a convolution of a Gaussian and a Lorentzian peak - synchrotron radiation produces a Lorentzian peak, the instruments used to collect the signal will add a Gaussian contribution. The individual Bragg peak positions are obtained through refinement of the unit cell dimensions *i.e.* the lattice parameters a , b , and c , and the angles between them. This method does not provide any information about the atomic positions, the scale factor or the site occupancies. This is the second case: no structural informations about the studied sample are known. The first step is to find the spacegroup. This is done using the software CheckGroup which will look for systematic extinctions of Bragg peaks. The second step is to refine the cell parameters using the Le Bail, method as well as the background to the diffraction profile. Finally the atomic positions within the unit cell can be refined using the Rietveld method [75]. The Rietveld method requires a high-quality powder data to have reliable intensities for each integrated Debye-Scherrer ring, as it can be seen in eq. 6.2 that the intensity contains the information about the atomic positions. For diffraction profiles of quasi-single crystals or powders with a strong preferred orientation a Rietveld refinement is not possible. The Rietveld structure refinement method carries out a least-squares refinement on the entire observed diffraction profile. The Rietveld process will refine the adjustable parameters until the residual $S = \sum_i \frac{(y_i - y_{ci})^2}{y_i}$ is minimised, where y_i and y_{ci} are respectively the observed and the calculated diffraction pattern at the i th step, *i.e.* a best fit of the entire

²We call powder a sample where every possible crystalline orientation is represented equally or with very little texturing.

calculated pattern for the observed diffraction pattern is obtained. In order to check for the quality of the fit, the following two values are often looked at:

$$\begin{aligned} R - \text{Bragg Factor} \quad R_B &= \frac{\sum |I_{Kobs} - I_{Kcalc}|}{\sum I_{Kobs}} \\ R - \text{weighed pattern} \quad R_{wp} &= \left[\frac{\sum w_i (y_{iobs} - y_{icalc})^2}{\sum w_i y_{iobs}^2} \right]^{\frac{1}{2}} \end{aligned}$$

These values should be the lowest possible. Combining these numerical criteria with a visual evaluation allows to judge for the quality of the proposed solution. An example of Rietveld refinement performed on the powder of a sample of FeH₃ with a simple cubic unit cell is shown in figure 6.4.

Part III

Structural changes in hydrides under pressure: AlH_3 and BeH_2

Chapter 7

Motivations

The first step of my Ph.D. thesis was to study the high pressure behaviour of a relatively well known hydride in order to develop a suite of diagnostics to characterize the structural and electronic properties of hydrides under pressure using the different techniques of investigation exposed in the previous part, and to develop new methods to synthesize an hydride from its elements under pressure. Aluminum hydride, AlH_3 , appeared to be a good candidate as it had been recently studied up to 120 GPa with the observation of an insulator-to-metal phase transition. Yet there was a need for a more detailed understanding of its pressure evolution. Also, some discrepancies between experimental results and theoretical predictions were pushing for a more thorough investigation of this compound.

The developed methods of synthesis could then be applied to another hydride which had not been studied in its crystalline form under high pressure up to now: beryllium hydride, BeH_2 . The synthesis of a high-purity crystal enabled the first study of the high-pressure behaviour of this hydride and hence to confirm some of the theoretical predictions that had been published on this subject.

The following two chapters report the evolution under pressure of the structural, vibrational and electronic properties of AlH_3 and BeH_2 . This part addresses the following points:

- Understanding the high-pressure behavior of hydrides (high compressibility, possible amorphization, facing the issue of poor recrystallization after a phase transition...).
- Developing a portfolio of techniques to characterize such low-Z compounds.
- Experimentally confirm the awaited predominant role of hydrogen in covalent hydrides.
- Developing an efficient synthesis technique in hydrogen medium using either a resistive heater or an infra-red YAG-laser.

Chapter 8

Aluminum Hydride AlH_3 under Pressure

8.1 Introduction

Aluminum hydride, also called alane, is a crystalline solid metastable at ambient temperature. Its volumetric hydrogen density of $148 \text{ g}\cdot\text{H}_2/\text{L}$ is more than twice that of liquid hydrogen. Combined with a rapid hydrogen rate at low temperatures ($\leq 100 \text{ }^\circ\text{C}$), these properties explain the interest this compound arouse over the past 60 years: it has been used as a solid rocket propellant, an explosive, a reductant agent or as a hydrogen source for portable power systems. Recently this interest has been renewed by the rapid development of hydrogen storage devices for automotive applications.

One of the very first publication on the synthesis of aluminum hydride in 1942 reported the formation of an impure form of alane $\text{AlH}_3 \cdot 2\text{N}(\text{CH}_3)_3$ [76]. Five years later a simpler process was proposed by Finholt *et al.* resulting in an ethereal solution of aluminum hydride [77] and the first synthesis of pure alane was realized in 1955 by Chizinsky [78]. After this first synthesis of a pure form of alane, very little work has been published in the open literature as a lot of classified work was being done by scientist of the former Soviet Union and of the United States. 20 years after the synthesis by Chizinsky, Bower *et al.* proposed an improved method to produce larger quantities of alane with larger crystallite sizes [79]. Moreover they had prepared and identified seven different polymorphs of AlH_3 called $\alpha, \alpha', \beta, \gamma, \delta, \epsilon, \zeta$ - AlH_3 , each polymorph exhibiting a unique morphology, the α -phase being the thermodynamically stable form at ambient conditions. Nowadays the common way to synthesize pure microcrystalline α - AlH_3 is to perform an ethereal reaction between LiAlH_4 and AlCl_3 followed by desolvation by heating the solution in a mixture of ether and benzene. However this method is time-consuming and not very well adapted for an industrial production. The synthesized α -polymorph is metastable under ambient conditions and only becomes stable at room temperature under pressure ($\sim 0.7 \text{ GPa}$), which means that to keep α - AlH_3 under ambient conditions a thin film is often deposited on its surface.

The crystal structure of α - AlH_3 was determined by Turley and Rinn in 1969 [80]: it crystallizes in the trigonal $R\bar{3}c$ space group with lattice parameters $a=4.449 \text{ \AA}$ and $c=11.804 \text{ \AA}$. As it can be seen in figure 8.1a its structure consists of corner shared AlH_6 octahedra with each H connecting two octahedra.

Experimentally, the high-pressure behaviour of α - AlH_3 remained relatively unknown up until very recently. In 2008, Goncharenko *et al.* published the first major study on alane under pressure [81], motivated by the recent predictions of a possible high-temperature superconductivity in hydrides by Ashcroft [26]. By compressing α - AlH_3 in hydrogen medium in a diamond anvil cell and using X-ray diffraction they identified two phase transitions. The first one takes place at 63 GPa towards a new phase that could not be clearly identified, yet the new structure was indexed by a triclinic symmetry, space group $P1$. Upon further compression, this intermediate phase transforms at 100 GPa into a new cubic phase with

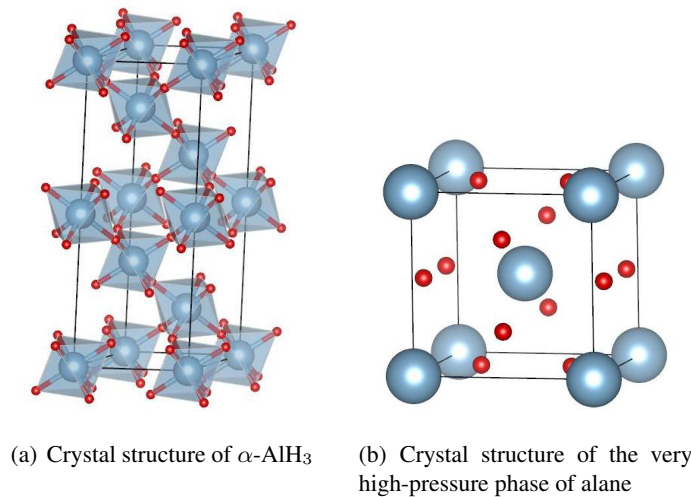


Figure 8.1: Structures of two AlH₃ polymorphs. Al atoms are represented in blue, H atoms in red.

the symmetry $Pm\bar{3}n$ with a lattice parameter $a=3.08 \text{ \AA}$, represented in figure 8.1b, and theoretically predicted a few months earlier by Pickard and Needs [82]. Interestingly the H-H distance in this structure is the shortest ever reported in an hydride, except for the H₂ molecule. *Ab initio* calculations performed in the study by Goncharenko *et al.* predicted that this phase should be metallic and should exhibit a high-temperature superconductivity of $T_c \sim 24 \text{ K}$ at 110 GPa. The metallic character of the cubic phase was confirmed in the same study by resistive measurements under pressure on a powder of alane but the superconductivity was not observed down to 4 K and up to 160 GPa [81]. A tentative explanation of this discrepancy between theory and experiment on high-temperature superconductivity was proposed by Rousseau *et al.* [83]: anharmonicity effects, not taken into account in the previous calculations, drastically affect superconductivity lowering it down to $\sim 2 \text{ K}$ at 110 GPa, which could explain why it was not observed. Islam *et al.* in another study also showed that these anharmonic effects could be reduced by lowering the pressure which would in turn lead to an increase of the temperature of superconductivity, up to 37 K at 70 GPa [24].

The first Raman study under pressure was published in 2008 [84]. The four Raman active modes predicted by the point group theory could be observed up to 16.9 GPa. A second Raman study was performed in 2010 up to 30.3 GPa, along with absorption measurements [85]. The conclusions of this study were in contradiction with the results from Goncharenko *et al.* as they measured an indirect gap of 1.0 eV at 50 GPa, expected to close around 60 GPa, *i.e.* AlH₃ should become metallic at much lower pressure than the one previously measured.

Aluminum hydride also received a lot of attention from Density Functional Theory (DFT) calculations. Such calculations aim to predict the sequence of structural phase transitions under pressure and to determine the physical properties of the different stable phases obtained. Two independent studies, by Pickard and Needs [82] and by Vajeeston *et al.* [86], both predicted two structural phase transitions under pressure with the metallic cubic structure being the most stable phase at high pressure. However two different structures are proposed for the intermediate phase: Pickard and Needs found a layered orthorhombic structure (space group $Pnma$) while Vajeeston *et al.* proposed an hexagonal structure (space group $P6_3/m$). The technique used in the two studies to determine these structures was different. In the first one Pickard and Needs used the "random searching" technique: a set of initial structures is created by

choosing random unit cells. Each of these structures is then relaxed to a minimum in the enthalpy at fixed pressure until the most stable ones are obtained several times. On the contrary Vajeeston *et al.* chose 58 potentially applicable structure types by analogy with other known compounds and compared their Gibbs free energies over a large pressure range.

A lot of DFT calculations also focused on the high pressure cubic phase. Kim *et al.* showed that this metallic phase is both mechanically and dynamically stable down to 72 GPa [87]. A recent study by Gurtabay *et al.* also showed the dominant role of hydrogen in this phase: cubic AlH_3 should be equivalent to an hydrogen sub-lattice weakly perturbed by Al atoms [88]. Such a description of the cubic AlH_3 revealed the existence of a low-energy plasmon, inducing an abrupt decrease of the reflexivity around 1 eV.

In this context, a lot of questions remained unanswered, namely:

- The influence of impurities: our laboratory got freshly synthesized pure AlH_3 powder at the start of this Ph.D. thesis, provided by the Université of Poitiers. No thin film was deposited on this powder, unlike the samples used by Goncharenko *et al.* [81], and it was conserved under an inert atmosphere of argon. Such samples were a real opportunity as the chemical synthesis of a high-purity powder is complicated and time-consuming. Moreover it would allow us to test for the possible influence of this thin film on the high-pressure behaviour of AlH_3 .
- Following the previous point: can AlH_3 be easily synthesized from its constituents under pressure?
- The influence of non-hydrostatic stresses: in their high-pressure study Goncharenko *et al.* used hydrogen as a pressure transmitting medium. Could it have an influence on the compound, slightly modifying its high-pressure behaviour or the stoichiometry for instance?
- The previous question leads to another one: is AlH_3 the most stable stoichiometry under pressure?
- What is the structure of the intermediate phase and can it be identified with a structure predicted by DFT calculations [82, 86]?
- A discrepancy between the resistivity measurements and the results of absorption of visible light on the pressure of metallization of alane remains. Another technique is required to determine the pressure of metallization and to determine if this metallization is induced by a progressive gap closure under pressure or by a phase transition.
- The stability of the cubic phase needs to be studied as it is predicted to be metastable down to 72 GPa which would be particularly interesting to study the influence of the anharmonic effects on the superconductivity.
- Can the predominant role of hydrogen in the cubic phase proposed by Gurtabay *et al.* be experimentally observed?

A systematic study was therefore performed on aluminum hydride by means of X-ray diffraction, synchrotron infra-red spectroscopy and Raman spectroscopy, covering the pressure range [0-120 GPa]. X-ray diffraction results confirmed the sequence of phase transitions observed in the precedent study by Goncharenko *et al.* and revealed that the intermediate was very poorly crystallized, explaining the previous difficulties to determine its structure. After a slight laser heating this phase recrystallizes and the symmetry of this structure is monoclinic, space group $P2_1/c$. This structure was not predicted by DFT calculations. Using X-ray diffraction we also confirmed that AlH_3 is the most stable stoichiometry and

that it can easily synthesized by laser heating an aluminum foil in hydrogen medium above 10 GPa. The metallic phase, appearing above 100 GPa, was found to be metastable down to 40 GPa which should be very encouraging for future measurements of superconductivity. Raman spectroscopy was extended up to 90 GPa. Infrared spectroscopy confirmed the metallic character of the cubic phase and revealed that the metallization is induced by the phase transition and not by a progressive band gap closure. Moreover this technique allowed us to observe an abrupt decrease in reflexivity at 1.15 eV in good agreement with the value of 1 eV predicted by Gurtabay *et al.* when considering the metallic phase as a weakly perturbed hydrogen sub-lattice.

These results have submitted to the journal *Physical Review B* in an article entitled "*Structural, vibrational and electronic properties of AlH₃ up to 120 GPa*" and attached in the following pages.

8.2 Article: "Structural, vibrational and electronic properties of AlH₃ up to 120 GPa"

Structural, vibrational and electronic properties of AlH_3 up to 120 GPa

Charles M. Pépin¹ and Paul Dumas² and Michael Hanfland³ and Paul Loubeyre^{1*}

¹*Dpartement de Physique Throrique et Applique,
CEA/DAM/DIF, F-91680 Bruyres-le-Chtel, France*

²*Synchrotron SOLEIL, BP48, F-91192 Gif-sur-Yvette, France and*

³*European Synchrotron radiation Facility (ESRF), BP22, F-38043 Grenoble, France*

(Dated: July 2, 2015)

A complete study of AlH_3 was realized using x-ray diffraction and infrared spectroscopy in the pressure range 0-120 GPa and by means of Raman scattering up to 60 GPa. At $P \sim 64$ GPa $\alpha\text{-AlH}_3$ undergoes a structural transition resulting in a poorly crystalized phase of lower symmetry and exhibiting a very strong ionic character. This phase was found to be monoclinic of space group $P2/m$ and when recrystallized by laser heating it was well described with a monoclinic cell of space group $P2_1/c$. A second transition to a metallic cubic phase was observed at 107 GPa. The infrared spectroscopy revealed no progressive gap closure with the pressure in the intermediate monoclinic phase, meaning that metallization is induced by the phase transition.

I. INTRODUCTION

Considerable interest for the hydrides arose in the past few years due to their very large hydrogen content (10.1wt.% for AlH_3 for instance) which makes them a promising hydrogen and energy storage material. For example AlH_3 , also called alane, already has many applications: it can be used as a solid rocket propellant, as an explosive or as an hydrogen source for portable devices. On the other hand a recent suggestion by N.Ashcroft¹ renewed the interest for hydrides under pressure. In fact it was suggested that "covalent-bonded hydrogen-rich materials" could exhibit features similar to those of metallic hydrogen. Metallic hydrogen is predicted to be a high-temperature superconductor^{2,3} and to exhibit a new state of matter which has not yet been observed in any other system⁴⁻⁶. However metallization of pure hydrogen appears to require a pressure greater than 400 GPa^{4,7} which remains beyond the reach of high pressure devices. On the contrary covalent hydrides being very compressible the application of pressure should induce a progressive overlap of electronic bands and finally the metallization at sufficiently high pressure but still easily attainable with the current pressure devices. Among those covalent hydrides AlH_3 quickly became a reference as Goncharenko *et al.*⁸ recently achieved metallization of alane at the predicted pressure of 100 GPa⁹ proving the viability of this theory.

Six metastable polymorphs of AlH_3 have been identified¹⁰, the α -phase being the most stable one under ambient conditions. $\alpha\text{-AlH}_3$ is rhombohedral of space group $R\bar{3}c$ with Al in 2b (000) and H in 6e (x, -x+1/2, 1/4) (x=0,878)¹¹. The behavior of alane under pressure was studied using DFT calculations and reported two structural transitions^{9,12}. Ref. [9] predicted a first transition at $P \sim 34$ GPa to a $Pnma$ structure whereas Ref. [12] predicted a transition at $P \sim 64$ GPa to a $P6_3/m$ structure. Both studies predicted a second transition resulting in a cubic $Pm\bar{3}n$ metallic phase taking place at $P \sim 73$ GPa in Ref. [9] and at $P \sim 104$ GPa in Ref. [12]. Goncharenko *et al.* observed two structural

transitions by X-Ray diffraction⁸: above 63 GPa alane transforms into a low-symmetry structure, described as a trigonal insulating phase (space group $P1$, $a=3.83\text{\AA}$, $b=5.12\text{\AA}$, $c=6.72\text{\AA}$, $\alpha=112.6^\circ$, $\beta=111.9^\circ$, $\gamma=56.6^\circ$), and above 100 GPa this trigonal unit cell transforms into a metallic phase with the predicted structure of space group $Pm\bar{3}n$ ($a=3.08\text{\AA}$). This high-pressure phase was predicted to be superconductive but no superconductivity was observed down to 4K and up to 165 GPa. Studying AlD_3 , Besedin *et al.* were recently able to stimulate by laser irradiation a new structural phase transition at $P \sim 53$ GPa¹³. The new high-pressure phase was described as a lattice of Al atoms with a monoclinic unit cell (space group $P2_1/c$, Al in 4e(0.288, 0.358, 0.020), $a=6.292\text{\AA}$, $b=4.074\text{\AA}$, $c=8.789\text{\AA}$, $\beta=160.46^\circ$) and was reported to be metastable down to $P \sim 35$ GPa. As some discrepancies between the theoretical and the experimental published studies still remain and knowing that a clear understanding of the evolution of alane under pressure is very important to act as a model for other hydrides but is still lacking, we undertook a new systematic study in which the behavior of $\alpha\text{-AlH}_3$ under pressure is being investigated by means of Raman scattering, Infrared (IR) absorption and X-Ray diffraction. Considering our results we propose a slightly revised equation of state (EOS). The intermediate insulating phase appearing between 63 and 107 GPa was found to be monoclinic of space group $P2/m$. In addition we show that each phase transition is accompanied by an evolution in bonding: alane undergoes a covalent to ionic bonding transition at 63 GPa followed at 107 GPa by a ionic to metallic bonding transition, confirming the electrical measurements from Ref. [8]. Interestingly the intermediate phase we propose is close to the one induced by laser irradiation by Besedin *et al.* on AlD_3 . We were also able to reproduce this phase transition on AlH_3 using infrared laser heating. X-ray diffraction allowed us to characterize this phase. It was found to be monoclinic of space group $P2_1/c$ with aluminum atoms in general positions 4e (x,y,z), close to what was found for AlD_3 .

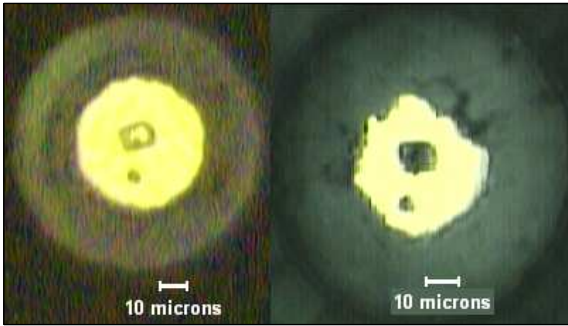


FIG. 1. Left: Single crystal of AlH_3 loaded in neon at 8 GPa. The samarium used as pressure scale is seen below the sample. Right: the same sample at 120 GPa, showing its complete blackening.

II. EXPERIMENTS

The samples of high-purity were synthesized by the Universit of Poitiers only a few months before the experiment¹⁴. The samples were checked by x-ray diffraction and showed no sign of contaminant phases.

X-Ray diffraction. To determine the EOS high pressure was generated using a diamond-anvil cell (DAC) with culets of $100 \mu\text{m}$ and a gasket made of rhenium preindented to $22 \mu\text{m}$ and drilled with a hole of $70 \mu\text{m}$. A single crystal of the freshly synthesized $\alpha\text{-AlH}_3$ with $\sim 8 \mu\text{m}$ was then placed in the center of the hole. Neon was used as a pressure transmitting medium. The pressure was measured using the samarium fluorescence¹⁵. Figure 1 gives a view of the sample used for the EOS of the α -phase.

A DAC loaded with powder was used to determine the structure from section III B. In this case the gasket had been coated with 800\AA of gold to ensure the confinement of hydrogen if dehydrogenation would happen.

Diamond anvil cells with single-crystals of $\alpha\text{-AlH}_3$ and Al loaded with hydrogen as pressure medium were used to search for the most stable phases of alane under pressure and to look for possible new stoichiometries. Confinement of the hydrogen was ensured by a gold coating of the gasket and LiF was used as a thermal insulator on each diamond. These DACs were also characterized by means of Raman spectroscopy.

The x-ray diffraction experiments were performed at beamline ID9A of the European Synchrotron Radiation Facility (ESRF) using wavelength of 0.41404\AA .

Raman spectroscopy. Raman spectroscopy was performed in DACs with culets of $300 \mu\text{m}$ and gaskets made of rhenium. Single crystals were placed at the center of the culets and neon was used as a pressure transmitting medium. Pressure was measured by the ruby-fluorescent technique¹⁶. Raman was measured with 6mW of the 647.1nm radiation of an Ar-Kr laser. Exposure time var-

ied between 30 and 70 seconds at low and high pressure respectively.

Infrared spectroscopy. High pressure generated using a DAC equipped with synthetic CVD diamond anvils with culets of $70 \mu\text{m}$ and a gasket made of rhenium preindented to $13 \mu\text{m}$ and drilled with a hole of $31 \mu\text{m}$. Measurements were made on a powder of selected crystals with no pressure medium. Pressure was determined using the Raman shift of the A_{1g} mode of $\alpha\text{-AlH}_3$ up to 59 GPa and from Raman shift of the high-frequency edge of the stressed diamond at higher pressure.

Infrared (IR) experiments were carried out at the SMIS beamline of the SOLEIL synchrotron, using a custom-made horizontal infrared microscope for large volume samples, equipped with two Schwarzschild objectives (47mm working distance, NA 0.5) that produces a $22 \mu\text{m}$ (FWHM) IR spot.

III. STRUCTURAL EVOLUTION UNDER PRESSURE

A. Cold-compression of pure $\alpha\text{-AlH}_3$

At low pressure our results are in good agreement with the ones reported by Goncharenko *et al.*⁸ (see Fig. 2). The proposed space group $R\bar{3}c$ (phase I) was clearly identified up to 63 GPa. In table I a summary of the results found in the literature is presented. Our results are close to what had been proposed in other experimental studies. However a large difference is observed between our results and the values proposed in the theoretical study of Ref. [12].

Upon increasing pressure the monoclinic distortion corresponding to a small deviation of the Bragg peaks from the calculated positions of the $R\bar{3}c$ space group and proposed by Ref. [8] and [19] was also observed on our single-crystal. At 63 GPa the first transition occurred - this transition occurred at the same pressure when using a single-crystal with neon as a pressure medium or powder without pressure medium, meaning that it is independent of the compression conditions. As it can be seen in the inset of figure 2 this transition appears when the c/a ratio in phase I begins to saturate. We observed that the low pressure phase and the new phase (phase II) coexist on a few GPa and that the maximum distortion appeared along the plane (AB) in the hexagonal axes. On the contrary very little distortion appears along the plane (AC) (see fig.3B). Moreover we can conclude that this first transition is displacive with a $\frac{\Delta V}{V}$ of -8.5% .

In Ref. [8] phase II was described in a trigonal unit cell (space group $P1$) with 6 formula units, but it was also suggested that the real symmetry might be lower due to difficulties to resolve the structure. On the other hand theoretical calculations using random structure searching from Pickard *et al.*⁹ and Vajeeston *et al.*¹² predicted structure with higher symmetry (space group $Pnma$ and $P6_3/m$ respectively). We tested all three proposed solu-

TABLE I. Parameters of the Murnaghan-Birch and Vinet¹⁷ fits from our data compared with the results from other references.

| V_0 ($\text{\AA}^3/\text{at}$) | K_0 (GPa) | K'_0 | Fit | Reference |
|------------------------------------|-------------|---------|------------|-----------|
| 33.54(2) | 42.28(3) | 3.97(1) | Mur.-Birch | Our data |
| 33.54(fixed) | 40.75(6) | 4.39(1) | Vinet | Our data |
| 33.5(1) | 42.3(5) | 3.5(1) | Mur.-Birch | [8] |
| | 47.9(1.0) | 3.3(2) | Mur.-Birch | [18] |
| 34.098 | 37.4(6) | 4.2(16) | Vinet | [13] |
| 33.90(4) | 40(2) | 3.1(2) | Mur.-Birch | [19] |
| 34.43 | 28 | 5.4 | Mur.-Birch | [12] |

tions to find any compatibility with our diffraction plate but none of them was able to reproduce our results. We found that phase II could be described by a monoclinic unit cell of symmetry $P2/m$ with $a=7.891\text{\AA}$, $b=3.335\text{\AA}$, $c=7.805\text{\AA}$, $\alpha=90^\circ$, $\beta=160.38^\circ$ and $\gamma=90^\circ$. However because of the very low signal to noise the full structure determination was not possible and the positions of the aluminum atoms could not be determined. Furthermore it appeared that this phase was very poorly crystallized which is confirmed by the measurement of the Full Width at Half Maximum (FWHM) as a function of pressure shown in figure 4: peaks were very broad and much less well-resolved than in phases I and III.

Upon compression we observed a new phase transition at 107 GPa, which is 7 GPa above the transition observed in Ref. [8], with a $\frac{\Delta V}{V}$ of -4%. This phase (phase III) corresponded to the one proposed in Ref. [8,9,12]: a cubic structure of symmetry $Pm-3n$. At 108 GPa we found $a=3.0866\text{\AA}$ with less than one percent difference between each diffraction peak [110], [200] and [211] meaning that we were able to achieve very good hydrostatic conditions.

B. Stability of the AlH_3 stoichiometry under pressure

As many nontraditional stoichiometries have been predicted for many other hydrides (see for instance Ref. [20],[21]) the stability of the AlH_3 stoichiometry is of prior interest.

To search for new stoichiometries at different pressures we used a laser heating method on samples of aluminum and AlH_3 loaded in hydrogen and AlH_3 loaded in LiF. Confinement of the hydrogen within the gasket hole was ensured by a gold coating and a thin layer of LiF (or a coating of Al_2O_3) was pressed onto each diamond to act as a thermal insulator in order to achieve high temperature and to protect the diamonds. Samples were heated using a YAG laser ($\lambda = 1064\text{nm}$). The resulting samples were then analyzed by means of Raman spectroscopy and x-ray diffraction.

Pressure range 10-30 GPa. When heated in this pressure range in presence of hydrogen aluminum reacted to transform into phase I of $\alpha\text{-AlH}_3$ which we clearly identified by its Raman spectra. When heated once again after the first transformation no other changes were observed.

As well, no changes were noticed when heating AlH_3 with and without hydrogen.

Pressure range 30-100 GPa. When heated above 30 GPa aluminum exhibited a different Raman spectrum than the one from phase I. Figure 7 shows this new Raman spectrum at 67 GPa. As it can be seen the new spectrum exhibits five new well-resolved peaks, which were attributed to a new phase (phase II'). X-ray diffraction measurements were then performed on similar samples for which Raman spectra showed no remaining presence of the phase I meaning that the whole sample had been laser heated and transformed. Diffraction results were analyzed using the FULLPROF software and are shown on figure 5. The calculated structure was found to be monoclinic with space group $P2_1/c$ containing 4 formula units with atoms in position $4e$ (xyz) (see details in table II) with the same volume as Phase II. Interestingly this phase had already been identified by Besedin *et al.*¹³ working on AlD_3 but had been obtained by a different way: the transition was light-induced and no heating had been performed. However our results are quite similar concerning the Raman spectra and the diffraction measurements. A slight difference appeared nevertheless in the parameters of the unit cell: we found that our diffraction pattern was better described with $a>c$. Also Ref. [13] reported the appearance of new weak peaks in their diffraction spectrum at $P=53.2$ GPa that they interpreted as the development of a superstructure by regular displacements of Al atoms. On the contrary we did not observe any other peaks than the ones indexed with our structure meaning that such superstructure was not identified in our results.

On table II we also reported the unit cell found for the phase II'. It has to be noted that these two phases are remarkably similar. Interestingly when heating AlH_3 (in presence of hydrogen or not) the same phase appeared up to 90 GPa. During the heating of AlH_3 in LiF no trace of hydrogen was detected by Raman spectroscopy meaning that no dehydrogenation from the sample was observed. Therefore it can be concluded that AlH_3 should be the most stable stoichiometry in this pressure range.

These results also brought us to another conclusion: the phase II described in section III and this new laser heating induced phase are the same phase. The difference between the two can be explained by the fact that the first one is very poorly crystallized, as we mentioned it

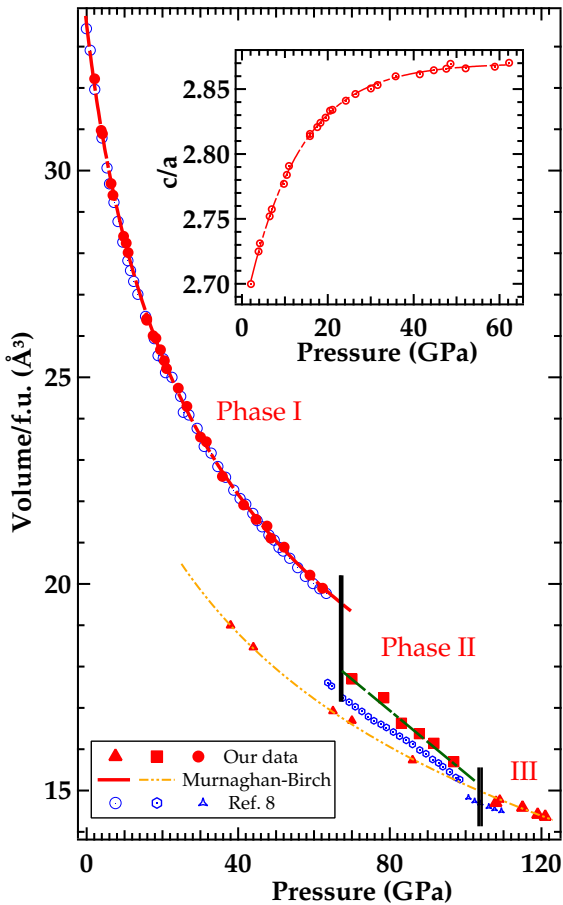


FIG. 2. Volume per formula unit in AlH_3 as a function of pressure. Inset: c/a ratio in phase I as a function of pressure. Experimental points were fitted by the Murnaghan-Birch equation with the following parameters (for comparison results from Ref. [8] are given in square brackets): $V_0=33.54(2)\text{\AA}^3$ [33.5(1)], $B_0=42.28(3)$ GPa [42.3(5)], $B'=3.97(1)$ [3.5(1)], for phase I, $V_0=26.1(2)\text{\AA}^3$ [27.0(5)], $B_0=65.20(1)$ GPa [50.4(10)], $B'=3.81(1)$ [3.5(2)], for phase III.

earlier. When slightly heated phase II finally crystallizes and gives rise to phase II' which is stable in the pressure range 30-100 GPa at least.

Above 100 GPa. A sample of aluminum deposited on 3 grains of $\sim 2\mu\text{m}$ size (picture presented on Fig.6) has been laser heated at 110 GPa. Before heating no spontaneous reaction of aluminum with hydrogen is observed. We only noted a small expansion of the unit cell (\sim) due to a small diffusion of hydrogen inside the aluminum lattice. After laser heating the sample exhibits the characteristic diffraction pattern of the cubic phase III with cell parameters in agreement with those found for pure AlH_3 . On decompression we found this phase to be visible to pressures as low as 36 GPa with onset of decomposition visible by a decrease of the scattering intensity at 44 GPa, al-

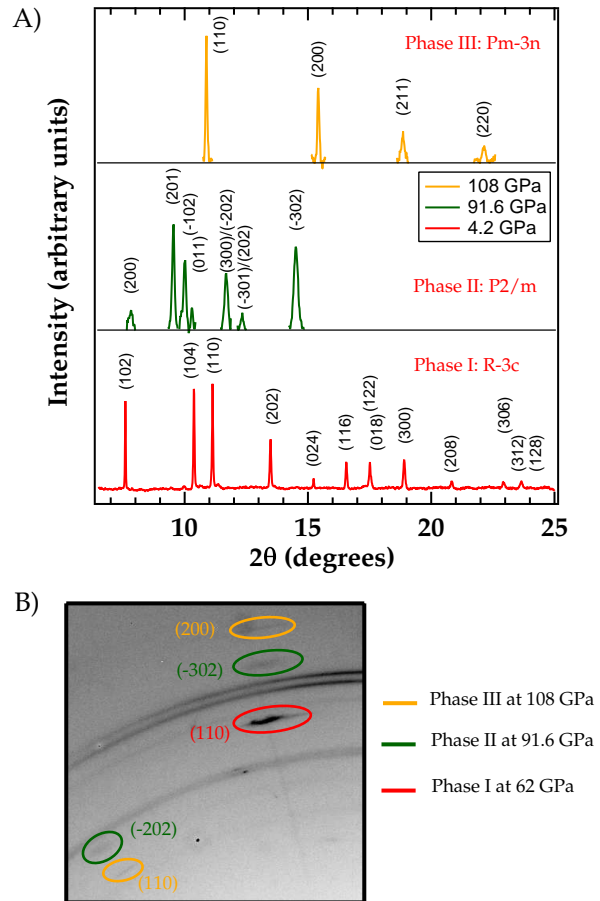


FIG. 3. A) Integrated x-ray diffraction patterns of phases I, II, and III for $\lambda = 0.41404\text{\AA}$. Phase I and II coexisted on a few GPa. Phase II can be described by a monoclinic unit cell of symmetry $P2/m$ with $a=7.891\text{\AA}$, $b=3.335\text{\AA}$, $c=7.805\text{\AA}$, $\alpha=90^\circ$, $\beta=160.38^\circ$ and $\gamma=90^\circ$. B) Addition of image plates at 62, 91.6 and 108 GPa showing the preferred distortion planes.

lowing to refine the equation of state of this phase (fig;2). Interestingly below 36 GPa the sample doesn't transit back to phase I or to fcc-aluminum+hydrogen. On the contrary no diffraction signal from the sample could be observed meaning that below this pressure the sample dissociates giving rise to an amorphous or highly porous phase of aluminum.

IV. SPECTROSCOPIC STUDY AND BONDING CHARACTERIZATION

A. Raman spectroscopy

Raman spectra of the rhombohedral phase of AlH_3 were successfully measured in the wavenumber range 500-

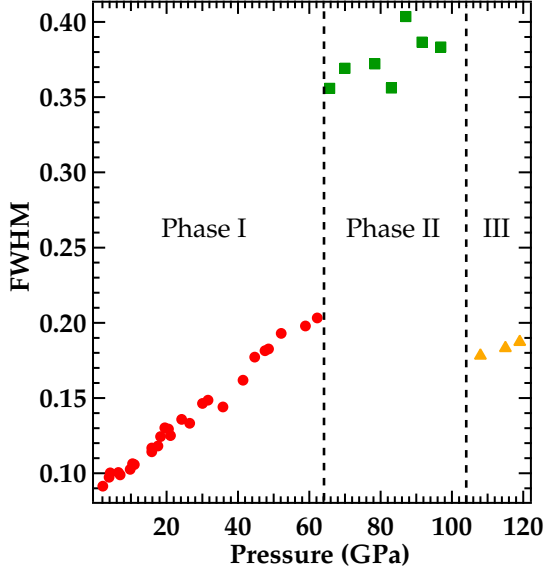


FIG. 4. Full Width at Half Maximum as a function of pressure showing a clear broadening of the peak of Phase II followed by the recrystallization of the sample at 107 GPa. Peaks used to measure the FWHM are [110] for Phase I, [-302] for Phase II, [200] for Phase III, which can be seen on the image plate from figure 3B.

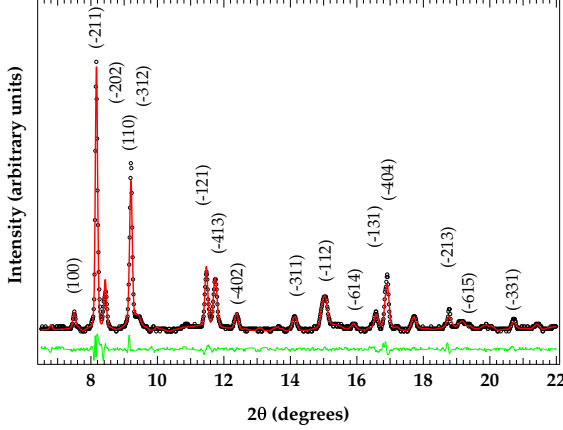


FIG. 5. Phase II' at 70 GPa, black points are the observed diffraction pattern, red solid line is the refined diffraction pattern ($R_F=10.9\%$)

2300 cm^{-1} up to 60 GPa. Fig. 7 shows a typical Raman spectrum at 18.2 GPa. As it is known that alane will decompose quickly with laser irradiation under ambient conditions but is stabilized when pressure is increased we only began to acquire raman spectra above 1 GPa. The point group theory allows us to predict the Raman active modes : knowing that in the α -phase aluminum atoms are in positions C_{3i} and hydrogen atoms in positions C_2

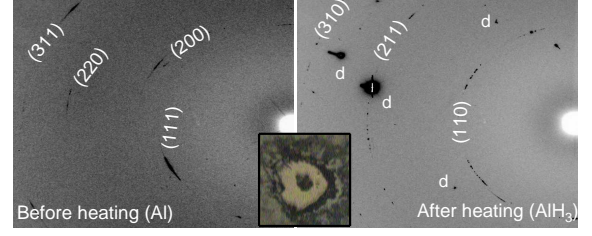


FIG. 6. Diffraction patterns of aluminum at 110 GPa (left) and $\text{AlH}_3\text{-HP}_2$ (right) after laser heating aluminum in presence of hydrogen. Diamond diffraction peaks are labeled d. Middle: picture of the sample of Al in hydrogen medium at 110 GPa before heating.

TABLE II. Comparison of the three structures. The parameters describe phase II' at 70 GPa, the structure from Ref. [13] at 53.2 GPa and Phase II at 69 GPa.

| | Phase II' ($P2_1/c$) Ref. [13] | Phase II ($P2_1/c$) | Phase II ($P2/m$) |
|---------|----------------------------------|-----------------------|---------------------|
| a (Å) | 8.566 | 6.292 | 7.891 |
| b (Å) | 4.021 | 4.074 | 3.335 |
| c (Å) | 6.134 | 8.789 | 7.805 |
| β | 160.42 | 160.46 | 160.38 |
| x | 0.272 | 0.288 | |
| y | 0.383 | 0.358 | |
| z | 0.008 | 0.02 | |

we can express the irreducible representation Γ_{AlH_3} of the factor group D_{3d} as follows :

$$\begin{aligned} \Gamma_{\text{AlH}_3} &= \Gamma_{\text{Al}} + \Gamma_{\text{H}} \\ &= A_{1g} + 3E_g + 2A_{1u} + 5E_u + A_{2g} + 3A_{2u} \end{aligned} \quad (1)$$

Knowing that there are two acoustic modes : $\Gamma_{\text{acous}} = A_{2u} + E_u$, we get:

$$\begin{aligned} \Gamma_{\text{AlH}_3}^{\text{vibr}} &= \Gamma_{\text{AlH}_3} - \Gamma_{\text{acous}} \\ &= A_{1g} + 3E_g + 2A_{1u} + 4E_u + A_{2g} + 2A_{2u} \end{aligned} \quad (2)$$

The character table of factor group D_{3d} then lets us know that there only 4 Raman active modes: 1 symmetric mode A_{1g} and 3 doubly degenerate modes E_g , and 6 IR active modes: 2 modes A_{2u} and 4 modes E_u . The remaining modes are silent. Let us remark that Ref. [22] reported five modes which is in contradiction with the point group theory . On our Raman spectra, as it can be seen on figure 7, we only observed the four predicted modes which were well-resolved and were indexed using Ref. [23] and Ref. [24]. Our results at low pressure are in very good agreement with those obtained in Ref. [22] and all four modes exhibit positive pressure shifts in frequency (Fig.8). At $P \sim 25$ GPa two modes merge together because of their different pressure shift rate and the E_g mode do not reappear until the phase transition.

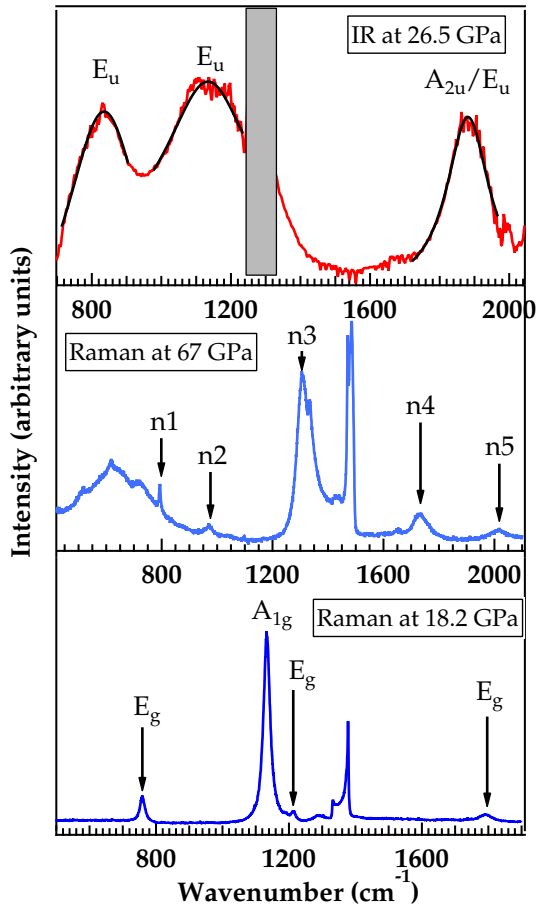


FIG. 7. Bottom: Raman spectrum of AlH_3 at 18.2 GPa showing the four observable modes. Middle: Raman spectrum of phase II after laser heating in presence of hydrogen at 67 GPa. Top: Infrared spectrum of Phase I at 26.5 GPa.

B. Infrared spectroscopy

Although $\alpha\text{-AlH}_3$ has been well studied experimentally only one study reported infrared spectroscopy results under pressure up to 25.4 GPa²⁵. An extended study of the compound under high pressure was therefore needed to improve our understanding of the bonding behavior of this archetypal hydride. As it has been shown in Sec.(IV A) alane exhibits six IR active modes, 2 modes A_{2u} and 4 modes E_u , however our spectral resolution and the relatively important thickness of our sample only permitted us to clearly identify three modes (see Fig.7).

Those three absorption bands were successfully monitored up to 50 GPa and the pressure shifts in frequency are shown in figure 10.

On this figure are also reported the points from Ref. [25]. We are in relative good agreement with these

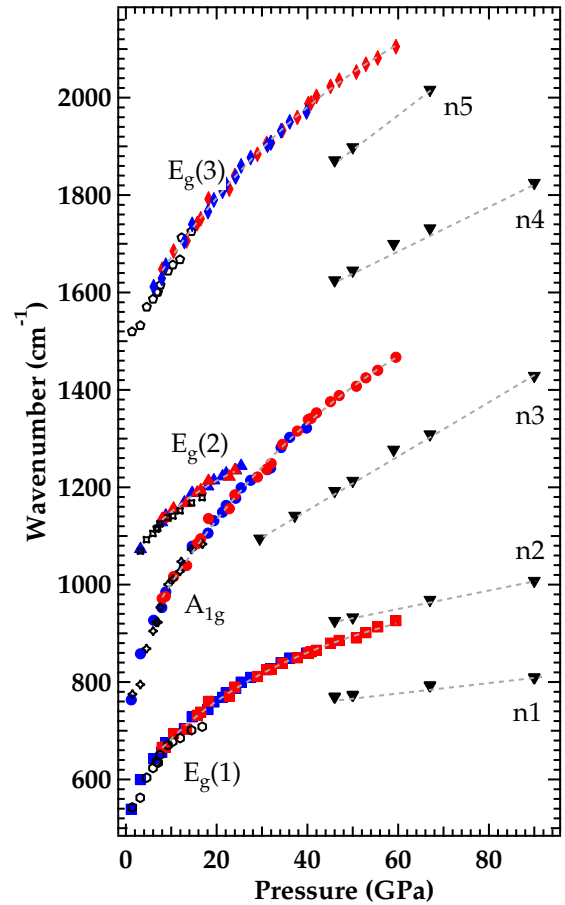


FIG. 8. Pressure dependance of Raman wavenumbers of alane upon compression. Empty symbols depict data obtained by Tkaz *et al.*²² (only the four modes in agreement with Ref. [23] were reported). Blue symbols correspond to the first run, red symbols to the second run. Black symbols correspond to the new phase II'

points, even if we were not able to identify the vibrational band at 1865 cm^{-1} . In agreement with our Raman and x-ray diffraction results, no changes are noticeable until $P \sim 59\text{ GPa}$. At this pressure changes in the IR spectrum occurred, as it is shown in figure 9: the sample exhibited a complete absorption in the wavenumber range $650\text{-}2300\text{ cm}^{-1}$.

A second transition was then observed between 111 and 115 GPa (Fig.11), corresponding to the structural transition Phase II \rightarrow Phase III identified by x-ray diffraction.

C. Discussion

A recent study²⁶ extended the Raman spectroscopy up to 30.3 GPa and reported an abrupt decrease in Ra-

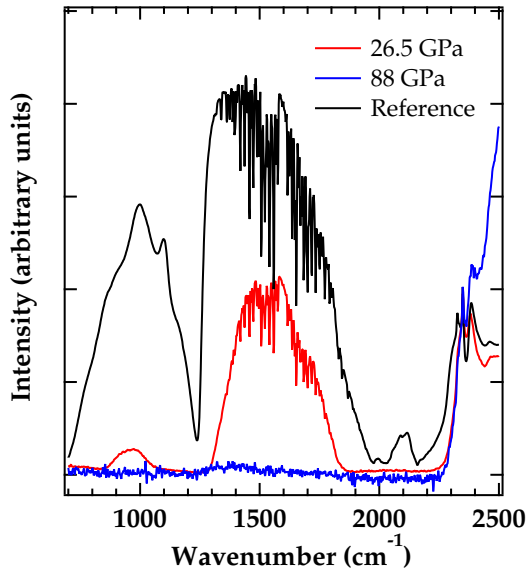


FIG. 9. Characteristic IR spectra of alane between 700 and 2500 cm^{-1} for phase I and II. The broad absorption band revealing the ionic character of phase II can be seen between 650 and 2300 cm^{-1} . The reference intensity has been recorded with the empty cell. Inset: Optical density of AlH_3 as a function of wavenumber. The black lines on the bottom-spectrum are fits of the absorption bands. Grey rectangles are used to mask the absorption due to the diamond.

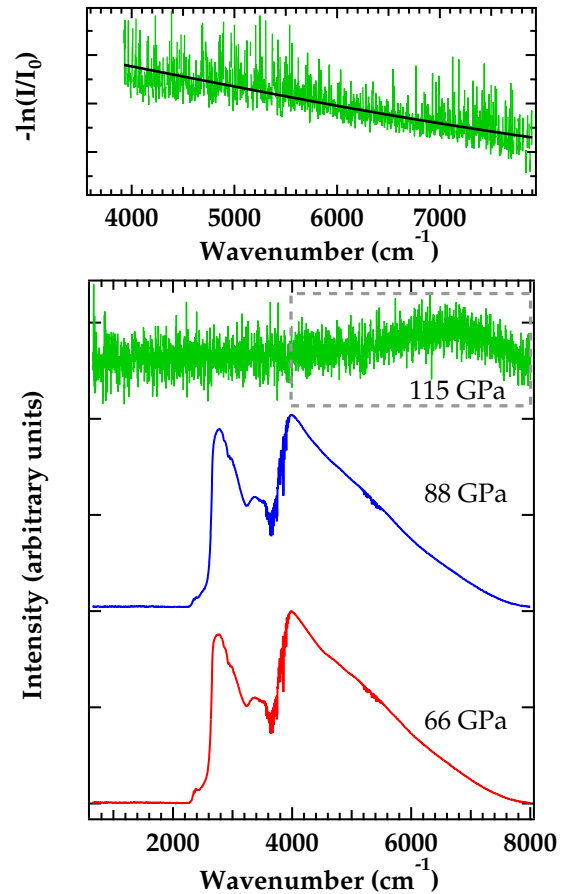


FIG. 11. IR spectra of phase II at 66 and 88 GPa and of phase III at 115 GPa showing that no progressive gap closure is observed under pressure. Upper graph: optical density of metallic AlH_3 corresponding to the grey framed part at 115 GPa. The black line is the fit from eq.3.

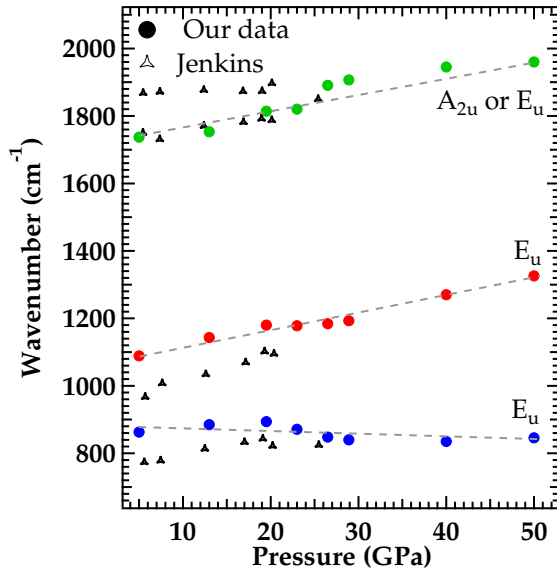


FIG. 10. Pressure dependence of Infrared absorptions peaks upon compression. The dashed grey lines are shown as guides for the eyes. Peaks were tentatively indexed using Ref. [23]

man intensity at this pressure which they attributed to a change in the structure. We did not observe any significant decrease in Raman intensity up to 60 GPa, suggesting that no phase transition is occurring below this pressure which is in agreement with our x-ray diffraction results. Above 60 GPa, when the first transition occurs, no Raman signal due to the sample was identified. However at this pressure we observed a loss in transparency of the sample (but no complete blackening) which we believe to be responsible for the loss of Raman signal. Raman and IR spectroscopy are closely related and present complementary results and one expects to observe a similar peak shift in both cases. However as it can be seen on figures 8 and 10 it is not the case for AlH_3 . We were not able to find a valid explanation for this difference in peak shift and additional work is needed to clarify this phenomenon. Interestingly the peaks of the Phase II' labelled n3, n4 and n5 show a very similar rate

of peak shift, whereas the peaks n1 and n2 exhibit a rate closer to the one observed in Infrared.

IR spectroscopy also allow us to deduce many information on the bonding behavior of the compound. The drastic changes in IR spectrum observed around 60 GPa on figure 9 is characteristic of ionic-bonded materials: absorption bands are very broad and merge together resulting in an unique very large absorption band. Therefore we can conclude that the transition Phase I \rightarrow Phase II is also accompanied with a change in bonding: the sample undergoes a covalent to ionic bonding transition. This result is then confirmed by the Raman spectra of the recrystallized Phase II: the peak frequencies are lower than in Phase I (see figure 8) which means that the bonds are weaker which agrees with the ionic character of this phase.

Finally the IR spectroscopy allowed the first confirmation of the electrical measurements realized in Ref. [8]. Indeed the spectrum from Phase III is a typical signal from a metallic sample. Complete blackening of the sample was observed at this pressure. We have interpreted this IR absorption data from figure 11 using a free electron Drude model. The absorption coefficient α can be expressed as:

$$\alpha(\omega) = \frac{\omega_p^2 \tau}{nc(1 + \omega_p^2 \tau^2)} \quad (3)$$

where ω_p is the plasma frequency, τ is the electron scattering relaxation time, n is the refractive index and c the speed of light in vacuum. α is experimentally given by:

$$\alpha(\omega) = -\frac{1}{d} \ln\left(\frac{I}{I_0}\right) \quad (4)$$

where d stands for the sample thickness. Assuming that $\tau = 4 * 10^{-15}$ s and that $d = 6 \mu\text{m}$ we were able to determine a plasma frequency $\omega_p = 1.15$ eV and a refractive index $n = 1.52$. This interpretation is admittedly only tentative knowing that a Drude model is better suited for simple metals, unlike AlH_3 . However this interpretation gives a first result which is very close to the value of 0.9 eV that has been calculated by Gurtubay *et al*²⁷ and thus confirm the existence of a low-plasmon at ~ 1 eV. Our results also add a new comprehension of the metallization mechanism of alane under pressure: as it can be seen on figure 11 metallization is not caused by a progressive gap closure like it is often the case under pressure, on the contrary here metallization is induced by the phase transition.

This IR study of $\alpha\text{-AlH}_3$ showed complementary results to the diffraction study allowing us to analyze the bonding behavior of the compound under pressure: each structural transition is accompanied by a modification in bonding, changing from mainly covalent to ionic first and then from ionic to metallic.

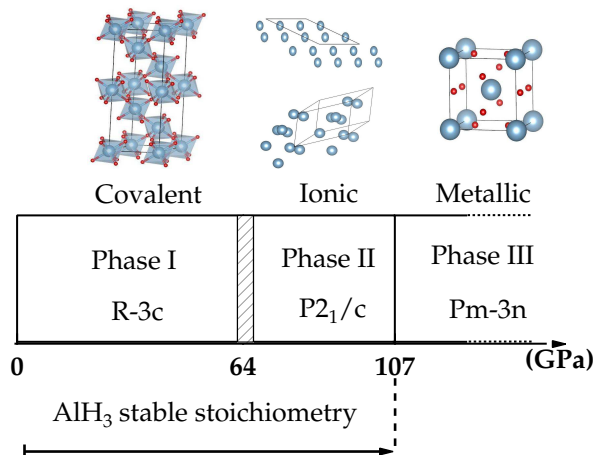


FIG. 12. Proposed phase diagram of AlH_3 at room temperature. Representations of the unit cells were visualized using VESTA²⁸. Aluminum atoms are shown in blue and hydrogen atoms in red. Phase II is shown on top along the b axis.

V. CONCLUSION

A new equation of state of the trivalent aluminum hydride has been proposed. Our measurements revealed that the intermediate phase II is a very poorly crystallized phase which could be better described when recrystallized. It was found to be monoclinic of space group $P2_1/c$ and to be stable in the pressure range 30-100 GPa at least. The difficulties encountered by phase II to crystallize could explain why the theoretical calculations failed to accurately describe it up to now. We also confirmed that in the pressure range 0-100 GPa the most stable stoichiometry of the Al-H system is AlH_3 . However additional work is now needed to search for new stoichiometries above 110 GPa, when alane is metallic. A conclusive phase diagram summarizing our results is shown in figure 12.

The bonding behavior of alane under pressure appeared to be related to its structural evolution: each phase transition is accompanied by a change in bonding. Firstly covalent the bonding then transforms to ionic and finally to metallic. Interestingly the metallic state is not the result of a progressive gap closure with pressure but is due to a phase transition. This means that all phase transitions must have been predicted and well studied when theoretically looking for a metallic state in hydrides.

Hydrogen-dominant alloys being predicted to be high-temperature superconductors AlH_3 appears to be a possible candidate as it metallizes at relatively low pressure (~ 100 GPa). Goncharenko *et al.* did not observe superconductivity down to 4 K at 120 GPa despite a predicted critical temperature of 24 K, pointing out that superconductivity could be hindered by other phenomena not taken into account at the time. It was later shown that anharmonicity effects had to be considered and the

recalculated temperature of superconductivity was then largely reduced, as low as 2 K at 110 GPa²⁹. Moreover two other studies, Ref. [30] and [31], showed that the cubic phase III should be dynamically stable upon decompression down to ~ 70 GPa and Ref. [31] also found a temperature of superconductivity of 2 K at 110 GPa, but more surprisingly they found that the critical temperature should increase upon decompression, up to 37 K at 70 GPa which is even higher than the first estimated temperature of 24 K at 100 GPa. In our study we

have confirmed the existence of a large metastability for phase III down to ~ 45 GPa. This result suggests that the question of whether phase III is a high-temperature superconductor upon decompression could now be answered by experiment.

VI. ACKNOWLEDGMENTS

Authors are grateful to ...

* pepin.charles@cea.fr

¹ N. Ashcroft, PRL **92**, 187002 (2004).

² N. Ashcroft, PRL **21**, 1748 (1968).

³ C. Richardson and N. Ashcroft, PRL **78**, 118 (1997).

⁴ S. Bonev, E. Schwegler, T. Ogitsu, and G. Galli, Nature **431**, 669 (2008).

⁵ N. Ashcroft, J. PHYS.: Condens. Matter **12**, A129 (2000).

⁶ E. Babaev, A. Sudbø, and N. Ashcroft, Nature **431**, 666 (2004).

⁷ P. Loubeyre, F. Occelli, and R. LeToullec, Nature **416**, 613 (2002).

⁸ I. Goncharenko, M. Eremets, M. Hanfland, J. Tse, M. Amboage, Y. Yao, and I. Trojan, PRL **100**, 045504 (2008).

⁹ C. Pickard and R. Needs, Phys. Rev. B **76**, 144114 (2007).

¹⁰ F. Brower, N. Matzek, P. Reigler, H. Rinn, C. Roberts, D. Schmidt, J. Snover, and K. Terada, J. Am. Chem. Soc. **98**, 2450 (1976).

¹¹ J. Turley and H. Rinn, Inorg. Chem. **8**, 18 (1969).

¹² P. Vajeeston, P. Ravindran, and H. Fjellvåg, Chem. Mater. **20**, 5997 (2008).

¹³ S. Besedin, A. Jephcoat, and A. Irodova, Phys. Rev. B **84**, 104111 (2011).

¹⁴ W. Cong, PhD thesis (2011).

¹⁵ F. datchi, R. LeToullec, and P. Loubeyre, J. Appl. Phys. **81**, 3332143 (1997).

¹⁶ H. Mao, J. Xu, and P. Bell, J. Geophys. Res. **91**, 4673 (1986).

¹⁷ P. Vinet, J. Ferrante, J. Smith, and J. Rose, J. Phys. C **19**, L467 (1987).

¹⁸ B. Baranowski, H. Hochheimer, K. Strssner, and W. Hnle, J. Less-Common Met. **113**, 341 (1985).

¹⁹ J. Graetz and J. Reilly, J. Alloys Compd. **424**, 262 (2006).

²⁰ E. Zurek, R. Hoffmann, N. Ashcroft, A. Oganov, and A. Lyakhov, PNAS **106**, 17640 (2009).

²¹ P. Zaleski-Ejgierd, V. Labet, T. Strobel, R. Hoffmann, and N. Ashcroft, J. Phys.: Condens. Matter **24**, 155701 (2012).

²² M. Tkacz, T. Palasyuk, J. Graetz, and S. Saxena, J. Raman Spectrosc. **39**, 922 (2008).

²³ C. Wolverton, V. Ozolins, and M. Asta, Phys. Rev. B **69**, 144109 (2004).

²⁴ P. Vajeeston, P. Ravindran, and H. Fjellvåg, J. Phys. Chem. A **115**, 10708 (2011).

²⁵ J. Ciezak-Jenkins, Army Research Laboratory (2011).

²⁶ N. Shimura, T. Takeichi, T. Kume, S. Sasaki, H. Shimizu, A. Ohmura, K. Ikeda, Y. Nakamori, and S. Orimo, J. of Phys.: Conf. Series **215**, 012047 (2010).

²⁷ I. Gurtubay, B. Rousseau, and A. Bergara, Phys. Rev. B **82**, 085113 (2010).

²⁸ K. Momma and F. Izumi, J. Appl. Crystallogr. **44**, 1272 (2011).

²⁹ B. Rousseau and A. Bergara, Phys. Rev. B **82**, 104504 (2010).

³⁰ D. Kim, R. Scheider, and R. Ahuja, Phys. Rev. B **78**, 100102 (2008).

³¹ A. Islam, M. Ali, and M. Ali, Physica C **470**, 403 (2010).

Chapter 9

Beryllium Hydride BeH₂

9.1 Introduction

Just like aluminum hydride, beryllium hydride BeH₂ has a unique set of physical properties which presents promising technological interest: made of low atomic mass constituents, a very large hydrogen content (18.28 wt. %), high calorific power and the lowest capture cross-section for thermal neutron by beryllium. These properties explain the early interest for this compound back to 1933, despite the toxic character of beryllium oxide.

The very first reported synthesis of beryllium hydride dates from 1933 [89]. It had been obtained by heating pristine beryllium between 170 and 260 °C in hydrogen medium during 7 hours. However the results could not be successfully reproduced by other teams and this synthesis method was quickly abandoned. Complex multi-stage processes involving the thermal decomposition of organoberyllium compounds then followed this first attempt to synthesize beryllium hydride, see for example [90] and [91]. While these synthesis methods can be reproduced they face two major issues: (i) the obtained material has a BeH₂ content of only 50 - 70 wt. %, *i.e.* it is highly impure and (ii) most of the time the synthesized product is an amorphous polymeric solid containing hydrogen bridged BeH₂Be groups. Recent neutron diffraction measurements indicate that this amorphous compound is composed of corner-sharing BeH₄ tetrahedra [92], [93].

A large improvement came from the use of pressure during the synthesis process. In 1978 the use of a piston-mold unit generating pressures up to 6.2 kbar combined with temperatures up to 200 °C allowed to synthesize crystalline beryllium hydride for the first time with a purity of 94.1 wt. % [94]. In that study two crystalline phases are identified: a first one at low temperature, which could not be resolved, and a second one appearing at higher temperature. This structure has an hexagonal symmetry with the following cell parameters: $a=4.20 \text{ \AA}$, $c=6.76 \text{ \AA}$ and $Z=4$. In 1992 this synthesis method was used by Konovalov and Bulychev in order to study the $p - T$ equilibrium diagram of the hydride [95]. They also synthesized two crystalline phases but with opposite conclusions: their low-temperature phase corresponds to the previous high-temperature phase and the high-temperature phase to the previous low-temperature one. The low-temperature phase was named α -BeH₂ and the high-temperature phase β -BeH₂. The symmetry of the β -phase is hexagonal with cell parameters $a=7.8 \text{ \AA}$, $c=5.5 \text{ \AA}$ and $Z=12$. The structure of the α -phase had been accurately determined at ambient conditions in 1988 using synchrotron radiation by Smith *et al.* [96] and is represented in figure 9.1. This structure has a body-centered orthorhombic symmetry, space group $Ibam$, with the following cell parameters: $a=9.082(4) \text{ \AA}$, $b=4.160(2) \text{ \AA}$, $c=7.707 \text{ \AA}$ and $Z=12$ and contains corner-sharing BeH₄ units similar to the ones found in the amorphous phase. These three studies are the only published work on crystalline beryllium hydride and that is most likely due to the difficulty

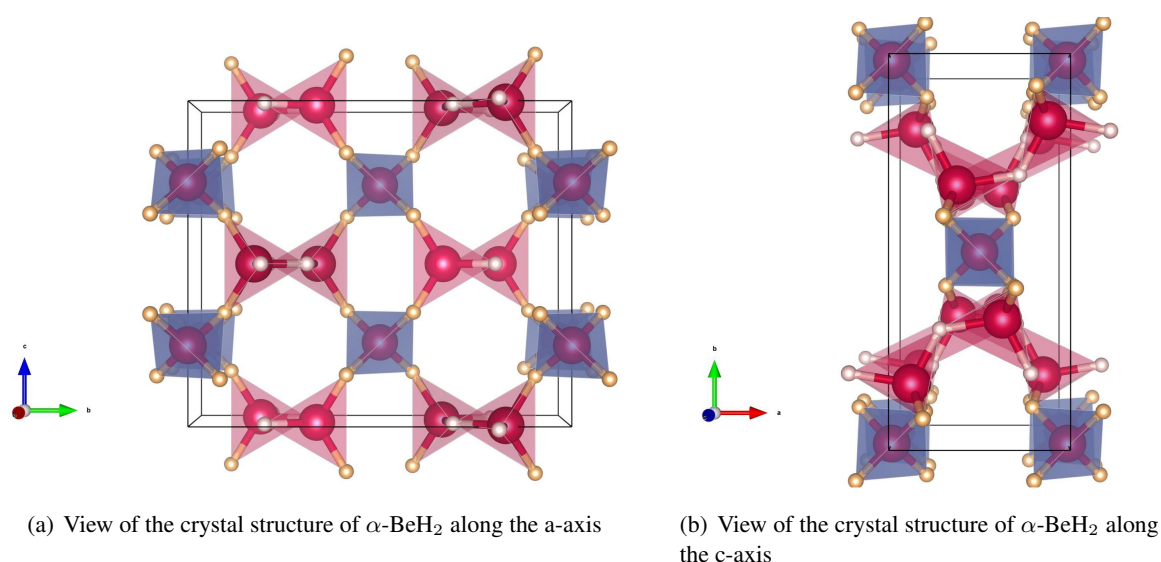


Figure 9.1: Structure of the known α -phase of BeH₂. Be atoms are represented in red, H atoms in gold.

to synthesize high-quality samples. These difficulties can be explained by the facts that: (i) the difference in cohesive energy between the α -phase and the polymeric one is very small [97] ($\Delta E \approx 3 \text{ kJ}\cdot\text{mol}^{-1}$) and (ii) the amorphous and the crystalline form share structural similarities: both contain corner-shared tetrahedral units of BeH₄ with similar interatomic distances [98], [93].

With the popularization of *ab initio* methods BeH₂ has gained a renewed interest as it is one the favourite target molecule for testing new *ab initio* quantum chemical methods (e.g. [99]). One of the very first theoretical work to extensively study the high-pressure behaviour of BeH₂ was published by Hantsch *et al.* in 2003 [100] following the remark by Haines *et al.* that the orthorhombic structure of α -BeH₂ is closely related to that of moganite, a monoclinic form of silica [101]. Hantsch *et al.* therefore proposed new stable BeH₂ structures based on the known structures of several SiO₂ polymorphs and a high-pressure structural transition towards a stishovite-like structure was predicted at 33 GPa. It was later suggested by Vajeeston *et al.* that before transforming to this phase, BeH₂ should undergo two phase transitions, at 7.07 GPa and 51.41 GPa respectively [102]. The stishovite-like phase should become more stable above 86.56 GPa and transforms to an ϵ -phase at 97.55 GPa. Just like for AlH₃, Vajeeston *et al.* chose 24 potentially applicable structures and compared their Gibbs free energy. A recent study by Wang *et al.*, using the "random searching" method, proposed a different sequence of phase transitions: α -BeH₂ is expected to transform to a new phase with a 1T-structure at 25 GPa that is found to be stable up to 140 GPa [29]. This 1T-structure is a trigonal phase (space group $P\bar{3}m1$), commonly found in metal dichalcogenides, which consists of stacking layers of edge-sharing BeH₆ octahedra as seen in figure 9.2. Such phase transition would then imply that the coordination number for the Be atoms increases at the transition. Above 140 GPa two more phase transitions are predicted, first towards a rhombohedral structure and then towards a metallic orthorhombic phase. This sequence of transition was also found by Yu *et al.* using a random searching method [28]. In both articles from Wang *et al.* and Yu *et al.* the metallic orthorhombic phase was predicted to be superconductive with $T_c \sim 40 \text{ K}$. Finally it has to be noted that a theoretical study by Hooper *et al.* [48] and the work from Yu *et al.* both showed that no changes of H-stoichiometry are expected for beryllium hydride under pressure.

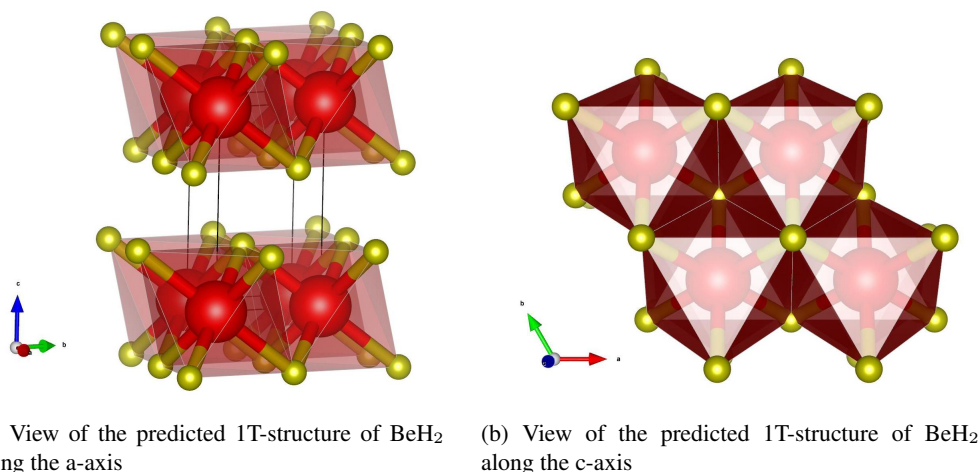


Figure 9.2: Representation of the 1T-structure of BeH₂ predicted by Wang *et al.* . Be atoms are represented in red, H atoms in gold.

The aim of our work was then to answer the following questions:

- Can BeH₂ be easily synthesized from its constituents under pressure to form a high-purity crystalline compound?
- DFT calculations predict different sequences of phase transitions under pressure. A detailed study of the high-pressure behaviour of crystalline beryllium hydride is therefore needed in order to test for these different predictions.
- Can metallic beryllium hydride be synthesized, in order to test its possible high-temperature superconductivity?
- Is BeH₂ the most stable stoichiometry under pressure, like it has been suggested [48], [28]?

Crystalline beryllium hydride was successfully synthesized by heating pristine beryllium in hydrogen medium at 2.4 GPa, using the external heater presented in section 2.1, and by laser heating metallic beryllium in hydrogen medium above 10.5 GPa using the method presented in section 2.2. Interestingly these two methods did not produce the same phase. In the first case the known α -phase, with the *Ibam* structure, was synthesized and its volume as a function of pressure could be measured up to 27.3 GPa. Above 27.3 GPa a dissociation of the α -phase into the elements is observed. The second phase, resulting from the laser heating technique and called β -phase in our study, could be indexed in a tetragonal unit cell, space group $P4_12_12$, which corresponds to the polymorph of BeH₂ isotypical to the crystalite-low structure proposed by Hantsch *et al.* . Above 17 GPa a new phase appears but its structure could not be determined. These different phases and phase transitions could be observed using X-ray diffraction, infra-red spectroscopy and Raman spectroscopy.

Between 40 and 70 GPa laser heating of pristine beryllium in hydrogen medium could not result in the formation of beryllium hydride, confirming the dissociation of the α -phase observed at lower pressure. Above 80 GPa laser heating resulted in the appearance of a new strong Raman spectrum and of a new X-ray diffraction pattern of a crystalline sample, suggesting the synthesis of a new phase. The XRD pattern could be easily indexed as the trigonal structure proposed by Wang *et al.* [29]. Its volume as a function of

pressure was measured up to 100 GPa. None of the different synthesized phases was found to be metallic, in agreement with the theoretical predictions which suggest that metallic beryllium hydride should appear above 200 GPa. BeH₂ is the only stoichiometry observed between 0 and 100 GPa.

These results have submitted to the journal *Journal of Chemical Physics* in an article entitled "*High pressure study of Crystalline Beryllium Hydride: New Structures and Re-entrant Disproportionation*" and attached in the following pages.

9.2 Article: "High pressure study of Crystalline Beryllium Hydride: New Structures and Re-entrant Disproportionation"

High Pressure Study of Crystalline Beryllium Hydride: New Structures and Re-entrant Disproportionation

Charles M. Pépin^{a)} and Paul Loubeyre^{b)}
CEA, DAM, DIF, F-91297 Arpajon, France

(Dated: 2 July 2015)

A detailed experimental study has been carried out on the characterization of pure crystalline beryllium hydride, BeH₂, up to 100 GPa using synchrotron x-ray diffraction and Raman spectroscopy. The already known *Ibam* structure has been synthesized at 2.4 GPa at 550 K and is stable up to ~ 27 GPa. This phase then dissociates into beryllium and hydrogen. At low pressure another stable polymorph of BeH₂ was synthesized: its structure is identified as isotypical to the crystoballite-low SiO₂ structure. Above 80 GPa the recently predicted 1T-structure for BeH₂ is synthesized using laser annealing of hydrogen-embedded beryllium. BeH₂ is the only stoichiometry observed up to 100 GPa.

I. INTRODUCTION

Beryllium hydride, BeH₂, presents promising technological interest due to its very large hydrogen content (>18 wt.%). It is viewed as a potential material for hydrogen storage in fuel cells, for solid rocket propellant or as an hydrogen source in energy-conversion portable devices. Beryllium deuteride has for instance been proposed as the ablator material for inertial confinement targets¹ and new ablators composed of Be have recently been tested at the National Ignition Facility (NIF)², hence experimental data on the high-pressure behaviour of this compound are needed. BeH₂ also appears to be of great importance for fundamental science research because of its small number of electrons (6), providing a popular testing tool for quantum chemical methods³.

Recently, the application of pressure has been proposed as a means to tune the properties of hydrides and consequently several works have been devoted to the theoretical study of beryllium hydride under pressure⁴⁻⁸. Three interesting effects are expected to appear with the application of pressure. The first one is the stabilization of new structures with a possible improved hydrogen capability, like it has been seen for LiBH₄⁹. Second, as proposed by Zurek *et al.*¹⁰ and recently demonstrated experimentally^{11,12}, the hydrogen content in hydrides should significantly increase with pressure. Third, pressure can turn hydrides with large hydrogen content, which tend to be covalent or ionic insulator, into metals with analogous properties to metallic hydrogen, such as a high T_c superconductivity¹³. The recent predictions^{7,8} of metallic BeH₂ at 200 GPa with a T_c of ~ 40 K tends to confirm that interesting properties can be expected for hydrogen dominant compounds. However the remarkable high pressure behavior of this hydride has been awaiting a clear experimental confirmation as the studies of crystalline BeH₂ remains very scarce, mostly due to the difficulties to synthesize pure crystalline samples.

In this paper, we present two different *in situ* synthesis methods to grow crystal of beryllium hydride. The high pressure behaviour of pure crystalline BeH₂ is investigated up to 100 GPa by means of Raman spectroscopy and synchrotron x-ray diffraction. The goals of this study were: (i) to investigate the sequence of phase transition under pressure of this compound; (ii) to identify the structures of the new phases; and (iii) to test the stability of the BeH₂ stoichiometry.

II. SAMPLE SYNTHESIS AND METHODS

In eight independent runs, pristine beryllium powder consisting of single crystalline grains was loaded together with hydrogen compressed to 1400 bars into diamond anvil cells (DACs). Hydrogen also acted as a pressure medium and the beryllium sample was always surrounded by excess hydrogen even at the highest pressures achieved. To reach pressures below 60 GPa we used diamonds with 300 μm culets and 100 μm beveled diamonds to achieve pressures in the 1 Mbar range. In all cases rhenium gaskets were used, coated with 2 μm of gold so as to prevent any diffusion of hydrogen.

Two different methods were used to synthesize pure crystalline beryllium hydride. The hydride was first synthesized by heating the sample between 2.4 GPa and 6 GPa at 550 K during 3 days using an external heater. Under those conditions, Be and H₂ react to form BeH₂, the solid expands as to fill a larger area of the cavity. The visual evolution is presented in Figure 1. The successful synthesis of the hydride was then characterized by the visual volume expansion of the sample and by the appearance of new Raman peaks. The second technique consists of YAG-laser heating the sample in hydrogen medium. In this case temperatures of ~ 1500 K are achieved. The temperature is measured by analysing the pyrometric signal emitted at the center of the hot spot. This technique was used to synthesize beryllium hydride at 10.5 GPa and at 82 GPa. So as to prevent an important heat loss due to the extremely high thermal conductivity of the diamond, the Be sample was thermally insulated from

^{a)}charles.pepin@cea.fr

^{b)}paul.loubeyre@cea.fr

the diamond culets either by thin layers of LiF ($\sim 2 \mu\text{m}$, pressed onto each diamond before loading) or grains of c-BN. Experimental runs performed with these different sample assemblies gave consistent results, which proves that no parasitic chemical reaction with the insulating media or the diamond culet occurred.

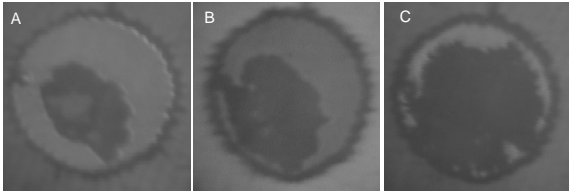


FIG. 1. Evolution of a beryllium sample at 2.4 GPa in hydrogen medium, heated at 550 K using an external heater. A: Initial Be sample in H_2 . A ruby is visible on the left side of the sample, near the gold ring used to confine hydrogen. B: After 12 hours at 550 K. C: After 60 hours at 550 K.

In all cases the pressure was determined using the revised hydrostatic ruby gauge up to 80 GPa and the equation of state of gold¹⁴ above 80 GPa.

Angle dispersive x-ray diffraction (XRD) patterns using monochromatic synchrotron radiation were collected at the European Synchrotron Radiation Facility beamlines ID09a, using a MAR555 flat panel detector with $\lambda=0.41548 \text{ \AA}$, and ID27, using a CCD detector with $\lambda=0.3738 \text{ \AA}$. The signal of the image plate was circularly integrated using the FIT2D software¹⁵ and analyzed using the FULLPROF software.

Raman spectra were measured using the 487.965 nm radiation of an Ar-Kr laser and a 0.5 m focal length AnDor spectrograph equipped with 1200-g/mm grating. The calibration of the spectrometer was performed using the calibrated spectral lines of a neon lamp. Exposure time varied between 2 and 10 seconds.

III. RESULTS AND DISCUSSION

Amorphous polymeric beryllium hydride can be obtained with great purity by complex multi-stage processes involving the thermal decomposition of organoberyllium compounds (e.g. Refs. (16, 17)) and has been the subject of several recent studies, see for instance Refs. (18,19,20). On the other hand, experimental studies on crystalline BeH_2 have been very limited because of the difficulty to synthesize a high purity crystalline sample. Until now there has been only one structure determination available²¹. The $\alpha\text{-BeH}_2$ has a body-centered orthorhombic structure (space group $Ibam$, $Z = 12$). The difficulties to synthesize pure crystalline samples can be explained by the facts that: (i) the difference in cohesive energy between the α -phase and the polymeric one is very small²² ($\Delta E \approx 3 \text{ kJ}\cdot\text{mol}^{-1}$) and (ii) the

amorphous and the crystalline form share structural similarities: both contain corner-shared tetrahedral units of BeH_4 with similar interatomic distances^{18,23}. This unique orthorhombic structure has been shown to be related to that of moganite, a monoclinic form of silica²⁴. SiO_2 being known to crystallize in a large variety of tetrahedral framework structure under pressure, the existence of a possible isomorphism between BeH_2 and SiO_2 motivated the first *ab initio* study of this hydride under pressure by considering possible polymorphs of BeH_2 isotypical to known SiO_2 structural frameworks⁴. In that study all the calculated structures were found to be stable and a high pressure transition toward a stishovite-like structure was predicted at 33 GPa. It was later suggested by Vajeeston *et al.* that before transforming to this phase, BeH_2 should undergo two phases transitions, at 7.07 GPa and 51.41 GPa respectively⁵. The stishovite-like phase should become more stable above 86.56 GPa and transforms to an ϵ -phase at 97.55 GPa. However a recent theoretical study by Wang *et al.* proposed a revised sequence of phase transition under pressure: $\alpha\text{-BeH}_2$ transforms at 25 GPa to a new phase with a 1T-structure (space $P\bar{3}m1$)⁷. This phase was found to be more stable than the ones previously predicted, up to 140 GPa. Above 140 GPa it further transforms to a rhombohedral structure (space group $R\bar{3}m$) previously predicted by Hooper *et al.*⁶, and then at 200 GPa transforms to a metallic $Cmcm$ structure. This sequence of phase was later reproduced by Yu *et al.*⁸. In both studies from Refs. (7) and (8) the $Cmcm$ structure was predicted to be superconductive with $T_c \sim 40 \text{ K}$.

A. Low-Pressure Behavior

In the present study, the diffraction pattern of the crystalline sample, synthesized using an external heater at pressure as low as 2.4 GPa, is perfectly indexed as the known $Ibam$ structure of $\alpha\text{-BeH}_2$, as shown on Figure 2A.

The volume versus pressure of $\alpha\text{-BeH}_2$ could be measured up to 27.3 GPa and is plotted in Figure 3. It is compared with previous experimental measurements on amorphous sample from Ref. (20) and with theoretical results from Refs. (5) and (7). To provide useful physical parameters (volume V_0 , bulk modulus B_0 and its pressure derivative B'_0 under ambient conditions) the $V(P)$ data points have been fitted by the Vinet-type functional form²⁵ which expresses the pressure as a function of $X = (\frac{V}{V_0})^{\frac{1}{3}}$ through:

$$P(V) = 3 \frac{B_0(1-X)}{X^2} \exp\left[\frac{3}{2}(B'_0 - 1)(1-X)\right] \quad (1)$$

The fitting parameters obtained are $V_0 = 24.31 \pm 0.09 \text{ \AA}^3/\text{f.u.}$, $B_0 = 26.6 \pm 1.0 \text{ GPa}$ and $B'_0 = 3.2 \pm 0.1$. The volume V_0 is very close to the one measured in Ref. (21) of $24.266 \text{ \AA}^3/\text{f.u.}$ Crystalline BeH_2 is less compressible than the amorphous form for which a bulk modulus of

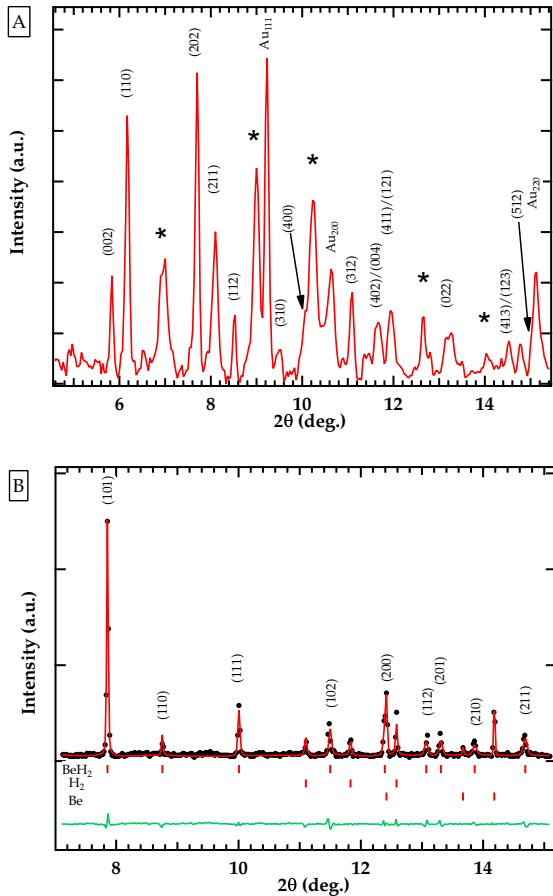


FIG. 2. A - Integrated x-ray diffraction pattern of α -BeH₂ for $\lambda=0.3738$ Å. Black asterisks correspond to Bragg peaks β -BeH₂. B - Integrated x-ray diffraction pattern of β -BeH₂ for $\lambda=0.41548$ Å. Black dots are the observed diffraction spectrum, red solid line corresponds to the LeBail fit of the experimental points. β -BeH₂ has been indexed as a tetragonal unit cell, space group $P4_12_12$ with $a=3.849(2)$ Å, $c=4.922(1)$ Å and $Z=2$.

14.2 ± 3.0 GPa was found. This trend is in agreement with the theoretical calculations of Refs. (5) and (26) who found a bulk modulus of 23.79 and 22.60 GPa, respectively, for α -BeH₂.

As it can be seen in Figure 2A some diffraction peaks, signaled with black asterisks, could not be indexed as the *Ibam* structure nor as non reacted beryllium, meaning that another phase, called β -phase, is synthesized when using an external heater. The presence of another phase when synthesizing α -BeH₂ had already been evidenced previously but its structure could not be solved experimentally^{27,28}. It was suggested in Ref. (28) that the temperature and the cooling rate could influence its synthesis. Using the laser heating technique, previously described in Section II, allowed us to test for this sug-

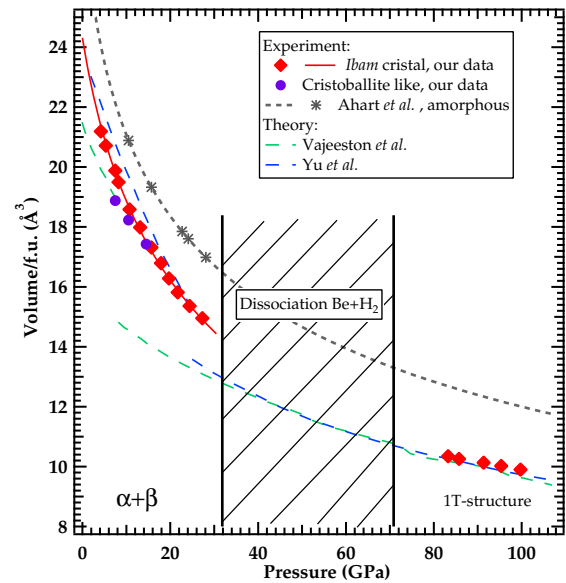


FIG. 3. Volume per BeH₂ formula unit versus pressure. The red and violet filled symbols correspond to our experimental data points, compared with results from Refs. [5, 8, 20] (other symbols).

gestion. The diffraction pattern of the crystalline sample synthesized at 10.5 GPa with this technique is presented in Figure 2B and correspond to the β -phase. The Bragg peaks of β -BeH₂ can be indexed in a tetragonal unit cell, space group $P4_12_12$ with $a=3.849(2)$ Å, $c=4.922(1)$ Å and $Z=2$. A complete structural refinement (atomic positions of Be and H) was not possible because of the very low signal to noise ratio and the existence of the a preferred orientation in our powder. Interestingly, this structure corresponds to the polymorph of BeH₂ isotypical to the cristobalite-low structure proposed by Hantsch *et al.*, with cell parameters in good agreement with the ones calculated at ambient pressure ($a=4.182$ Å, $c=5.622$ Å)⁴. The observation of this β -phase further confirms that BeH₂ might behave similar to SiO₂. From the XRD data, we could index the unit cell volume as a function of pressure up to 17 GPa at three different pressures, shown on Figure 3. Its volume is very close to the one measured for the α -phase but its pressure behavior seems different, although it would require more data points to confirm this trend. Above 17 GPa, changes in the XRD pattern were observed: the (101) diffraction peak begins to split into two peaks and overall the diffraction signal is much weaker. These changes are attributed to the appearance of a new phase, called β' . The structure of the β' -phase could not be successfully determined. However, the existence of a strong isotypism of BeH₂ and SiO₂ suggests that this phase transition could originate from a monoclinic of the cristobalite-like β -phase like it has been observed for SiO₂²⁹, which could explain the splitting of

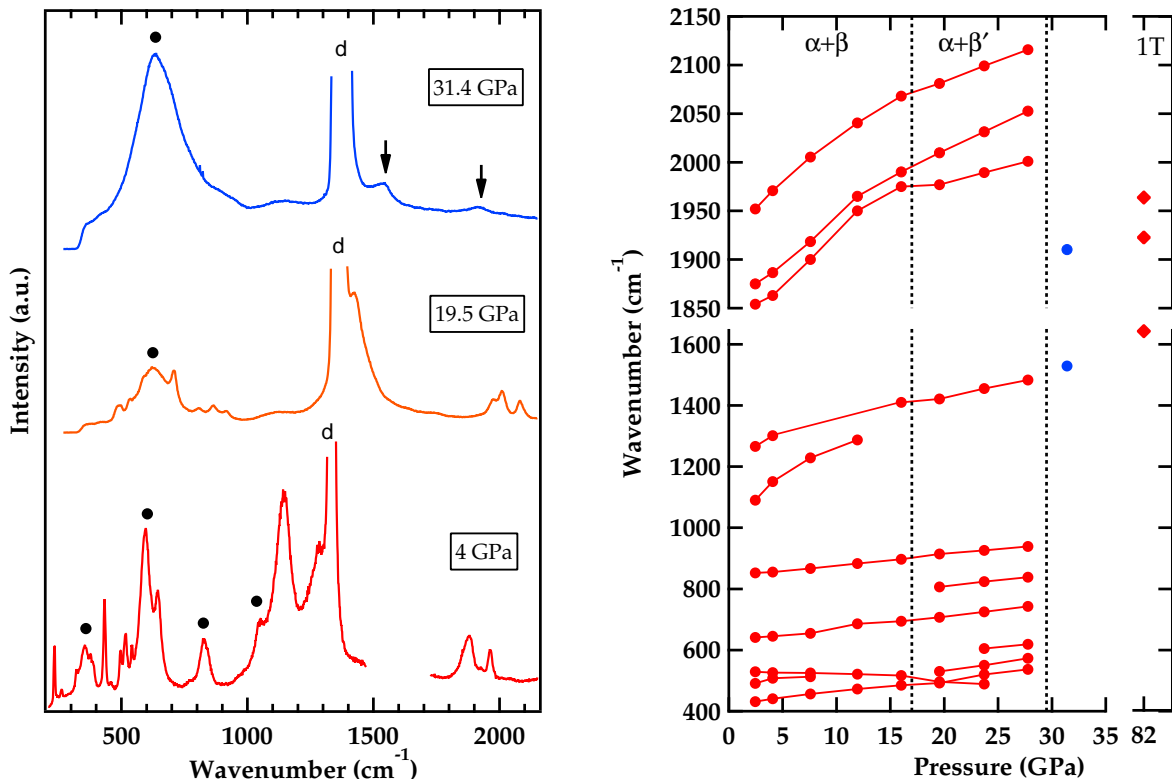


FIG. 4. Left: Characteristic Raman spectra of BeH₂ at 4 GPa (red line), 19.5 GPa (orange line) and at 31.4 GPa (blue line), with black arrows showing the two weak remaining peaks. Raman bands of diamond anvil are labeled d. Black points denote the roton modes of hydrogen. Right: Pressure dependence of the Raman shifts of a mixture of α and β -BeH₂ (red circles), of the amorphous phase (blue circle) and of the 1T-structure (red diamonds).

(101) diffraction peak.

Raman spectroscopy under pressure, realized on a sample synthesized using an external heater, and therefore containing both α and β -BeH₂, is presented in Figure 4. 10 Raman active modes and 3 IR active modes were well resolved and their shifts as a function of pressure followed up to 17 GPa. The highest frequencies around ~ 1900 cm⁻¹ are in agreement with the results from Refs. (4) and (30) and can be compared to the stretching mode measured at 2179 cm⁻¹ for free BeH₂³¹. Above 17 GPa a new Raman mode appears at 806 cm⁻¹ and the pressure dependence of the Raman shifts changes related to Be-H bond above 1900 cm⁻¹ softens indicating a change of crystal field. These changes further confirm the existence of a phase transition toward a β' -phase observed by XRD at this pressure and the similarities of the Raman spectra suggest that the two phases are closely related.

Above 27 GPa drastic changes are observed both in the diffraction pattern and in spectroscopy (see Fig. 4). Between 27 and 30 GPa the diffraction peaks from the α -phase disappear while peaks from the β -phase are still

observed and peaks indexed as pure beryllium, using the equation of state of Ref. [32], appear and grow in intensity. Above 30 GPa the remaining diffraction peaks of the β' -phase also disappear. At this transition no new diffraction peaks, apart from the ones of pure beryllium, could be observed. However, very weak broad Raman modes could still be observed as indicated by arrows in Figure 4, meaning that the β' -phase transforms at this pressure to an amorphous phase that could not be observed by XRD. We therefore propose that above 30 GPa a pressure-induced reentrant disproportionation of α -BeH₂ into Be+H₂ occurs while β' -BeH₂ transforms to an unidentified amorphous phase.

The investigation of the existence of various (meta)stable polymorphs of BeH₂ and of a large dissociation pressure range, which had not been predicted by the latest studies^{7,8}, should be very interesting to refine the understanding of this compound under pressure.

B. High-Pressure Behavior

Laser heating of pristine beryllium in hydrogen medium between 35 and 70 GPa could not result in the formation of beryllium hydride.

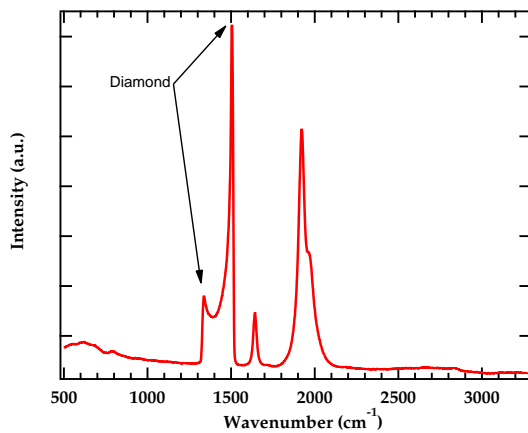


FIG. 5. Characteristic Raman spectrum of the 1T-structure at 82 GPa. Three characteristic modes are observed between 1600 and 2000 cm^{-1} .

When laser heating the sample at 82 GPa around ~ 1500 K a new strong Raman spectrum is observed and presented in Figure 5. The XRD pattern of the crystalline sample, presented on Figure 6, is indexed as the trigonal structure (space group $P\bar{3}m1$, $Z=1$) proposed by Wang *et al.*⁷ and Yu *et al.*⁸, called phase II and represented on Figure 6. The structure of phase II is commonly found in metal dichalcogenides and is referred as 1T-structure. It consists of stacking layers of edge-sharing BeH_6 octahedra, with H-H van der Waals bonds between two layers. This 1T-structure holds promising electronic and optic properties with transition metal dichalcogenides³³. However it has been shown in Ref. [7] that these properties could not be reproduced in phase II of BeH_2 . The lattice parameters and unit cell volume could be obtained from the XRD data up to 100 GPa. The volume per formula unit of phase II as a function of pressure has been reported in Figure 3. The measured cell parameters at 100 GPa are $a = b = 1.985(2)$ Å and $c = 2.890(2)$ Å. These parameters are in very good agreement with the ones calculated by Wang *et al.* who proposed $a = b = 1.97254$ Å and $c = 2.88702$ Å at the same pressure, i.e. 1.3% error on the volume. In this phase II, Wang *et al.* predicted an average Be-H bond length of 1.42 Å at 100 GPa, which is comparable to the measured value of 1.44(2) Å measured for the *Ibam* phase at ambient pressure²¹, while one would expect a decrease of this bond length under pressure. In our Raman measurements, the highest Raman vibration in phase II at 80 GPa is observed at 1970 cm^{-1} while it is observed at 1953 cm^{-1} at 2.4 GPa and extrapolated at 2330 cm^{-1} at

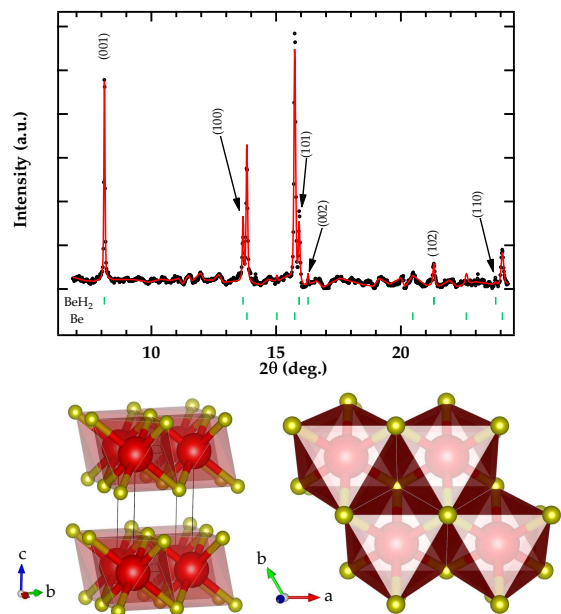


FIG. 6. Integrated x-Ray diffraction pattern of phase II of BeH_2 at 83.5 GPa for $\lambda=0.41548$ Å. Black dots are the observed diffraction spectrum, red solid line corresponds to the LeBail fit of the experimental points. Phase II has been indexed as a tetragonal unit cell, space group $P\bar{3}m1$ with $a=2.014(3)$ Å, $c=2.934(1)$ Å and $Z=1$ and is represented below the diffraction pattern along the *a* and *c* axis, using VESTA³⁴. Be atoms are represented in red and H atoms in yellow.

80 GPa (Fig. 5 and 4). Raman spectroscopy providing an indirect probe of the Be-H bond length, this result is in agreement with the counter-intuitive evolution of this bond length. Moreover such behavior is similar to that observed for SiO_2 : when transforming from a tetrahedral framework structure to an octahedral framework structure a negative difference of ~ 250 cm^{-1} is predicted³⁵.

To what extent hydrides with a high H:metal ratio are analogous to metal hydrogen is of great fundamental interest¹³. At 2.4 GPa, in α - BeH_2 , the nearest H-H distance is 2.22 Å and it diminishes down to 1.64 Å, between two layers in phase II at 100 GPa. This value is much larger than the 1.2 Å value in CaH_6 , which is characteristic of a weak covalent bond³⁶, in agreement with the description of H-H van der Waals bonds between two layers. The H-H distance in this hydride is expected to decrease slowly with pressure, going down to 1.35 Å at 400 GPa⁸, which is significantly larger than the expected 1.0 Å H-H distance for metal hydrogen at 450 GPa³⁷. However, the highly anisotropic structure of phase II might offer the possibility to drastically reduce this H-H distance in BeH_2 at much lower pressures: compression along the *c* axis in order to squeeze the van der Waals spaces should efficiently reduce the H-H distance

without requiring much higher pressures.

IV. CONCLUSION

The pressure behavior of pure crystalline beryllium hydride has been experimentally investigated for the first time up to 100 GPa and compared with the predictions of state-of-the-art *ab initio* calculations published recently. The *Ibam* structure, α -BeH₂, is found stable up to \sim 27 GPa, and then dissociates into the elements, which contradicts recent predictions^{5,7,8}, and calls for a revision in the 35-70 GPa pressure range. Stable polymorphs of BeH₂ isomorph to SiO₂ have been identified at low pressure and transforms to an unidentified poorly crystallized phase above 30 GPa. Such isotypism of BeH₂ and SiO₂ has been suggested by Hantsch *et al.* and offers an interesting alternative approach to the comprehension of the behaviour under pressure of this hydride.

Above 80 GPa the predicted 1T-structure^{7,8} is synthesized by laser heating beryllium in hydrogen medium. The use of laser heating, necessary to overcome kinetic barrier, also allows to search for new stable stoichiometries, like it has been shown for iron hydrides¹¹. In the case of beryllium, BeH₂ was the only stoichiometry, confirming the predictions of Refs. (6) and (8).

The two different methods to form crystalline beryllium hydride, use of external heater and of laser heating, and its results should have important implications for the synthesis and the study of metal hydrides in general, and we hope that our findings will motivate further experimental works.

ACKNOWLEDGMENTS

The authors acknowledge the European Synchrotron Radiation Facility for provision of synchrotron radiation on beam line ID09a (proposal HC-1074) and ID27. We wish to thank M. Hanfland, M. Mezouar and G. Weck for their help with XRD experiments and sample synthesis and T. Plisson for fruitful discussions.

¹S. Y. Gos'kov, N. V. Zmitrenko, Y. E. Markushkin, and Y. A. Merkul'ev, *J. Russian Laser Res.* **28**, 148 (2007).

²NIF internal publication (2014).

³P. G. Szalay and R. J. Barlett, *J. Chem. Phys.* **103**, 3600 (1995).

⁴U. Hantsch, B. Winkler, and V. Milman, *Chem. Phys. Lett.* **378**, 343 (2003).

⁵P. Vajeeston, P. Ravindran, A. Kjekshus, and H. Fjellag, *Appl. Phys. Lett.* **84**, 34 (2004).

⁶J. Hooper, B. Altintas, A. Shamp, and E. Zureck, *J. Phys. Chem. C* **117**, 2982 (2013).

⁷Z. Wang, Y. Yao, L. Zhu, T. Iitaka, H. Wang, and Y. Ma, *J. Chem. Phys.* **140**, 124707 (2014).

⁸S. Yu, Q. Zeng, A. R. Oganov, C. Hu, G. Frapper, and L. Zhang, *AIP Advances* **4**, 107118 (2014).

⁹Y. Filinchuk, D. Chernychov, A. Nevidomskyy, and V. Dmitriev, *Angw. Chem. Int. Ed.* **47**, 529 (2008).

¹⁰E. Zurek, R. Hoffmann, N. Ashcroft, A. Oganov, and A. Lyakhov, *PNAS* **106**, 17640 (2009).

¹¹C. M. Pépin, A. Dewaele, G. Geneste, P. Loubeyre, and M. Mezouar, *Phys. Rev. Lett.* **113**, 265504 (2014).

¹²C. M. Pépin, P. Loubeyre, F. Occelli, and P. Dumas, *PNAS* **00**, 00 (2015).

¹³N. W. Ashcroft, *Phys. Rev. Lett.* **92**, 187002 (2004).

¹⁴A. Dewaele, P. Loubeyre, and M. Mezouar, *Phys. Rev. B* **70**, 094112 (2004).

¹⁵A. P. Hammersley, S. O. Svensson, M. Hanfland, A. N. Fitch, and D. Husermann, *High Press. Res.* **14**, 235 (1996).

¹⁶R. W. Baker, G. J. Brendel, B. R. Lowrance, J. R. Mangham, E. M. Marlett, and L. H. Shepherd, *J. Organomet. Chem.* **159**, 123 (1978).

¹⁷M. D. Senin, V. V. Akhachinskii, Y. E. Markushkin, N. A. Chirin, L. M. Kopytin, I. P. Mikhaleenko, N. M. Ermolaev, and A. V. Zabrodin, *Inorg. Mat.* **29**, 1416 (1993).

¹⁸S. Sampath, K. M. Lantzky, C. J. Benmore, J. Neuefeind, J. E. Siewenie, P. A. Egelstaff, and J. L. Yarger, *J. Chem. Phys.* **119**, 12499 (2003).

¹⁹S. Sampath, A. I. Kolesnikov, K. M. Lantzky, and J. L. Yarger, *J. Chem. Phys.* **128**, 134512 (2008).

²⁰M. Ahart, J. L. Yarger, K. M. Lantzky, S. Nakano, H. K. Mao, and R. J. Hemley, *J. Chem. Phys.* **124**, 014502 (2006).

²¹G. S. Smith, Q. C. Johnson, D. K. Smith, D. E. Cox, R. L. Snyder, R.-S. Zhou, and A. Zalkin, *Solid State Comm.* **67**, 491 (1988).

²²A. D. Zdetsis, M. M. Sigalas, and E. N. Koukaras, *Phys. Chem. Chem. Phys.* **16**, 14172 (2014).

²³S. V. Marchenko, V. F. Petrunin, Y. E. Markushin, M. D. Senin, and N. A. Chirin, *Sov. Phys. Solid State* **24**, 1308 (1982).

²⁴J. Haines, C. Chateau, J. M. Léger, A. L. Sauze, N. Diot, R. Marchand, and S. Hull, *Acta Cryst.* **B55**, 677 (1999).

²⁵P. Vinet, J. Ferrante, J. Smith, and J. Rose, *J. Phys. C* **19**, L467 (1987).

²⁶B.-T. Wang, P. Zhang, H.-L. Shi, B. Sun, and W.-D. Li, *Eur. Phys. J. B* **74**, 303 (2010).

²⁷G. J. Brendel, E. M. Marlett, and L. M. Niebylski, *Inorg. Chem.* **17**, 3589 (1978).

²⁸S. K. Kononov and B. M. Bulychev, *Russian J. of Inorg. Chem.* **37**, 1361 (1992).

²⁹M. T. Dove, M. S. Craig, D. A. Keen, W. G. Marshall, S. A. T. Redfern, K. O. Trachenko, and M. G. Tucker, *Mineralogical Magazine* **64**, 569 (2000).

³⁰H. Iddir, P. Zapol, and A. I. Kolesnikov, *Phys. Rev. B* **80**, 134111 (2009).

³¹P. F. Bernath, A. Shayesteh, K. Tereszchuk, and R. Colin, *Science* **297**, 1323 (2002).

³²A. Lazicki, P. Loubeyre, F. Occelli, R. J. Hemley, and M. Mezouar, *Phys. Rev. B* **85**, 054103 (2012).

³³Q. H. Wang, K. Kalantar-Zadeh, A. Kis, J. N. Coleman, and M. S. Strano, *Nature Nanotechnology* **7**, 699 (2012).

³⁴K. Momma and F. Izumi, *J. Appl. Crystallogr.* **44**, 1272 (2011).

³⁵B. B. Karki, M. C. Warren, L. Stixrude, G. J. Ackland, and J. Crain, *Phys. Rev. B* **55**, 3465 (1997).

³⁶H. Wang, J. S. Tse, K. Tanaka, T. Iitaka, and Y. Ma, *PNAS* **109**, 6463 (2012).

³⁷J. M. McMahon and D. M. Ceperley, *Phys. Rev. Lett.* **106**, 165302 (2011).

Part IV

Changing the stoichiometry of hydrides: iron hydrides and lithium hydrides

Chapter 10

Motivations

After familiarizing with the different investigation techniques to study hydrides under pressure the next step was to test the hypothesis of an increase of the hydrogen stoichiometry in hydrides under pressure. We naturally focused on lithium hydride first as the theoretical work published by Zurek *et al.* had been the first one to really envisage the possibility to induce stoichiometric changes in hydrides under pressure and subsequently is at the origin of most of the recent theoretical papers predicting new hydrides with unusual stoichiometries and exciting properties (high-temperature superconductivity, improved hydrogen storage...) all across the periodic table. Trying to experimentally reproduce these results on lithium hydride seems therefore to be a relevant starting point.

The second system we studied is the mixture of iron and hydrogen. In this case recent theoretical predictions had shown the possibility to drastically increase the hydrogen content in the hydride, FeH transforming under pressure to FeH₃ and then to FeH₄. This system therefore appeared as an ideal candidate to confirm the hypothesis stating that the H-stoichiometry in hydrides should increase with pressure. Moreover iron and hydrogen are both two of the main constituents of planetary interiors. Thus studying the stability of novel iron hydrides under pressure seemed to be of high interest as it could have an impact on future planetary interiors and in particular for the Earth's core, mainly composed of iron and for which hydrogen is considered as a possible light element.

The following two chapters report the changes of H-stoichiometry induced under pressure in the systems lithium-hydrogen and iron-hydrogen.

Chapter 11

Lithium Hydrides

11.1 Introduction

Lithium hydride, LiH, is the most elementary ionic compound with only four electrons per unit cell. Like other light elements hydrides LiH is a prospective candidate for hydrogen storage having a large hydrogen content of 12.59 wt.% [103]. However its decomposition of temperature of 720 °C is too high to be efficiently used in storage devices at the moment and a lot of studies are currently undergoing to try to find alternative ways to improve this temperature of operation. LiH is also a material of choice for neutron-shielding nuclear reactors [104] and is extensively used as a precursor to complex metal hydrides, since LiH itself can be easily produced through the reaction $2\text{Li} + \text{H}_2 \rightarrow 2\text{LiH}$ at moderate temperature.

Lithium hydride crystallizes in the rock-salt structure (space group $Fd\bar{3}m$), the so-called *B1* phase. Despite this simplicity, the high pressure behaviours of LiH and LiD are attractive for the study of solid-state physics and interesting properties are expected because of the quantum properties of the protons and of the growing interaction of the core electrons. For instance it has been shown that the zero-point motion gives a measurable isotopic shift in its equation of state [105]. A long awaited effect of the pressure on LiH is the metal-insulator transition and has motivated a lot theoretical and experimental work in different groups. At ambient conditions the electronic band-gap of LiH is $E_g=4.9$ eV and it decreases steadily under pressure (-11 meV/GPa) [106]. Using these results the band gap closure is expected to occur around ~ 450 GPa which is beyond the reach of the actual high-pressure devices. However it has been predicted that metallization could occur at lower pressure after a phase transition towards a metallic *B2* phase with a CsCl structure. In fact such *B1-B2* phase transition has already been observed in all heavier alkali hydrides and various theoretical models have made predictions for this transition in LiH between 220 and 400 GPa [107, 108, 109, 110]. Experimentally, X-ray diffraction has been performed on a single crystal up to 250 GPa: XRD lines from the *B1*-phase of LiH could be monitored up to the highest pressure achieved meaning that no phase transition nor metallization (no blackening of the sample) was observed [111]. Lazicki *et al.* also examined the vibrational properties of LiH using Raman spectroscopy to measure the second-order Raman up to 120 GPa. In the case of alkali halides, also exhibiting a *B1 – B2* phase transition, the transition has been predicted to be accompanied by a softening of the transverse-acoustic (TA) phonon mode at the zone boundary *X* point [112] and a parallel was proposed for lithium hydride. The Raman data from Lazicki *et al.* suggest the onset around 200 GPa, hinting that the transition may not be far beyond 250 GPa.

In 2009 an alternative to this high-pressure $B1 - B2$ phase transition was proposed by considering the stabilization of new surstoichiometric phases LiH_2 and LiH_6 [27], presented in figure 11.1. Both phases were found to be energetically favoured above ~ 100 GPa relatively to LiH and H_2 . Very interesting features are predicted for these new phases:

- LiH_2 contains a guest hydrogen part made of H_2 units in a LiH host lattice, with a H-H distance at 150 GPa of 0.76 \AA *i.e.* close to that of an H_2 molecule. LiH_6 also contains H-H bonds but slightly stretched.
- Both phases are found to become metallic above 100 GPa as a result of an electron transfer from the electropositive Li ion.
- LiH_6 should be superconductor with a critical temperature of 31 K at 100 GPa [113].

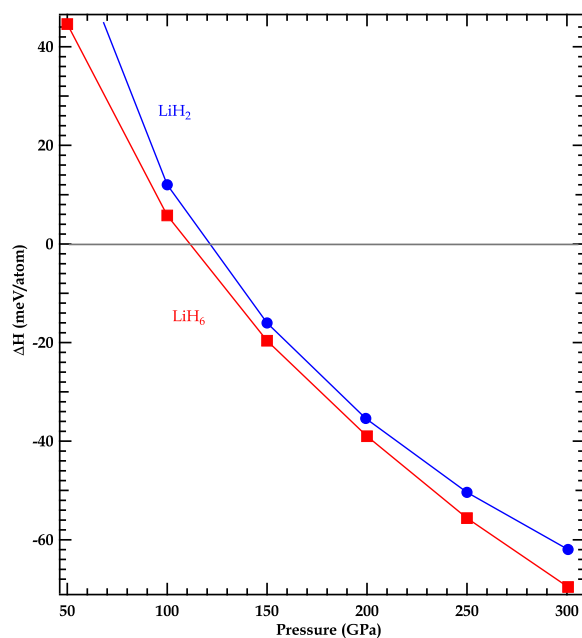
The metallic character of these new phases was obtained by Zurel *et al.* through the calculations of band gaps with DFT methods. However it is well known that DFT tends to underestimate the band gap of a material and thus the pressure necessary to metallize. Xie *et al.* therefore studied the LiH_2 as a function of pressure using the GW approximation [113]. Metallization, occurring through a progressive band gap closure, is then predicted at 175 GPa with this method. The case of LiH_6 is quite different as it is a native metal even at pressures where it is thermodynamically unstable against decomposition into LiH and H_2 . Experimentally attempts were made to synthesize these new compounds by compressing elemental lithium and hydrogen in a diamond anvil cell using Raman spectroscopy or X-ray diffraction to detect the possible synthesis of the overstoichiometric phases [111, 114]: no structural changes nor new high-frequencies Raman vibrations, predicted for LiH_2 and LiH_6 , could be observed. A subsequent study by Kuno *et al.* laser heated a sample of Li in hydrogen at low-pressure (~ 30 GPa) and reported the possible synthesis of LiH_x as they observed new Raman vibrations as well as a change of structure by X-ray diffraction [115]. The synthesized compounds was a transparent insulator up to 62 GPa.

In view of the literature two main issues needed to be addressed:

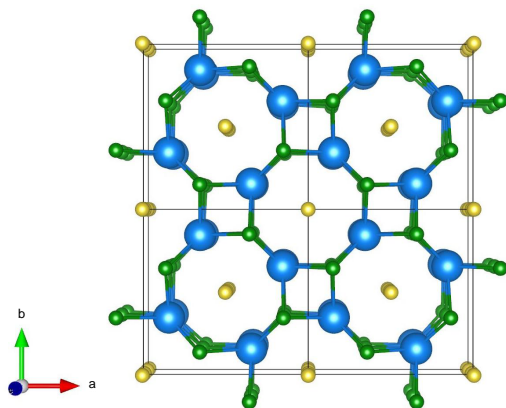
- Can the $B1 - B2$ transition be observed at ambient temperature and what is the pressure of transition?
- Can novel stoichiometries be stabilized and observed under pressure as it has been predicted?

We have chosen to perform measurements on LiH only using infra-red absorption spectroscopy as it presented several key advantages:

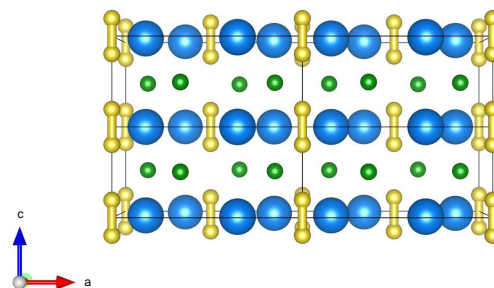
- It is a non-invasive probing technique and will therefore greatly reduce the probability to induce undesired chemical reactions.
- It is very sensitive to chemical changes, like the formation of a H-H bond in our case.
- This probing technique is ideally suited to detect semi-metallic or metallic states, which is exactly what we are looking for in the case of the $B1 - B2$ transition or in the case of the formation of metallic LiH_x compounds.
- It offers the possibility to measure the high pressure evolution of the longitudinal and transverse optical (LO-TO) phonon modes of LiH , and compare it with the extrapolation proposed by Lazicki *et al.* [111].



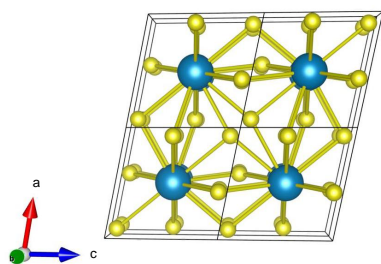
(a) Enthalpies of formation of LiH₂ and LiH₆ as a function pressure calculated by Zurek *et al.* where $\Delta H = H(\text{LiH}_n) - \frac{n-1}{2} H(\text{H}_2) - H(\text{LiH})$



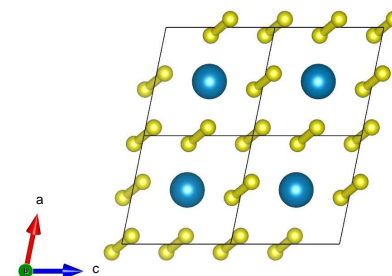
(b) View of LiH₂ along the *c* axis. Li atoms are represented in blue and the H atoms in two inequivalent positions in green and yellow respectively.



(c) View of LiH₂ along the *b* axis showing the presence of H₂ units.



(d) View of LiH₆ along the *b* axis. Li atoms are represented in blue and H atoms in yellow.



(e) View of LiH₆ along the *b* axis showing the presence of stretched H₂ units.

Figure 11.1: LiH₂ and LiH₆, as described by Zurek *et al.* .

As the expected pressures were all above the 200 GPa range, diamond anvil cells with culet sizes ranging from 25 to 40 μm were used. A high-purity LiH sample was loaded without pressure transmitting medium in the cell. Due to the very high reactivity of LiH with oxygen and water, the loading was performed in a glove box at the synchrotron SOLEIL, in an inert argon environment with less than 3 ppm of oxygen and water. Despite this precaution some samples were contaminated by water, evidenced in infra-red absorption by the presence of a broad absorption band at $\sim 3300\text{ cm}^{-1}$ shifting negatively under pressure and characteristic of the presence of LiOH [116]. Each time a new sample was reloaded.

When compressing pure LiH below 130 GPa the only observed absorption came from the LO-TO modes and their evolution under pressure was in good agreement with the results from Lazicki *et al.* even though we noticed a large broadening due to non-hydrostatic stresses. Above 130 GPa drastic changes in the absorption spectra were observed: two new weak absorption bands could be observed around 2500 cm^{-1} , in agreement with the predictions from Zurek *et al.* for LiH₆. The LO-TO absorption from LiH could still be observed. As the pressure increases the intensity of the two new absorption bands became stronger. Above 160 GPa a third absorption appeared around 4000 cm^{-1} and the three new peaks could be monitored up to 215 GPa before the systematic failure of our diamonds. The predicted vibron frequency for LiH₂ suggests its formation above 160 GPa. Our experimental observation of LiH_{*n*} products implies that a disproportionation into layers takes place in the LiH sample at high pressure: we were able to simultaneously observe characteristic absorptions from LiH, LiH₂ and LiH₆. Moreover we propose that the disproportionation mechanism involves a diffusion of Li in diamond: the affinity of Li with carbon sucks the Li from the LiH sample at the interface with diamond and the transformed interface layer evolves to the LiH_{*n*} compound having the minimum enthalpy, predicted to be LiH₆. After the formation of LiH₆ through diffusion of Li, it is in presence of LiH which leads to the formation of LiH₂ as illustrated by the convexity of the convex Hull proposed by Zurek *et al.* .

Further experiments were conducted at lower temperatures: 77 K and 18 K. The appearance of the two new vibrons, hence the transformation to LiH₆, occurs at higher pressure for lower temperatures: 180 GPa at 77 K and it was not observed up to 250 GPa at 18 K. The Li/C reactivity is hindered at lower temperature, explaining the increase of the pressure transition at lower temperature. Moreover such activation law, fitted by an Arrhenius law in our case, suggests that the B1 – B2 phase transition in LiH might never be observed by compressing pure LiH in contact with a diamond even down to 4 K, as it would be in concurrence with LiH₆ formation.

These results have been published in June 2015 in the journal *Proceedings of the National Academy of Science* in an article entitled "*Synthesis of Lithium polyhydrides above 130 GPa at 300 K*", attached in the following pages.

11.2 Article: "Synthesis of Lithium polyhydrides above 130 GPa at 300 K"

Synthesis of lithium polyhydrides above 130 GPa at 300 K

Charles Pépin^a, Paul Loubeyre^{a,1}, Florent Ocelli^a, and Paul Dumas^b

^aCommissariat à l'Énergie Atomique, Centre DAM - Ile de France, F-91297 Arpajon, France; and ^bSynchrotron SOLEIL, F-91192 Gif-sur-Yvette, France

Edited by Michael L. Klein, Temple University, Philadelphia, PA, and approved May 15, 2015 (received for review April 17, 2015)

The prediction of novel lithium hydrides with nontraditional stoichiometries at high pressure has been seminal for highlighting a promising line of research on hydrogen-dense materials. Here, we report the evidences of the disproportionation of LiH above 130 GPa to form lithium hydrides containing H₂ units. Measurements have been performed using the nonperturbing technique of synchrotron infrared absorption. The observed vibron frequencies match the predictions for LiH₂ and LiH₆. These polyhydrides remain insulating up to 215 GPa. A disproportionation mechanism based on the diffusion of lithium into the diamond anvil and a stratification of the sample into LiH₆/LiH₂/LiH layers is proposed. Polyhydrides containing an H₂ sublattice do exist and could be ubiquitously stable at high pressure.

high pressure | hydride chemistry | hydrogen stoichiometry

Over the past 5 y, and since the prediction of stable LiH_n compounds at high pressure has been proposed (1), numerous calculations have unveiled a novel view on the chemical combination of hydrogen with metals under pressure (2–7). Three remarkable trends have been identified: (i) Hydrogen stoichiometry should drastically increase under pressure in metals. (ii) Polyhydrides with nontraditional stoichiometries, in some cases containing an H₂ sublattice, should be stable. (iii) These hydrogen-dense systems may become metallic at much lower pressure than expected for metallic hydrogen and could have a high-temperature superconductivity (8, 9). These theoretical results have impelled an active experimental search (e.g., refs. 10 and 11).

Very recently, a few experimental results have particularly illustrated the richness of this line of research. A significant change of the H content in a transition metal has been reported by directly compressing rhodium in fluid hydrogen. The transition from RhH to RhH₂ is associated with the change of interstitial hydrogen from octahedral to tetrahedral sites (12). Two novel iron hydrides, FeH₂ and FeH₃, have been discovered under pressure, in the sequence FeH–FeH₂–FeH₃ that follows the expected drastic increase of hydrogen content upon pressure increase (13). Moreover, FeH₂ and FeH₃ adopt intriguing structures with layers of atomic hydrogen. Finally, a superconducting critical temperature (*T_c*) of 190 K has been measured in H₂S compressed to about 200 GPa, which breaks the cuprate record of superconductivity temperature (14, 15). The understanding of such a high *T_c* suggests that decomposition of H₂S sample to form the H₃S superconducting phase occurs at high pressure in the diamond anvil cell. Here, we directly show the existence under pressure of novel forms of lithium polyhydrides, possibly LiH₆ and LiH₂, each containing a sublattice of H₂ units.

Results and Discussion

Previous works have investigated the stability of new Li–H compounds by compressing pure Li in hydrogen, LiH in hydrogen, or pure LiH (16, 17). Stoichiometric LiH is invariably formed. Solid LiH has a rock salt structure (B1) that was observed to remain stable up to 160 GPa and 250 GPa, using Raman spectroscopy and X-ray diffraction, respectively. Any appearance of the predicted hydrogen-rich compounds in these experiments might have been

either hindered by the kinetics or not detected because the probing techniques were not sensitive enough. Heating of these Li–H samples in the diamond anvil cell (DAC) could help to overcome a possible kinetic barrier, but, since Li–H systems form transparent and reactive materials, a controlled heating without chemical contamination by the confinement materials is quite difficult to avoid. Instead we have chosen to perform the measurements using a noninvasive probing technique that has a great sensitivity to chemical changes, namely infrared (IR) absorption measurements. Moreover, IR absorption is ideally suited to detect a metallic character of the sample.

The pressure evolution in the IR transmission spectra of LiH collected at 300 K is illustrated in Fig. 1. The IR transmission of the unloaded empty DAC is used as the reference to obtain the IR absorption bands of the LiH_n sample. Up to 130 GPa, the only observed feature is a broad absorption band that rapidly shifts upward under pressure, from 800–1,200 cm^{−1} under a few gigapascals to 1,900–2,300 cm^{−1} at 100 GPa. This band corresponds to the longitudinal and transverse optical (LO–TO) modes of solid LiH that merge into a band due to nonhydrostatic pressure stress broadening, since no pressure-transmitting medium was used. Above 130 GPa, two well-resolved peaks become clearly identified between 2,500 cm^{−1} and 3,000 cm^{−1} while the broad band below 2,000 cm^{−1} is still present. We also note that there is no significant absorption in the lower wave numbers domain, indicating no sign of a semimetallic state. A chemical and/or structural change in the sample clearly occurs above 130 GPa at 300 K and was successfully reproduced in two independent experiments.

Fig. 2 shows more specifically the representative absorption spectra of LiH samples above 2,300 cm^{−1}. Two peaks, denoted ν_1 and ν_2 , appear around 2,500 cm^{−1} above 130 GPa. Their intensity increases with pressure. Above 160 GPa, another peak, ν_3 , is observed around 4,000 cm^{−1}. The frequency shift with pressure of these three IR peaks and of the absorption band below 2,000 cm^{−1} could be monitored up to 215 GPa, as plotted in Fig. 3. The ν_1 , ν_2 , and ν_3 peaks are ascribed to vibrons of H₂ entities. We use the calculated phonon density of states in LiH_n compounds to interpret our data and provide an assignment for these various peaks (1, 18). It should be noted first that the frequency as well as the

Significance

High hydrides with unusual stoichiometries have been predicted to become energetically favored in various hydrides of alkali and alkali earth metals under pressure. This paper reports on synchrotron infrared spectroscopic measurements on lithium hydride (LiH) compressed in a diamond anvil cell up to 215 GPa, showing that insulating lithium polyhydrides containing H₂ units are synthesized above 130 GPa at 300 K. The observed vibron frequencies are in good agreement with the predictions for LiH₂ and LiH₆.

Author contributions: C.P. and P.L. designed research; C.P., P.L., F.O., and P.D. performed research; C.P. and P.L. analyzed data; and C.P. and P.L. wrote the paper.

The authors declare no conflict of interest.

This article is a PNAS Direct Submission.

¹To whom correspondence should be addressed. Email: paul.loubeyre@cea.fr.

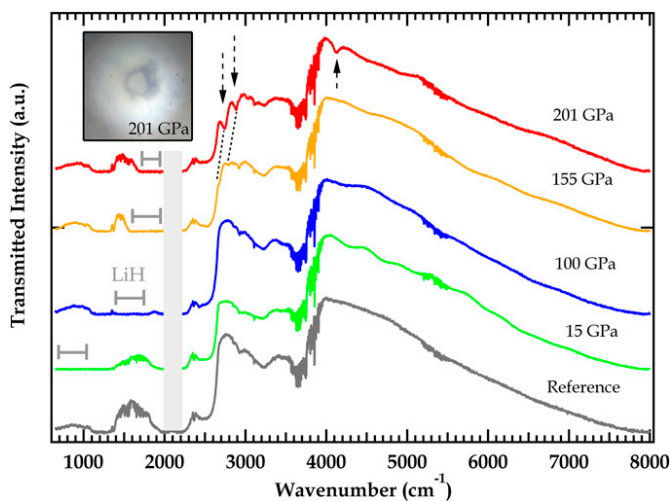


Fig. 1. IR transmission spectra at selected pressures, at 300 K. The broad absorption band corresponding to the LO-TO modes of LiH is visible at low wavenumbers and is framed by the gray cursor as a guide for the eyes. The new absorption peaks originating from LiH₂ and LiH₆ are indicated by black arrows at 201 GPa. The absorption peaks below 3,000 cm⁻¹ can be observed at 155 GPa. (Inset) Photograph of the optically transparent sample at 201 GPa. The frequency range of the high two-phonon absorption of the diamond has been masked for clarity purposes.

positive pressure-induced frequency shift of these peaks does not match with the infrared absorption spectra of pure solid H₂ (19). The latter is at higher frequency and exhibits a negative pressure dependence. This rules out the possibility of a dissociation of LiH to form LiH_x ($x < 1$) and solid H₂ that was recently predicted around 90 GPa (20). LiH₂ is thought of as containing interpenetrating Li⁺H⁻ and H₂ sublattices, with a weak interaction between them. The H–H distance should be similar to the one in pure solid H₂. Thus, the H₂ vibron frequency in LiH₂ is predicted around 4,000 cm⁻¹ with a positive pressure frequency shift. In

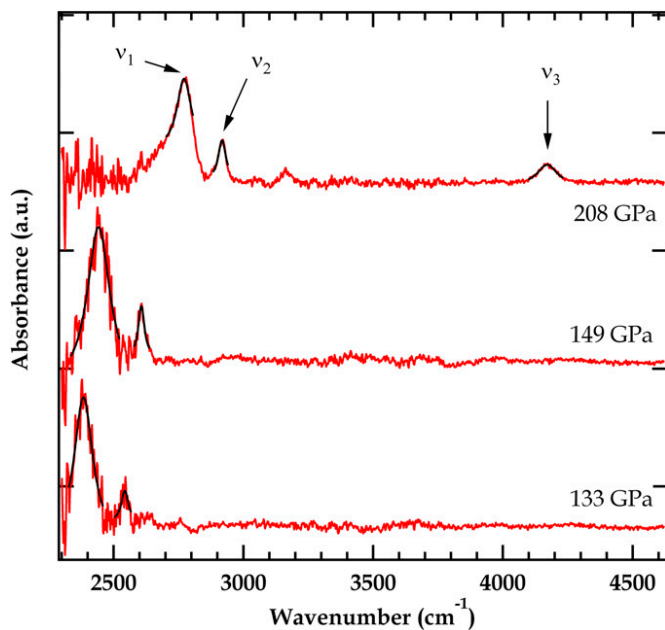


Fig. 2. Selected IR absorbance spectra at 300 K above 2,300 cm⁻¹. The absorption peaks labeled ν_1 and ν_2 both appeared above 130 GPa. A third peak, labeled ν_3 , appeared upon further compression above 160 GPa.

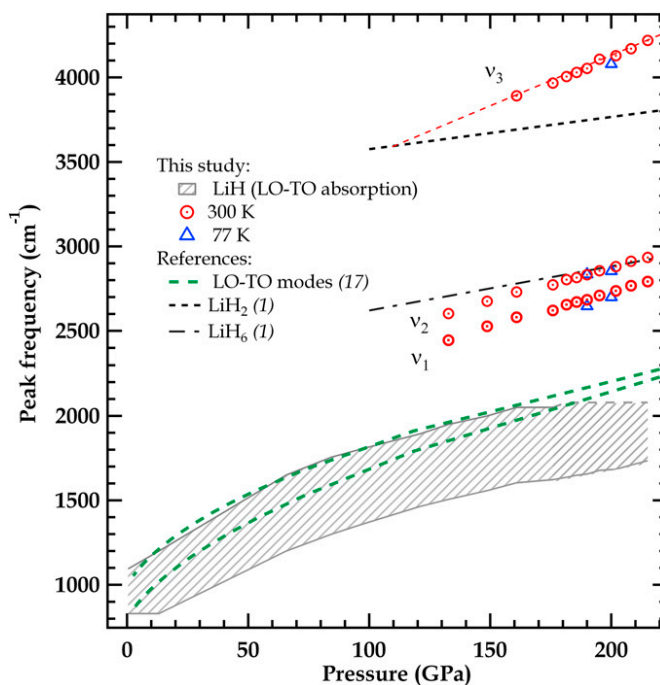


Fig. 3. Pressure dependence of the absorption peaks at 300 K and 77 K. Estimation of the LO-TO frequencies from Raman measurements from Lazicki et al. (17) are shown, as well as the most intense calculated frequencies for LiH₂ and LiH₆ by Zurek et al. (1). The measured lower and upper bounds of the LO-TO absorption band of LiH are shown.

contrast to LiH₂, LiH₆ and other LiH_n ($n = 4-8$) contain H₂ units with slightly stretched H–H bonds, since the Li atom transfers its valence electron to H₂ molecules, hence populating the anti-bonding state and weakening the H₂ molecule. In this case, vibron frequencies are predicted to be in the 3,000 cm⁻¹ range. The predicted vibron frequencies for LiH₂ and LiH₆ are plotted in Fig. 3 and compared with our data. The reasonable agreement between ν_1 , ν_2 , and ν_3 with LiH₆ and LiH₂ vibrons frequencies suggests their formation. In all LiH_n compounds, the other phonon modes, associated with Li atoms or intermolecular vibrations, fall below 2,000 cm⁻¹, i.e., in the measured broad band. As seen in Fig. 3, the evolution of the band is also in good agreement with the evolution of the LO-TO frequencies of LiH, as measured from Raman measurements (17). Therefore, this low-frequency band is not a distinctive criterion for a stoichiometry change in the LiH sample.

The observation of LiH_n products implies that a disproportionation reaction has taken place in the LiH samples under pressure. Other evidence contributes to disclose a possible mechanism of this transformation. In all our LiH compression experiments, the diamond anvils always broke at an unusually low pressure compared with the numerous other studies performed with our DACs. Each failure was identified by a crack propagating from the tip of the anvil. Since no formation of Li could be detected in the sample from a change of the IR absorption, we assume that the excess Li is diffusing into the diamond anvils, as has been reported for pure Li, and so making the crack (21). The convex hull diagram of the relative enthalpies calculated for LiH_n compound indicates that LiH should be always stable if the compressed sample keeps an equal ratio of Li and H (1). In the present case, the affinity of Li with carbon sucks the Li from the LiH sample at the interface with diamond, and the transformed interface layer evolves to the LiH_n compound having the minimum enthalpy, predicted to be LiH₆. The hypothesis of a Li/C chemical reaction was strengthened by

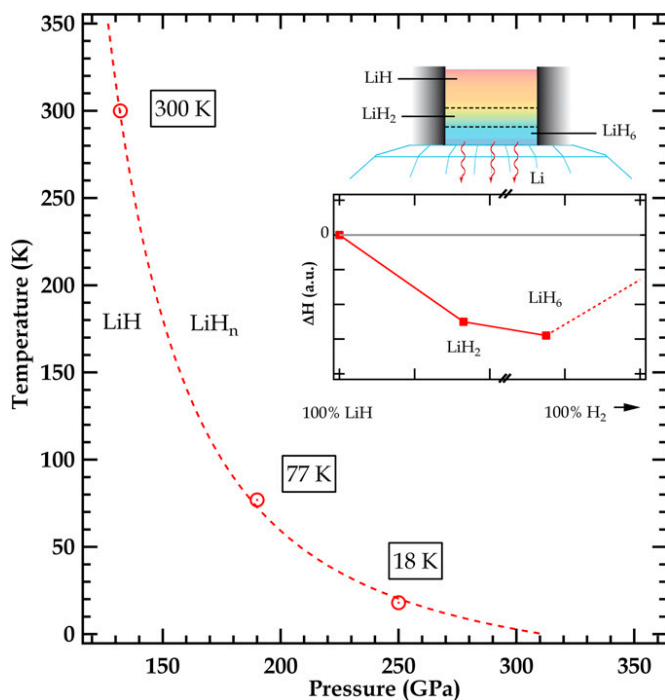


Fig. 4. Temperature dependence of the disproportionation mechanism fitted by an Arrhenius law. The B1–B2 pressure transition in LiH is predicted by Lebègue et al. (22) to take place at 329 GPa and is never intersected by the transition line. The pressure at 18 K corresponds to a lower estimation, as the transition was not observed up to 250 GPa. (Inset) Schematic mechanism of the structuration of the sample in layers via the chemical reaction of lithium with the anvils and according to the convex hull proposed by Zurek et al. (1).

performing the LiH compression experiments at low temperature. The appearance of the ν_1 and ν_2 vibrons, hence the transformation to LiH_6 , occurs at higher pressure for lower temperatures—180 GPa at 77 K—and it was not observed up to 250 GPa at 18 K. As seen in Fig. 4, the Arrhenius law fitted for this transition line is indicative of an activation mechanism that is in agreement with the reactivity–diffusion mechanism of Li with diamond. Hence, the Li/C reactivity somehow helps to change the hydrogen composition of the sample and to overcome the energy barrier of the disproportionation reaction [the reaction barrier hindered the transformation of LiH compressed in hydrogen to 160 GPa at 300 K (16)]. It is also interesting to note that the B1–B2 transition, and hence the metallic form of LiH, predicted to occur around 329 GPa (22) might never be observed by compressing pure LiH in a DAC, even at 4K.

By going up in pressure, the appearance of LiH_6 and LiH_2 is, in fact, an illustration of the convexity of the hull diagram. Above

130 GPa, the diffusion of Li in C favors the formation of a LiH_6 layer in contact with the anvil. However, at the interface between this LiH_6 layer and LiH, the formation of a LiH_2 layer lowers the enthalpy due to the convexity of the hull diagram. This mechanism of the structuration of the sample in layers is illustrated in Fig. 4, Inset. The appearance of such layers also explains why the diffraction peaks of LiH were still measured up to 250 GPa, since the central part of the sample was still a single crystal of LiH. However, it should be noted that the detection of the diffraction peaks corresponding to LiH_6 or LiH_2 would be nearly impossible, since only the diffraction of a single crystal can give a measurable signal.

Finally, the compressed LiH sample remained optically transparent up to 215 GPa, and the infrared absorption did not show any characteristic feature of a semimetallic state. Such observation is at odds with calculations, since LiH_6 is predicted to have a structure with one formula unit in the unit cell and so to be a native metal (1, 18). Our observation hence implies either that the structure of LiH_6 has more than one formula unit or that another stoichiometry corresponds to the minimum enthalpy of the convex hull diagram. The band gap of LiH_2 is also predicted to close above 170 GPa (18), but it could be that the metallic transition pressure was underestimated.

To summarize, novel forms of polyhydrides with nontraditional stoichiometry and containing H_2 units, ubiquitously predicted for alkaline and alkaline earth metals, do exist. Such counterintuitive compounds, like LiH_6 (18), are expected to be high- T_c superconductors (8). These experimental results, alongside the recent findings on sulfur hydride (14, 15), should stimulate further experimental and theoretical efforts to achieve their metallization and study their metastability.

Methods

Four different experiments were conducted by compressing LiH in a membrane diamond anvil cell equipped with 40- μm diamond anvil culet size at various temperatures: two at 300 K, one at 77 K, and one at 18 K. Careful loading of high-purity LiH grains was handled in a glove box in an inert argon environment with less than 3 ppm oxygen and water. No pressure medium was used, and LiH was directly compressed in rhenium gaskets coated with gold. A photograph of a sample under white light transmission is shown in Fig. 1. No trace of chemical contamination of the sample could be detected in the IR absorption spectra. The IR experimental configuration is the one used previously for our measurements in solid H_2 to 290 GPa at the SMIS beamline of the SOLEIL synchrotron (23). A home-made horizontal IR microscope, equipped with two Schwarzschild objectives (47-mm working distance, numerical aperture 0.5) enables the use of a He flow cryostat. Infrared spectra were taken with a 4 cm^{-1} resolution and 512 scans. A Raman system, mounted on the same bench, enables measurement of the high-frequency edge of the T_{2g} Raman band of the diamond at the anvil/sample interface and estimation from it of the sample pressure by using the calibration of ref. 24.

ACKNOWLEDGMENTS. The authors acknowledge the SOLEIL synchrotron for provision of beam time.

- Zurek E, Hoffmann R, Ashcroft NW, Oganov AR, Lyakhov AO (2009) A little bit of lithium does a lot for hydrogen. *Proc Natl Acad Sci USA* 106(42):17640–17643.
- Wang H, Tse JS, Tanaka K, Iitaka T, Ma Y (2012) Superconductive sodalite-like clathrate calcium hydride at high pressures. *Proc Natl Acad Sci USA* 109(17):6463–6466.
- Baettig P, Zurek E (2011) Pressure-stabilized sodium polyhydrides: NaH_n ($n > 1$). *Phys Rev Lett* 106(23):237002.
- Hooper J, Zurek E (2012) Rubidium polyhydrides under pressure: Emergence of the linear H_3 species. *Chemistry* 18(16):5013–5021.
- Zaleski-Ejgierd P, Labet V, Strobel TA, Hoffmann R, Ashcroft NW (2012) WH_n under pressure. *J Phys Condens Matter* 24(15):155701.
- Bazhanova ZG, Oganov AR, Gianola O (2012) Fe–C and Fe–H systems at pressures of the Earth's inner core. *Phys. Usp* 55(5):489.
- Gao G, et al. (2013) Theoretical study of the ground-state structures and properties of niobium hydrides under pressure. *Phys Rev B* 88(18):184104.
- Ashcroft NW (2004) Hydrogen dominant metallic alloys: High temperature superconductors? *Phys Rev Lett* 92(18):187002.
- Duan D, et al. (2014) Pressure-induced metallization of dense $(\text{H}_2\text{S})_2\text{H}_2$ with high- T_c superconductivity. *Sci Rep* 4:6968.
- Eremets MI, Trojan IA, Medvedev SA, Tse JS, Yao Y (2008) Superconductivity in hydrogen dominant materials: Silane. *Science* 319(5869):1506–1509.
- Goncharenko I, et al. (2008) Pressure-induced hydrogen-dominant metallic state in aluminum hydride. *Phys Rev Lett* 100(4):045504.
- Li B, et al. (2011) Rhodium dihydride (RhH_2) with high volumetric hydrogen density. *Proc Natl Acad Sci USA* 108(46):18618–18621.
- Pépin CM, Dewaele A, Geneste G, Loubeyre P, Mezouar M (2014) New iron hydrides under high pressure. *Phys Rev Lett* 113(26):265504.
- Strobel TA, Ganesh P, Somayazulu M, Kent PRC, Hemley RJ (2011) Novel cooperative interactions and structural ordering in $\text{H}_2\text{S-H}_2$. *Phys Rev Lett* 107(25):255503.
- Drozdov AP, Eremets MI, Trojan IA (2015) Conventional superconductivity at 190 K at high pressures. arXiv:1412.0460.
- Howie RT, Narygina O, Guillaume CL, Evans S, Gregoryanz E (2012) High-pressure synthesis of lithium hydride. *Phys Rev B* 86(6):064108.

17. Lazicki A, Loubeyre P, Occelli F, Hemley RJ, Mezouar M (2012) Static compression of LiH to 250 GPa. *Phys Rev B* 85(5):054103.
18. Xie Y, Li Q, Oganov AR, Wang H (2014) Superconductivity of lithium-doped hydrogen under high pressure. *Acta Crystallogr C Struct Chem* 70(Pt 2):104–111.
19. Hanfland M, Hemley RJ, Mao HK, Williams GP (1992) Synchrotron infrared spectroscopy at megabar pressures: Vibrational dynamics of hydrogen to 180 GPa. *Phys Rev Lett* 69(7):1129–1132.
20. Hooper J, Zurek E (2012) Lithium subhydrides under pressure and their superatom-like building blocks. *ChemPlusChem* 77(11):969–972.
21. Guillaume CL, et al. (2011) Cold melting and solid structures of dense lithium. *Nat Phys* 7(3):211–214.
22. Lebègue S, Alouani M, Arnaud B, Pickett WE (2003) Pressure-induced simultaneous metal-insulator and structural-phase transitions in LiH: A quasiparticle study. *Eur. Lett.* 63(4):562.
23. Loubeyre P, Occelli F, Dumas P (2013) Hydrogen phase IV revisited via synchrotron infrared measurements in H₂ and D₂ up to 290 GPa at 296 K. *Phys Rev B* 87(13):134101.
24. Akahama Y, Kawamura H (2006) Pressure calibration of diamond anvil Raman gauge to 310 GPa. *J Appl Phys* 100(4):043516.

Chapter 12

Iron hydrides

12.1 Introduction

The Earth's core is primarily made up of iron but experimental constraints on the density of iron at the core conditions show that pure iron is ~ 3 to 5% denser than the solid inner core [117]. The incorporation of one or more light elements has been suggested to resolve this core-density deficit, as the resulting alloy would have an expanded volume and a reduced average atomic mass compared to pure iron [118]. Hydrogen is considered as a possible light element as it was likely introduced in the form of water during the Earth formation with the possibility for a Fe+H₂O to react to form FeO and FeH_x [119]. Thus the iron-hydrogen system has been the subject of several studies and the low-pressure part of its phase diagram is relatively well-known, as it can be seen in figure 12.1. At ambient conditions the solubility of hydrogen in body-centered cubic iron (α -Fe) is very low and FeH_x with $x \sim 1$ only forms around ~ 3 GPa [121]. The first observation of an iron hydride was made in 1980 [122] and the structure determination at ambient temperature of this hydride, called ϵ' -FeH _{$x \sim 1$} , was performed a few years later, alongside its equation of state up to 60 GPa [123]. It consists of double hexagonal close-packed (dhcp) structure with close-packed iron layers stacked along the c-axis in an ABAC sequence (Wickoff positions 2a for atoms in the layer A, and 2c for atoms in the layers B and C), with hydrogen occupying all available octahedral interstitial sites as determined by neutron powder diffraction [121]¹. Neutron powder refinements also proposed the existence of a small vertical displacement (0.06 Å) of the hydrogen atoms towards the iron atoms in positions 2a. Consequently the electron density near the Fermi level is significantly altered, inducing a ferromagnetic ordering, while this magnetism is lost in pure ϵ -Fe [124, 125]. Experimentally the ferromagnetic-nonmagnetic transition has been shown to occur near ~ 30 GPa at 300 K [126, 127].

The low-pressure part of the FeH phase-diagram has also been extensively studied and the results published in a recent study by Sakamaki *et al.* [120] were reproduced in figure 12.1. At high-temperature a face-centered cubic phase is formed, γ -FeH_x, with the same structure than γ -Fe with hydrogen occupying the octahedral sites. The correct estimation of the stoichiometry is still needed as only x-ray diffraction have been performed on this phase γ -FeH_x, predicting $x = 1.1$ to 1.2 which suggests that some tetrahedral interstitial sites are occupied or that the method used to determine the stoichiometry (based on the cell volume expansion of 1.9 Å³/H determined from degassing experiments of γ -Fe_{0.65}Mn_{0.29}Ni_{0.06}H_{0.96}) is incorrect [120, 128]. High-temperature experiments also revealed the existence of a melting point depression around ~ 5 GPa [119] and showed the melting curve is drastically affected by the incorporation of

¹The neutron powder diffraction refinements also allowed to determine the stoichiometry of the hydride of 0.98. From now on we will then assume that this phase has an ideal stoichiometry of 1 and will be referred as ϵ' -FeH.

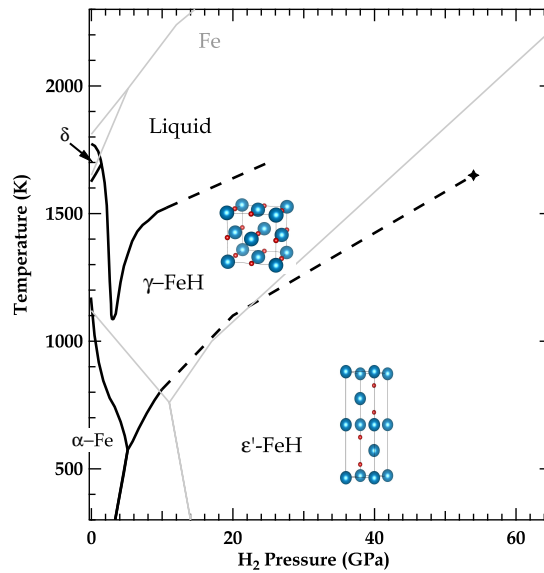


Figure 12.1: Known phase diagram of FeH adapted from ref. [120].

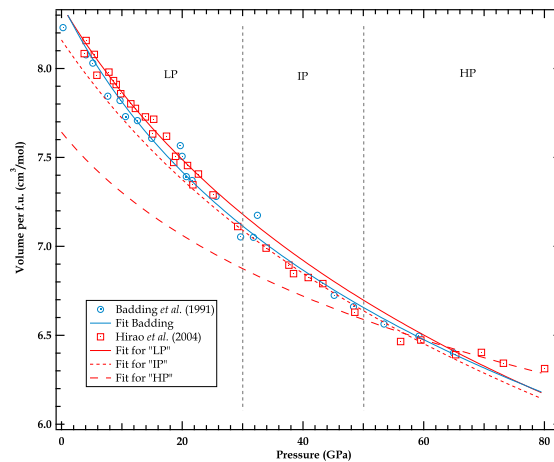


Figure 12.2: Pressure-volume data points for dhcp-FeH.

hydrogen, lying ~ 800 K below the melting curve of γ -Fe [120, 129]. Based on these results a γ - ϵ' -liquid triple point has been predicted near 60 GPa and 2000 K. A later study by Narygina *et al.* revised the position of this triple point around 80 GPa and 2000 K.

The high-pressure part of this phase diagram on the other hand drastically lacks informations despite the clear need of experimental data relevant for the Earth's core (pressures > 130 GPa) or planetary cores. The pressure-volume relationship for ϵ' -FeH has been studied up to 60 GPa in 1991 by Badding *et al.* [123] and extended up to 80 GPa by Hirao *et al.* in 2004. These results are presented in figure 12.2. Hirao *et al.*, unlike Badding *et al.*, identified three distinct compression regimes : low-pressure "LP" between 0 and 30 GPa, intermediate pressure "IP" between 30 and 50 GPa, high-pressure "HP" between

50 and 80 GPa. As no phase transition was observed in the studied pressure, the anomalous compression behaviour was attributed either to the FM-NM transition or to a change of hydrogen solubility in iron between 30 and 50 GPa. This change in compressibility was later interpreted in a theoretical study by Isaev *et al.* as a dhcp→hcp phase transition [130]. Another phase transition was predicted in this study to occur above 80 GPa towards a face-centered cubic phase.

Recently the possibility to stabilize new phases with greater H-stoichiometry under high-pressure was considered theoretically for the first time in 2012 by Bazhanova *et al.* [35]. Using a random searching method this study predicts the stability of a simple cubic FeH₃ phase and of a monoclinic FeH₄ at pressures of the Earth's inner core (*i.e.* above 330 GPa).

In this context our study was focused on the following issues:

- What is the high-pressure of dhcp-FeH? Can the progressive increase in compressibility observed by Hirao *et al.* be reproduced and does it extend at higher pressure?
- Can the two phase transitions predicted for FeH by Isaev *et al.* be experimentally confirmed?
- Are new stoichiometries stabilized under pressure like it has been suggested by Bazhanova *et al.* and can we measure their equation of state?
- If new phases with a greater stoichiometry are synthesized under pressure, can they be recovered at ambient conditions?

Previous experimental studies on dhcp-FeH encountered two major issues: first the increased reactivity of hydrogen under high pressure and high temperature greatly limited the available pressure range, second, when dhcp-FeH forms at 3.5 GPa and 300 K the resulting compound is a poorly crystallized powder exhibiting broad diffraction peaks. The later effect deteriorates the accuracy of the volume determination which explains the scattering of data points in figure 12.2. Such poor recrystallization effect at a phase transition had already been encountered in the study of aluminum hydride: the same method, a mild laser heating of the sample in hydrogen medium at low pressure, was therefore used to improve the samples crystalline quality. The improvement is evidenced by sharper X-ray diffraction lines, as seen in figure 12.3. This method allowed us to reduce the volume uncertainty and hence to reduce the scattering of our data points. The volume as a function of pressure was then measured up to 136 GPa, allowing us to conclude that:

- No change in compressibility is observed up to the maximum studied pressure.
- No phase transition occurs in the [3.5 - 136 GPa] pressure range.

Laser heating of an iron foil in hydrogen medium was performed at several pressures: 12, 17, 27, 67, 70, 84, 86 and 90 GPa. At 12, 17 and 27 GPa the temperature was kept below 1000 K in order to avoid quenching the fcc-phase. Except for the improvement of the sample quality no phase nor volume change was observed. Laser heating between 67 and 86 GPa leads to the appearance of new XRD peaks that could not be indexed by any of the known or predicted phases for FeH_x. The Rietveld refinement of the integrated diffraction pattern gives a tetragonal unit cell with the symmetry $I4/mmm$ and four iron atoms in Wyckoff positions 4e (0, 0, 0.853). Because of the very low scattering of the H atoms, as seen in section 6.1, their positions could not be determined using XRD data. However, having determined the multiplicity of the Fe atoms we were able to determine that the volume per Fe atom of the new phase was $\sim 4 \text{ \AA}^3$ larger than the one of pure Fe and $\sim 2 \text{ \AA}^3$ larger than the one we had measured for dhcp-FeH at the same pressure. Such $\Delta V \sim 2 \text{ \AA}^3$ is very close to the value determined from the volume expansion

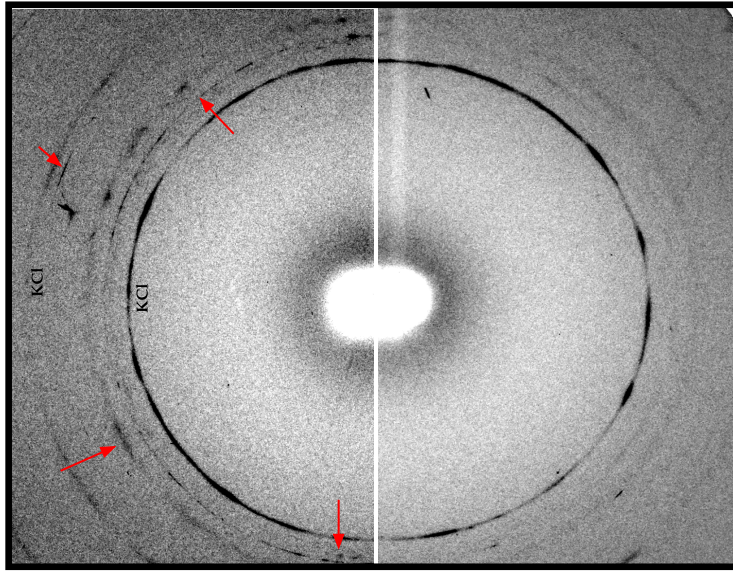


Figure 12.3: Image plates illustrating an example of recrystallization of dhcp-FeH. The image plate on the right shows the signal obtained before laser heating, and after laser heating on the left. The acquisition time is the same in both cases. The sharper XRD lines are evidenced by the red arrows.

associated to the formation of $3d$ metal monohydrides [46]. We then assumed a constant volume expansion upon the stoichiometry increase of 1 in FeH_x , which lead to the stoichiometry FeH_2 . Moreover the volume per formula unit of FeH_2 is smaller than the one of ideal mixing of Fe and H_2 solids at the same pressure, as expected for a compound formation at high pressure. Combining these volume considerations with *ab initio* calculations the positions of the H atoms were determined and the structure of this new FeH_2 phase is shown in figure 12.4.

Laser heating above 86 GPa then lead to the disappearance of the XRD lines of the FeH_2 phase. The Rietveld refinement gives a simple cubic unit cell with the symmetry $Pm\bar{3}m$, with Fe in position $1a$ (0,0,0), with a volume $\sim 2 \text{ \AA}^3$ larger than the one in FeH_2 , meaning that this phase is likely to have an FeH_3 stoichiometry. With H atoms in positions $3c$ ($0, \frac{1}{2}, \frac{1}{2}$) this structure corresponds to the one predicted by Bazhanova *et al.* [35]. The determination of these two new phases allowed us to propose a new phase diagram for the Fe-H system, as shown in figure 12.4.

Both FeH_2 and FeH_3 could be meta-stably recovered at lower pressure, down to 23 GPa and 39 GPa respectively, allowing us to determine their equation of state upon decompression.

it is important to note that upon pressure increase the stoichiometry in this hydride goes from Fe to FeH then to FeH_2 and finally to FeH_3 , *i.e.* the stoichiometry in the hydride increases with pressure with hydrogen not occupying interstitial sites anymore. This point, as we have seen in the general introduction, corresponds to the implicit rule emerging from numerous first-principles, namely that the hydrogen content in hydrides should significantly increase with pressure. This study is the first experimental observation and confirmation of such an increase of hydrogen stoichiometry in an hydride through discontinuous steps.

These results have been published in December 2014 in the journal *Physical Review Letters* in an arti-

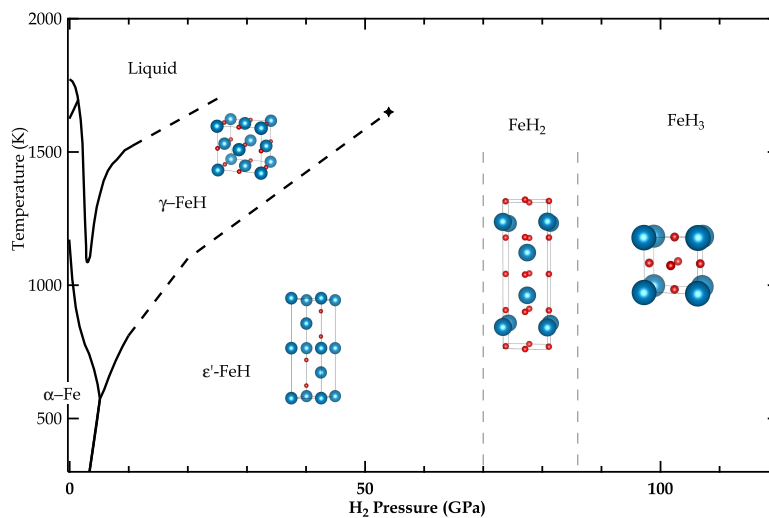


Figure 12.4: The revised phase diagram of the Fe-H system up to 130 GPa, showing for each different observed phases its structure and its stoichiometry. Iron atoms are represented in blue and hydrogen atoms in red.

cle entitled "*New Iron Hydrides under High Pressure*", attached in the following pages.

12.2 Article: "New Iron Hydrides under High Pressure"

New Iron Hydrides under High Pressure

Charles M. Pépin,^{*} Agnès Dewaele, Grégory Geneste, and Paul Loubeyre[†]
CEA, DAM, DIF, F-91297 Arpaçon, France

Mohamed Mezouar

ESRF, 6 Rue Jules Horowitz BP220, F-38043 Grenoble Cedex, France

(Received 25 July 2014; revised manuscript received 13 November 2014; published 30 December 2014)

The Fe-H system has been investigated by combined x-ray diffraction studies and total energy calculations at pressures up to 136 GPa. The experiments involve laser annealing of hydrogen-embedded iron in a diamond anvil cell. Two new FeH_x compounds, with $x \sim 2$ and $x = 3$, are discovered at 67 and 86 GPa, respectively. Their crystal structures are identified (unit cell and Fe positional parameters from x-ray diffraction, H positional parameters from *ab initio* calculations) as tetragonal with space group *I4/mmm* for FeH_{~2} and as simple cubic with space group *Pm3m* for FeH₃. Large metastability regimes are observed that allowed to measure the $P(V)$ equation of state at room temperature of FeH, FeH_{~2}, and FeH₃.

DOI: 10.1103/PhysRevLett.113.265504

PACS numbers: 81.40.Vw, 88.85.mh

Under pressure, most transition metals form hydrides, usually with a H:metal ratio close to 1 [1]. But this view of chemical combination should be considerably expanded by going in the 100 GPa pressure range. Indeed, a rough rule emerges from numerous first-principles calculations on the reaction of H₂ with various normal and transition metals, namely, that the hydrogen content of their hydrides should significantly increase with pressure. Therefore, predictions of polyhydrides with unusual stoichiometries abound such as LiH₂, LiH₆ [2], NaH₉ [3], CaH₆ [4], FeH₃, and FeH₄ [5]. Up to now, this remarkable high pressure behavior of hydrides has been awaiting clear experimental confirmation. In this Letter we show that under pressure the hydrogen content in Fe dramatically increases through discontinuous steps, leading to the formation of two new FeH_x compounds: FeH_{~2}, composed by alternate layers of atomic H and of Fe, and FeH₃.

Pure Fe and H₂ solids have been extensively studied under pressure over the past 30 years, disclosing very intriguing properties [6,7]. The study of FeH_x compounds could be as interesting. By significantly varying the Fe:H ratio in the iron hydrides, one can expect the properties of FeH_x to be tuned from ironlike to hydrogenlike. On the one hand, the phase diagram of FeH is related to the one of pure iron, with a face-centered cubic (fcc) structure under P - T conditions similar to the stability field of fcc Fe [8,9] (see Fig. 1). Also, FeH is ferromagnetic at low pressures and undergoes a magnetic collapse around 22 GPa [10], at a slightly higher pressure than the one in Fe. On the other hand, hydrogen rich compounds should have analogous properties to those of metallic hydrogen and so hold promise as high temperature superconductors [11], with predictions of superconductivity critical temperature as high as 220 K in CaH₆ [4]. As such, hydrogenlike properties could be expected for FeH_{x>1} compounds.

Apart from these fundamental issues, the observed stability of novel iron hydrides under high pressure should have a significant impact on planetary interior modeling since Fe and H are two of their main constituents [12,13]. In particular, hydrogen is considered as a possible light element in Earth's core, which is mainly composed of iron [14].

Previous diamond anvil cell (DAC)-based pressure studies of hydrides were performed at 300 K. Only three polyhydrides of transition metals have been observed by doing so: rhodium dihydride [15], tungsten hydride [16], and iridium trihydride [17]. The present experiments have been performed by laser heating hydrogen-embedded Fe

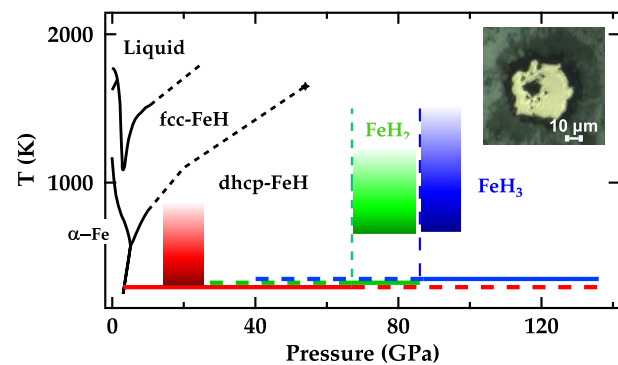


FIG. 1 (color online). Phase diagram of the Fe-H system. The black boundary lines for FeH have been taken from Refs. [8] and [9]. Colored rectangles depict the P - T regions where laser heating has been performed and the stability domains of dhcp-FeH, FeH₂, and FeH₃ are indicated. Horizontal solid and dashed lines indicate the pressure range over which these phases are stable and metastable, respectively, at 298 K. Inset: photograph of a typical sample configuration. The sample is embedded in hydrogen and sits on *c*-BN grains, the small black dots which can also be seen around it.

samples in the 100 GPa pressure range at temperatures between 300 and 1500 K. A very slow transformation kinetics exists in hydrogen-metal systems and, consequently, heating is mandatory to explore the stability field of polyhydrides under pressure.

Experiments were performed on 2 μm thick Fe polycrystalline samples loaded in diamond anvil cells with hydrogen as a pressure medium. Rhenium gaskets have been used, protected with a 800 \AA gold coating to prevent the loss of hydrogen by diffusion. Pressure was measured using the equation of state of a small piece of gold [18] loaded close to the sample. Powder diffraction patterns were analyzed using the FULLPROF software. The uncertainty in volume is $\pm 0.05 \text{ cm}^3/\text{mol}$ and in pressure $\pm 2\%$. YAG-laser heating of the sample, with an on-line setup on the ID27 x-ray diffraction (XRD) beam line (angular dispersive mode) of the European Synchrotron Radiation Facility, has been performed at several pressures: 12, 17, 27, 67, 70, 84, 86, and 90 GPa, keeping the temperature below 1500 K. The P - T phase diagram's space so explored is represented in Fig. 1. The Fe sample was thermally insulated from the diamond culets either by thin layers of KCl, LiF ($\sim 2 \mu\text{m}$, pressed onto each diamond before loading) or grains of c -BN. Experimental runs performed with these different sample assemblies gave consistent results, which proves that no parasitic chemical reaction with the insulating media or the diamond culet occurred. Because of the difficulty of laser heating in a hydrogen environment, because of its high reactivity [19,20] and increased diffusivity often resulting in the failure of the diamond anvils, XRD data were taken before and ~ 1 min after heating, but not during heating.

The Fe-H system has already been substantially studied up to 80 GPa and FeH is the only stoichiometry observed so far [8,9,21]. In the first part of this work, we revisit and extend the cold compression curve of double hcp (dhcp)-FeH up to 136 GPa. Four runs were performed. In three of them, a laser annealing of the sample during ~ 3 min was made at 12, 17, and at 27 GPa, respectively, keeping the temperature below the transition to fcc-FeH ($T \leq 1000$ K) (see Fig. 1). No phase nor volume change was observed after the heating cycle. Such laser heating enables us to significantly improve the sample crystalline quality, evidenced by sharper XRD lines, and, hence, to reduce the experimental uncertainty in the volume determination. A diffraction pattern is plotted in Fig. 2, typical of those in the 100 GPa pressure range. Our $V(P)$ data points are plotted in Fig. 3 together with literature data [22,23], with a good agreement. The present data are less scattered thanks to the improved volume accuracy. The $V(P)$ data points are fitted with a Vinet-type equation of state [24], yielding the zero pressure volume, the bulk modulus, and its pressure derivative. These values are reported in Table I. In a previous study, an anomalous compressibility behavior above 50 GPa was interpreted as a slight increase of the

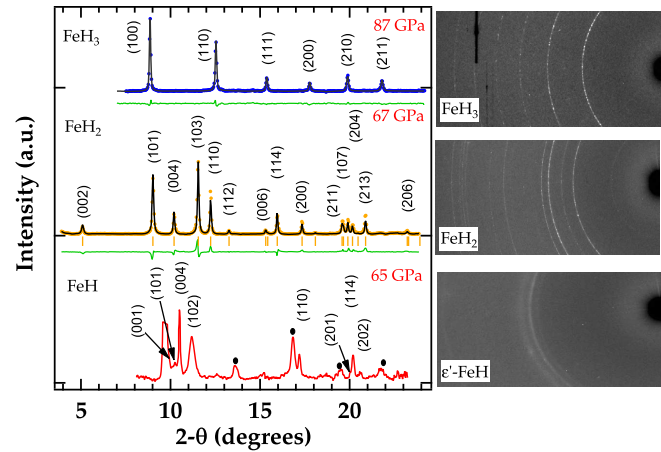


FIG. 2 (color online). X-ray diffraction patterns of FeH, FeH₂, and FeH₃ (right: image plates, left: integrated patterns). Bottom: dhcp-FeH at 64 GPa. Black dots mark the diffraction peaks from insulating material KCl. The significant broadening of the (102) peak relative to the others is attributed to random stacking faults [23]. Middle: FeH₂ at 67 GPa, described as a tetragonal $I4/mmm$ ($a = 2.479 \text{ \AA}$, $c = 8.415 \text{ \AA}$, $Z = 4$) unit cell, Fe in positions $4e$ (0,0,0.853). The Rietveld refinement is shown with a Bragg R factor $R_B = 12.1\%$. Top: Simple cubic $Pm\bar{3}m$ ($a = 2.437 \text{ \AA}$, $Z = 1$) phase of FeH₃ at 87 GPa. The Rietveld refinement with Fe in positions $1a$ (0,0,0) is shown with a Bragg R factor $R_B = 8.4\%$.

H concentration [23]. Such behavior is not observed here. Also, theoretical calculations have predicted two phase transitions below 100 GPa, first toward an hcp lattice and then to a fcc lattice [25] but none are observed here even by going up to 136 GPa. We thus conclude that under cold compression, there is no change of the H content nor of the structure of dhcp-FeH, even by going up to 136 GPa.

Laser heating between 67 and 86 GPa leads to the disappearance of the dhcp-FeH XRD peaks. The Rietveld refinement of the integrated new diffraction pattern after heating at 67 GPa shown in Fig. 2 gives a tetragonal unit cell with the symmetry $I4/mmm$ and four iron atoms in Wyckoff positions $4e$ (0, 0, 0.853). Because of the low atomic scattering power of H, it is impossible to determine the exact stoichiometry and the H atoms positions using the XRD data. At 67 GPa, the volume per Fe atom is 12.93 \AA^3 , i.e., $\sim 4 \text{ \AA}^3$ larger than the one in pure Fe and $\sim 2 \text{ \AA}^3$ larger than the one in dhcp-FeH at the same pressure. This $\Delta V \approx 2 \text{ \AA}^3$ is very close to the value determined from the volume expansion in the formation of $3d$ metal monohydrides [1]. Assuming a constant volume expansion upon the stoichiometry increase of 1 in FeH _{x} , we propose that this new phase is FeH _{~ 2} . Also, as seen in Fig. 3, the volume per formula unit of FeH _{~ 2} is smaller than the one of ideal mixing of Fe and H₂ solids at the same pressure, as expected for a compound formation at high pressure. Annealing conditions ($T \approx 1000$ K) were necessary to overcome kinetic barrier in the formation of FeH _{~ 2} , which explains why it has not been observed before [23]. At

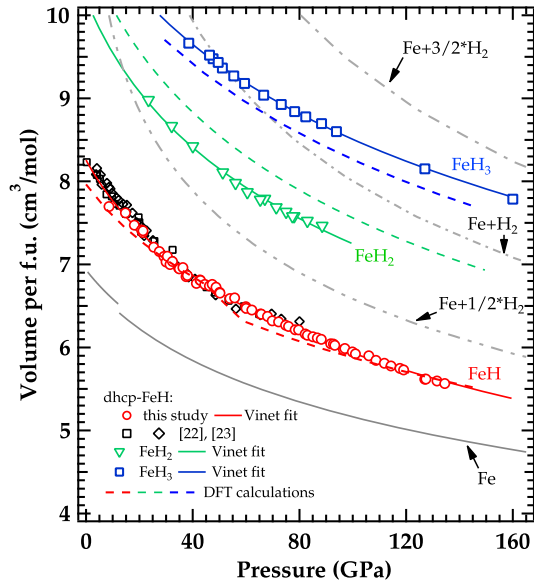


FIG. 3 (color online). Molar volume per formula unit as a function of pressure for iron hydrides. Experimental data for dhcp-FeH, $\text{FeH}_{\sim 2}$, and FeH_3 are represented together with literature data for FeH [22,23]. Error bars do not exceed the size of the data points. The Vinet fits [24] of the data are full lines and correspond to the parameters given in Table I. Dashed lines are results from the *ab initio* calculations with the most stable magnetic order (see text). Dash-dotted lines depict the molar volumes of ideal mixtures of iron and hydrogen with H:Fe ratio of 1, 2, and 3 using the equations of state of Refs. [26,27].

ambient temperature, FeH_2 is preserved upon pressure decrease down to 23 GPa and so its equation of state could be measured by going down in pressure (see Fig. 3). These data points are fitted by a Vinet-type equation of state, with the ambient pressure volume, bulk modulus, and its pressure derivative given in Table I.

A second compound replaces FeH_2 under laser heating at ~ 1400 K above 87 GPa, as shown in Fig. 2. The structural

determination gives a simple cubic unit cell with the symmetry $Pm\bar{3}m$ [with one Fe atom in Wyckoff positions $1a$ (0, 0, 0)], and a volume of 14.48 \AA^3 per Fe atom at 87 GPa, that is $\sim 2 \text{ \AA}^3$ larger than the one in $\text{FeH}_{\sim 2}$ at the same pressure. This volume expansion being very near to the one in going from FeH to $\text{FeH}_{\sim 2}$, this new phase is thus likely to have an FeH_3 stoichiometry. Moreover, the measured volume and the positional parameters of Fe atoms are almost identical to those of the FeH_3 compound recently predicted by Bazhanova *et al.* [5], in which the H atoms are in positions $3c$ (0, $\frac{1}{2}$, $\frac{1}{2}$). The same structure has been observed for IrH_3 , for the Ir/H system at high pressure [17]. At ambient temperature, FeH_3 can be preserved down to at least 39 GPa and was compressed up to 160 GPa. Its compression curve was measured over this pressure range, as shown in Fig. 3 and the parameters of the Vinet-type fit [24] of these data are reported in Table I.

First-principles density functional calculations using the ABINIT code [29] and the projector-augmented wave [30] method have been used to determine the structural positional parameters of the hydrogen atoms in FeH_2 , and to calculate the properties of dhcp-FeH, FeH_2 , and FeH_3 . In particular, the calculated equation of state is used below to validate the $x \sim 2$ and $x = 3$ concentrations attributed to the two FeH_x compounds discovered. We employed the generalized gradient approximation in the Perdew-Burke-Ernzerhof form (GGA-PBE) [31]. The lattice parameters and atomic positions in the different phases have been optimized, providing in each case the enthalpy at $T = 0$ K as a function of hydrostatic pressure. The calculations do not take into account the zero-point energy. For each phase, both non-spin-polarized and spin-polarized calculations in a ferromagnetic (FM) configuration have been performed. In particular, for FeH_2 , we started from the experimental determination of the space group and atomic positions of the Fe atoms (4 Fe/conventionnal cell) and we tested all the possibilities compatible with the Wyckoff positions of

TABLE I. Parameters (V_0 : volume, K_0 : bulk modulus, K'_0 : its pressure derivative, all at ambient conditions) of the equation of state obtained by the Vinet fit [24] of the experimental and *ab initio* data for Fe, FeH, FeH_2 , and FeH_3 . Numbers between parentheses represent fitting or published errors bars. FM: ferromagnetic; NM: nonmagnetic.

| Phase | V_0 (cm ³ /mol) | K_0 (GPa) | K'_0 | Reference |
|----------------|------------------------------|-------------|------------|-----------------------|
| Fe | 6.754(0.015) | 163.4(7.9) | 5.38(0.16) | [26] |
| FeH | 8.371(0.03) | 131.1(3.0) | 4.83 | Experimental |
| | 7.960(0.004) | 185.2(0.5) | 4.91(0.02) | <i>ab initio</i> , FM |
| | 7.58(0.05) | 227.2(0.02) | 4.8(0.1) | <i>ab initio</i> , NM |
| | 8.325(0.03) | 150.0(5.0) | 4 | [23] |
| | 8.371(0.07) | 121.0(19.0) | 5.31(0.9) | [22] |
| | 8.244 | 155 | 3.7 | [28], FM |
| FeH_2 | 7.642 | 248 | 4.3 | [28], NM |
| | 10.221(0.108) | 127.2(8.1) | 5 | Experimental |
| FeH_3 | 10.782(0.07) | 127.0(0.1) | 4.69(0.01) | <i>ab initio</i> , FM |
| | 11.171(0.04) | 190.1(0.05) | 5 | Experimental |
| | 10.858(0.003) | 205.5(0.7) | 4.38(0.01) | <i>ab initio</i> , NM |

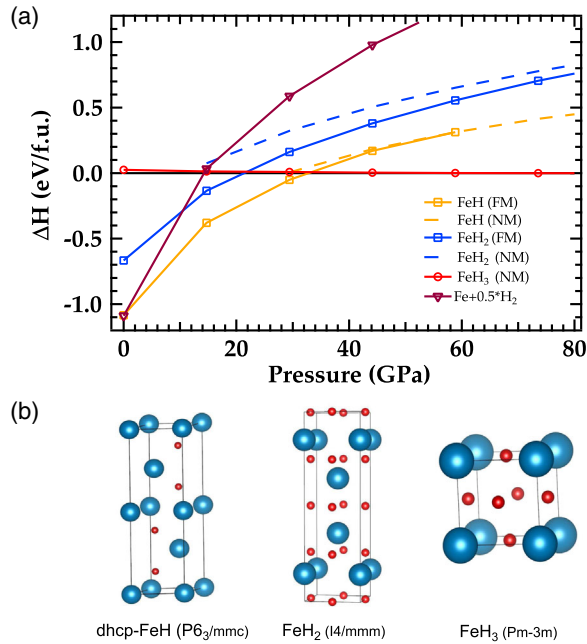


FIG. 4 (color online). (a) Calculated enthalpies as a function of pressure for the Fe-H structures proposed to match the experimental data. The magnetic phase of FeH₃ has been taken as reference so that $\Delta H = H(\text{FeH}_{3-n}) + (n/2)H(\text{H}_2) - H(\text{FeH}_3^{\text{FM}})$. (b) Representation of the structures of FeH, FeH₂, and FeH₃. Large blue and small red spheres represent the iron and hydrogen atoms, respectively.

space group $I4/mmm$. The structure, obtained at 67 GPa by placing 8 H atoms in the $4c$ $(0, \frac{1}{2}, 0)$ and $4d$ $(0, \frac{1}{2}, \frac{1}{4})$ positions, is the most stable, with relaxed cell parameters very close to the one measured at the same pressure. This structure is drawn in Fig. 4(b). It contains alternating layers of only Fe atoms and of only H atoms along the z direction. In FeH, a ferromagnetic to nonmagnetic transition is calculated to take place around 45 GPa, in good agreement with the predictions of Refs. [28,32]. In FeH₂, the ferromagnetic order is the most stable over the pressure range investigated here, with an even stronger effect on the enthalpy and on the equation of state than for FeH. In FeH₃, on the contrary, a ferromagnetic order appeared to have very little influence [Fig. 4(a)]. All structures were found to be metallic in the studied pressure range.

The calculated compression curves computed for FeH, FeH₂, and FeH₃ at $T = 0$ K are compared to experimental data in Fig. 3 and Table I. For FeH (with the FM to NM transition fixed around 45 GPa) and FeH₃, the calculated equilibrium volume and bulk moduli are, respectively, slightly lower and higher than the experimental ones, but the compression curves remain close in the scanned pressure range. These trends are similar to what is obtained for pure transition metals when the same GGA-PBE functional is used [33]. The inclusion of thermal expansion and zero point energy in the calculation could reduce the small difference. In contrast, the calculated compression

curve for FeH₂ at $T = 0$ K is above the experimental one. This could be a hint that the H:Fe ratio is slightly below 2 in the phase observed experimentally, which is possible if the proposed structure contains hydrogen vacancies.

The calculated enthalpies of the various phases of Fe-H systems observed here are compared in Fig. 4(a). They are plotted relative to the one of FeH₃^{FM}. The sequence of stable phases under pressure according to the present calculation is Fe + H₂, dhcp-FeH with FM order, and cubic FeH₃. FeH₂ is never energetically favored over dhcp-FeH even when a ferromagnetic order is taken into account, although it significantly stabilizes this phase. Inclusion of the zero point energy of H₂ molecules would tend to stabilize phases with high hydrogen stoichiometries over those with low hydrogen stoichiometries, and thus would favor FeH₂ compared to FeH. The enthalpy of FeH₂ could also be lowered if this phase contains H vacancies, as discussed above.

FeH and FeH₂ both exhibit a smaller bulk modulus than the one of pure iron, whereas FeH₃ has a greater bulk modulus (see Table I). It is interesting to note that FeH₃ and IrH₃ [17] have the same structure and an equal bulk modulus of 190 GPa, although the bulk modulus of their parent metals are very different, 163 and 383 GPa for Fe and Ir, respectively. This could suggest that the properties of these two hydrides are strongly influenced by the properties of the H sublattice. This has already been discussed for metal AlH₃ in which the electronic properties could be described as the ones of the hydrogen sublattice weakly perturbed by Al atoms [34]. To what extent hydrides with a high H:metal ratio are analogous to metal hydrogen is of great fundamental interest. At 110 GPa, the H-H nearest distance is 1.70 Å in FeH₃, significantly larger than the 1.54 Å value in AlH₃ [35] but shorter than the 1.84 Å value in IrH₃ [17]. In these hydrides, the H-H distance diminishes slowly with pressure, going to 1.66 Å in FeH₃ at 160 GPa. To reach the 1.0 Å H-H distance expected for metal hydrogen at 450 GPa [36] would require pressures of ~ 850 GPa. On the other hand, the layer of atomic H in FeH₂ or the H sublattice in FeH₃ could have interesting properties analogous to those of expanded metal hydrogen. In addition, FeH₃, nonferromagnetic above 40 GPa, is calculated to be metallic: it would be very interesting to investigate if it is a superconductor as it has been proposed for hydrogen dominant alloys [11].

To sum up, we have synthesized two novel Fe hydrides, FeH _{$x \sim 2$} at 67 GPa and FeH₃ at 86 GPa, thus providing the first experimental confirmation of the theoretically predicted trend of an increase of hydrogen content in hydrides with increasing pressure. We observe a large metastability of the Fe-H compounds and laser heating was necessary to achieve the synthesis of FeH _{$x \sim 2$} and FeH₃. The search of FeH₄ and even higher stoichiometry iron hydrides now looks promising and a strong motivation to extend the present work to Earth's core conditions. The investigation

of the electronic properties of these novel iron compounds should now be very interesting with operative effects of magnetism, dimensionality, proton zero point energy, and correlations.

The authors acknowledge the European Synchrotron Radiation Facility for provision of synchrotron radiation on beam line ID27 (proposal HC-839). We wish to thank S. Anzellini, V. Svitlyk and P. Parisiadis for their help with the XRD experiments, and Z. Bazhanova for an exchange on the FeH₂ calculation.

*charles.pepin@cea.fr

†paul.loubeyre@cea.fr

- [1] Y. Fukai, *The Metal-Hydrogen System: Basic Bulk Properties*, 2nd ed. (Springer, Berlin, 2005), Chap. 4.
- [2] E. Zurek, R. Hoffmann, N. Ashcroft, A. Oganov, and A. Lyakhov, *Proc. Natl. Acad. Sci. U.S.A.* **106**, 17640 (2009).
- [3] P. Baettig and E. Zurek, *Phys. Rev. Lett.* **106**, 237002 (2011).
- [4] H. Wang, J. S. Tse, K. Tanaka, T. Iitaka, and Y. Ma, *Proc. Natl. Acad. Sci. U.S.A.* **109**, 6463 (2012).
- [5] Z. Bazhanova, A. Oganov, and O. Gianola, *Phys. Usp.* **55**, 489 (2012).
- [6] S. S. Saxena and P. B. Littlewood, *Nature (London)* **412**, 290 (2001).
- [7] J. M. MacMahon, M. A. Morales, C. Pierleoni, and D. M. Ceperley, *Rev. Mod. Phys.* **84**, 1607 (2012).
- [8] K. Sakamaki, E. Takahashi, Y. Nakajima, Y. Nishihara, K. Funakoshi, K. Suzuki, and Y. Fukai, *Phys. Earth Planet. Inter.* **174**, 192 (2009).
- [9] O. Narygina, L. Dubrovinsky, C. McCammon, A. Kurnosov, I. Kantor, V. Prakapenka, and N. Dubrovinskaia, *Earth Planet. Sci. Lett.* **307**, 409 (2011).
- [10] W. Mao, W. Sturhahn, D. Heinz, H. Mao, J. Shu, and R. Hemley, *Geophys. Res. Lett.* **31**, L15618 (2004).
- [11] N. W. Ashcroft, *Phys. Rev. Lett.* **92**, 187002 (2004).
- [12] D. Stevenson, *Nature (London)* **268**, 130 (1977).
- [13] S. M. Wahl, H. F. Wilson, and B. Militzer, *Astrophys. J.* **773**, 95 (2013).
- [14] J.-P. Poirier, *Phys. Earth Planet. Inter.* **85**, 319 (1994).
- [15] B. Li, Y. Ding, D. Y. Kim, R. Ahuja, G. Zou, and H. K. Mao, *Proc. Natl. Acad. Sci. U.S.A.* **108**, 18618 (2011).
- [16] T. Scheler, F. Peng, C. L. Guillaume, R. T. Howie, Y. Ma, and E. Gregoryanz, *Phys. Rev. B* **87**, 184117 (2013).
- [17] T. Scheler, M. Marques, Z. Konopkova, C. L. Guillaume, R. T. Howie, and E. Gregoryanz, *Phys. Rev. Lett.* **111**, 215503 (2013).
- [18] A. Dewaele, P. Loubeyre, and M. Mezouar, *Phys. Rev. B* **70**, 094112 (2004).
- [19] T. Matsuoka, H. Fujihisa, N. Hirao, Y. Ohishi, T. Mitsui, R. Masuda, M. Seto, Y. Yoda, K. Shimizu, A. Machida *et al.*, *Phys. Rev. Lett.* **107**, 025501 (2011).
- [20] N. Subramanian, A. F. Goncharov, V. V. Struzhkin, M. Sommayazulu, and R. J. Hemley, *Proc. Natl. Acad. Sci. U.S.A.* **108**, 6014 (2011).
- [21] V. Antonov, E. Cornell, V. Fedotov, A. Kolesnikov, E. Ponyatovsky, V. Shiryayev, and H. Wipf, *J. Alloys Compd.* **264**, 214 (1998).
- [22] J. V. Badding, R. Hemley, and H. Mao, *Science* **253**, 421 (1991).
- [23] N. Hirao, T. Kondo, E. Ohtani, and K. Takemura, *Geophys. Res. Lett.* **31**, L06616 (2004).
- [24] P. Vinet, J. Ferrante, J. Smith, and J. Rose, *J. Phys. C* **19**, L467 (1986).
- [25] E. Isaev, S. Skorodumova, R. Ahija, Y. Velikov, and B. Johanson, *Proc. Natl. Acad. Sci. U.S.A.* **104**, 9168 (2007).
- [26] A. Dewaele, P. Loubeyre, F. Occelli, M. Mezouar, P. I. Dorogokupets, and M. Torrent, *Phys. Rev. Lett.* **97**, 215504 (2006).
- [27] P. Loubeyre, R. LeToullec, D. Hausermann, M. Hanfland, R. Hemley, H. Mao, and L. Finger, *Nature (London)* **383**, 702 (1996).
- [28] C. Elssner, J. Zhu, S. Louie, B. Meyer, M. Fähnle, and C. Chan, *J. Phys. Condens. Matter* **10**, 5113 (1998).
- [29] X. Gonze, G. M. Rignanese, M. Verstraete, J. M. Beuken, Y. Pouillon, R. Caracas, F. Jollet, M. Torrent, G. Zerah, M. Mikami *et al.*, *Z. Kristallogr.* **220**, 558 (2005).
- [30] M. Torrent, F. Jollet, F. Bottin, G. Zerah, and X. Gonze, *Comput. Mater. Sci.* **42**, 337 (2008).
- [31] J. P. Perdew, K. Burke, and M. Ernzerhof, *Phys. Rev. Lett.* **77**, 3865 (1996).
- [32] T. Tsumuraya, Y. Matsuura, T. Shishidou, and T. Oguchi, *J. Phys. Soc. Jpn.* **81**, 064707 (2012).
- [33] A. Dewaele, M. Torrent, P. Loubeyre, and M. Mezouar, *Phys. Rev. B* **78**, 104102 (2008).
- [34] I. G. Gurtubay, B. Rousseau, and A. Bergara, *Phys. Rev. B* **82**, 085113 (2010).
- [35] I. Goncharenko, M. I. Erements, M. Hanfland, J. S. Tse, M. Amboage, Y. Yao, and I. A. Trojan, *Phys. Rev. Lett.* **100**, 045504 (2008).
- [36] J. M. McMahon and D. M. Ceperley, *Phys. Rev. Lett.* **106**, 165302 (2011).

Part V

Discussion and conclusion

Chapter 13

Discussion

The present systematic study of four different hydrides under pressure allows us to derive some trends and propose some heuristic rules on high-pressure hydrides, obtained by compressing metals in hydrogen at 300 K.

A. Improving the crystal quality of hydrides under pressure

One of the first conclusion we can draw is that most of the time the samples are very poorly crystallized. Consequently, these samples are poorly characterized by X-ray diffraction with measurements of broad peaks. Such difficulties had been encountered before on several hydrides: in AlH_3 the structure of the intermediate phase could not be determined at first because of recrystallization issues [81], pure crystalline BeH_2 had never been easily synthesized and only the amorphous form had been the subject of experimental studies under pressure recently [131], dhcp-FeH poorly crystallizes when forming under pressure at 3.5 GPa as we have described in section 12.1. The first task of this thesis has been to find a way to overcome this issue as it can greatly impair our understanding of hydrides under pressure. A high-temperature synthesis method, using a YAG-laser or an external heater, was developed in this context. A mild laser heating of the sample in hydrogen medium, almost never exceeding 1500 K, allows to very efficiently recrystallize the sample and to synthesize high-quality, high-purity hydrides. However this method requires to pay particular attention to the sample configuration as unwanted and misleading chemical reactions can be very easily induced. An efficient insulation of the sample is needed to avoid any contamination: in our case thin layers of LiF or KCl and c-BN grains were used. The use of salt layers is easier to set up and does not interfere with Raman measurements but they produce intense XRD lines and strongly absorb infra-red light. On the contrary, c-BN grains will produce small Bragg peaks and have very weak infra-red absorption bands but it is more difficult to set up. Moreover, the sample configuration is less stable: laser heating below 10 GPa could not be performed with this arrangement as hydrogen would melt at low temperatures and convection movements would push the sample out of the c-BN grains on the diamond. An external heater was used to cover this pressure range.

B. Overcoming energetic barriers

Another observation is that energetic barriers can prevent the formation of the stable stoichiometry by compression of the metal in pure hydrogen medium at 300 K. The YAG-laser heating method is therefore needed to overcome such energetic barriers and to synthesize the stable phases that may have been missed otherwise. In AlH_3 , we have observed that with pure compression the first phase transition is found at

63 GPa while it can be observed at pressures as low as 30 GPa by laser heating the sample. Another example in the Fe-H system: pure compression of dhcp-FeH showed no phase transitions up to 136 GPa, while two new phases with a higher H-stoichiometry, FeH₂ and FeH₃, could be synthesized at 67 and 87 GPa respectively, by laser heating FeH in presence of hydrogen. Combining high-pressure and high-temperature allows to efficiently explore the stability landscape of the system.

C. Metallic state of hydrides under pressure: a universal volume increase

In this thesis, four different types of hydrides were studied: an alkali metal hydride (Li-H), an alkaline earth metal hydride (Be-H), a transition metal hydride (Fe-H) and a poor metal hydride (Al-H). The incorporation of hydrogen in the host cell had different effects depending on the system. In beryllium hydride and aluminum hydride a partly covalent hydrogen-metal bond is formed, drastically affecting the mechanical properties, the bulk modulus being reduced in the case of the hydride, while in lithium hydride an ionic bond is formed. These three hydrides are insulators at ambient pressure and are expected to become metallic under pressure. However the insulator-metal transition is only observed for AlH₃: for LiH this transition is prevented by the formation of LiH₆ and for BeH₂ it is expected to occur above 200 GPa, a pressure that was not reached in the present work. In the case of iron hydride the hydride is metallic when it forms at 3.5 GPa, with hydrogen occupying interstitial sites. In transition metals and despite their very different affinity with hydrogen, a general trend concerning the behaviour of hydrogen in the hydride phase has been observed. It was first reported by Baranowski *et al.* that the volume expansion caused by a hydrogen atom in *fcc* 3d-metals is $\sim 3 \text{ \AA}^3$ [132]. A following work by Fukai [133] compiled a large number of data and showed that the presence of one hydrogen atom expands the host lattice by 2-3 \AA^3 , depending on the host lattice. This empirical rule of the "size" of a hydrogen atom is verified in the case of iron hydride: the volume increase caused by a hydrogen atom is $\Delta V_H \sim 2.3 \text{ \AA}^3$ for dhcp-FeH at 3.5 GPa. Interestingly, this rule holds for the non-interstitial structures FeH₂ and FeH₃: the volume per Fe atom for both phases is $\sim 2 \text{ \AA}^3$ larger than the one of the previous stoichiometry. Moreover we note that $\Delta V_H \sim 2 \text{ \AA}^3$ in the metallic cubic phase of AlH₃ (it is only true for the metallic phase, the hydrogen volume in the covalent and ionic phases being much greater than 2 \AA^3). This empirical rule therefore seems to hold for metallic hydrides. A difficult issue related to the synthesis of new hydrides is the determination of the stoichiometry of the newly synthesized phase as the positions (and hence the multiplicity) of the hydrogen atoms cannot be determined by X-ray diffraction. Volume considerations using this empirical rule therefore could allow to quickly get a first estimation of the stoichiometry in the case of metallic hydrides. Having this information, *ab initio* calculations can then be undertaken to determine the relative positions for the hydrogen atoms in the experimentally determined unit cell.

D. Candidates for a high-T_c superconductivity and analogy with pure hydrogen

A reliable structure determination is indeed of prior interest as it will be a key point to determine the physical properties of the new phase. Once again it emphasizes the need for clear experimental data (fine powder with no preferred orientation, single crystal...) which can be achieved through a controlled use of the YAG-laser heating method. An accurate description of the structural parameters of our sample will for example help to refine the prediction of its temperature of superconductivity. The search for such high-temperature superconductors was in fact one of the goals of this thesis. Two possible candidates can be proposed here: the cubic phase of AlH₃ and FeH₂. Lithium hydrides and beryllium hydride are not considered as possible candidates as no metallic character was found in these hydrides up to the highest pressures achieved. Let us begin with aluminum hydride. This hydride first appeared as a very interesting candidate

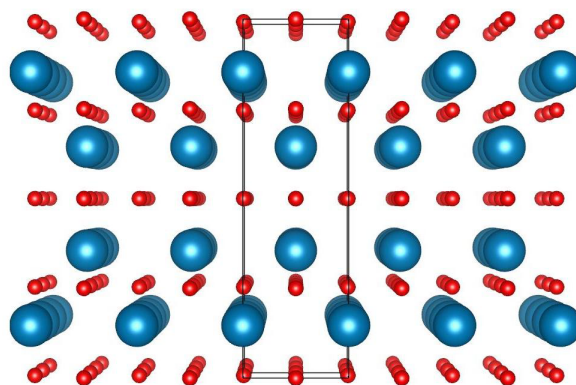


Figure 13.1: Crystal structure of FeH₂ showing the alternance of Fe and H layers. Fe atoms are represented in blue and H atoms in red

in the study of Goncharenko *et al.* [81], as it was found to become metallic at 110 GPa *,i.e.* at pressures four times lower than pure hydrogen, and a temperature of superconductivity of 24 K at 110 GPa was predicted for this metallic phase. However, no superconductivity was observed down to 4 K. It was later shown that anharmonic effects have to be taken into consideration and greatly reduce the temperature of superconductivity [83]. It was also shown that such anharmonic effects could be reduced at lower pressure which would in turn increase the temperature of superconductivity when releasing the pressure, up to 37 K at 70 GPa [24]. In our study we have shown that the metallic phase can be metastably recovered over a large pressure range, down to 40 GPa. In view of the theoretical predictions, such results are very encouraging and call for further experimental work in order to measure the temperature of superconductivity in this phase. A second route to promote superconductivity could be the study of aluminum deuteride AlD₃, as it has been shown in the case of palladium that such anharmonic effects are reduced in the deuterated sample [134] and could explain the inverse isotope effect on the temperature of superconductivity.

The second candidate is FeH₂. Although no theoretical predictions on a possible superconductivity have been published yet, several elements indicate that it could be a very promising candidate for high-temperature superconductivity. FeH₂ crystallizes in a tetragonal structure, space group $I4/mmm$, and is represented in figure 13.1. It consists of alternating layers of Fe and H atoms. Such layered structure is very interesting:

- MgB₂, exhibiting the highest temperature of superconductivity at 39 K observed so far in a conventional superconductor, presents a structure consisting of alternating layers of Mg and B. Even though the space group is different ($P6/mmm$ for MgB₂) it has been shown that this alternation of layers greatly influences the superconductivity.
- Surprisingly, layered structures with the same space group $I4/mmm$ are adopted by non-conventional superconductors (e.g. (La,Ba)₂CuO₄, T_c=38 K; Tl₂Ba₂CuO₄, T_c=95 K...) and by the recently discovered "122" iron-based superconductors [135]. This comparison is allegedly somewhat tentative as we are looking for a conventional superconductivity in our compounds. Nevertheless it is worth noting that layered structures tend to exhibit unexpected high-T_c's.
- The presence of "dense" planes of atomic hydrogen in a layered arrangement seems very close to the ideal case of the hydrogen dominant metallic alloy proposed by Ashcroft [26] and could be

analogous to pure atomic hydrogen expected above 550 GPa. A greater compression of these planes might however be needed as the H-H distance in FeH_2 is approximately 1.7 Å while it should be 0.98 Å in atomic hydrogen at 500 GPa [136].

Our experiments on AlH_3 tend to back up this latter point. Indeed, in the metallic phase of AlH_3 , exhibiting a H-H distance of 1.54 Å, we have confirmed that the properties of the hydride are strongly influenced by the properties of the hydrogen sublattice: the experimental observation of a low-energy plasmon predicted by Bergara *et al.* [137] showed that cubic AlH_3 can be described as a hydrogen sublattice weakly perturbed by Al atoms, thus confirming the strong analogy between hydrides with a high H:metal ratio and pure hydrogen.

E. Predictability of the DFT calculations

Over the past ten years a very large number of calculations had been published but very few had been confronted experimentally. In this thesis, we have shown that DFT calculations can be predictive in terms of structural stability under pressure: we confirmed the existence of new lithium polyhydrides under high pressure, one of the predicted structure for BeH_2 was identified and FeH_3 could be synthesized above 87 GPa. However some discrepancies remain and there is room for improvements: the predicted metallic character of the new lithium polyhydrides was not observed, the low-pressure behaviour of beryllium hydride appears to be much more complicated than predicted, the estimated pressures of phase transitions are poorly reproduced by DFT calculations and FeH_2 is never found stable theoretically. As we are looking for conventional superconductivity in these compounds, a property closely dependent on the structure of the material via the calculation within the DFT of the electron-phonon coupling, there is a need to understand any discrepancy between experiments and calculations to progress in the design of novel high-temperature superconductors. A textbook example illustrating this idea is the study of AlH_3 : at first there was the prediction of a possible high-temperature superconductivity in hydrides. This idea was then applied to the specific case of aluminum hydride and a high-temperature superconductivity was indeed predicted. It was followed by experiments, that did not observe the expected property and called for a revision of the description of the high-pressure phase of AlH_3 . A refined description was then proposed which agreed with experiments and proposed a new set of experiments which were partly realized by our group and should be followed by further works. More generally the same scheme is observed on hydrides and when this Ph.D. started three main challenges were open to experimentalists :

1. Show that new stoichiometries can be stabilized under pressure and their determined structures correspond to the ones predicted;
2. Observe the metallization of these hydrides at pressures within a range accessible by diamond anvil cells;
3. Measure a high temperature of superconductivity in these hydrides.

Through the systematic study of different systems this thesis has demonstrated the validity of the first point, confirming in different hydrides that new stoichiometries are stable at higher pressure and that the hydrogen content in hydrides can drastically increase with pressure. The metallic character of the new lithium polyhydrides could not be observed however and the second point therefore remains to be explored further. At the end of this thesis new experimental results on H_3S tend to confirm the third point: a conventional high-temperature superconductivity in the order of 200 K at 200 GPa has been measured in this hydride. The combination of these results is now extremely encouraging and should motivate future theoretical and experimental studies.

F. The next step

The discussions and results of this thesis only concerned binary hydrides. The next trend should be to incorporate these hydrides within greater unit cells *i.e.* study ternary hydrides in order to accentuate the chemical pre-compression as suggested by Ashcroft. This is closely related to one of the main challenge when studying hydrides: specifically designing a system with the desired physical properties and that can be synthesized at relatively low pressure, typically <10 GPa. Such compound should then be metastably recovered at ambient pressure. As we have seen in our experiments, it could be somewhat quite tricky: releasing the pressure on hydrides leads its dissociation into the elements and the formation of a porous material. Some solutions to this problem may be found in the use of nano-samples covered with a protecting layer permeable to hydrogen under high pressure but impermeable at low pressures [138] or through synthesis induced by ultrafast microexplosion [139].

General Conclusion

The aim of this thesis was to undertake a systematic experimental study on light elements hydrides under pressure. Prior to this work, numerous first-principles calculations awaited a clear experimental confirmation and the major key issues were clearly identified: Is the analogy between pure hydrogen and hydrides with a high hydrogen content relevant? Could the hydrogen stoichiometry in hydrides increase at higher density? Could high pressure allow the stabilization of new hydrides with unusual stoichiometries? In order to gain more insight on their high pressure behaviour diverse types of hydrides (ionic, covalent, metallic with interstitial hydrogen) have been studied, synthesized from the elements Li, Be, Al and Fe.

In this context the first part of this thesis has been dedicated to the development of a synthesis method from the elements under high pressure to produce high-quality and high-purity sample. This method relies on the generation of high-temperatures through the use of an external resistive heater or of a YAG-laser, combined with a specific sample configuration: a metallic foil is deposited on top of an insulating layer and embedded in a fine hydrogen powder. This technique offers the possibility to recrystallize samples and to overcome energetic barrier in order to synthesize new stable phases and was first applied to the study of two covalent hydrides, namely AlH_3 and BeH_2 .

Aluminum hydride was synthesized under pressure from its constituents and studied up to 120 GPa. A previously undetermined intermediate structure could be identified and the insulator-to-metal transition was confirmed at 107 GPa. A feature in reflectivity in the metallic phase, around 1.15 eV, confirmed the prediction of a plasmon peak as due to the H metallic lattice weakly perturbed. Thus it demonstrates the predominant role of hydrogen in hydrides and shows the relevance of the analogy between pure hydrogen and hydrides.

The first high-pressure study of crystalline beryllium hydride was presented. The behaviour of this compound appears to be more complicated than previously anticipated: at low pressure several polymorphs have been identified and an analogy with the high pressure behaviour of SiO_2 seems possible. Upon further compression BeH_2 decomposes, exhibiting a pressure-induced reentrant disproportionation and cannot be synthesized between 30 and 70 GPa. Above 80 GPa a new phase of higher coordination with the predicted 1-T structure is synthesized. No insulator-to-metal transition was observed in this hydride, up to 110 GPa.

In these two covalent hydrides no changes of stoichiometry could be observed. However in the cases of iron and lithium such changes could be successfully induced under high pressure.

The cold compression curve of iron hydride, dhcp-FeH, was measured and showed no changes up to the maximum pressure of 136 GPa. YAG-laser heating of the sample, on the other hand, allowed the synthesis of two new phases at 67 and 87 GPa, identified as FeH_2 and FeH_3 respectively. The experimental determination of the sequence of phase transitions $\text{FeH} \rightarrow \text{FeH}_2 \rightarrow \text{FeH}_3$ thus confirmed that the hydrogen stoichiometry in hydrides can increase with pressure. Moreover, it was observed that these new phases present very large metastability domains and can be recovered at much lower pressures.

Lithium hydride was studied by means of infra-red absorption spectroscopy as it is a non-invasive

technique and is ideally suited to detect any chemical changes or metallic states. The compression at ambient temperature of pure LiH revealed that new high-frequencies absorption bands appear at 130 GPa and 160 GPa, corresponding to the formation of LiH_6 and LiH_2 respectively, both phases containing molecular hydrogen in their structures. This experiment confirmed that pressure can promote the stabilization of new hydrides with unusual stoichiometries.

Although this study has enabled progress in the understanding and the synthesis of hydrides under pressure, some key questions still remain like the metallization of these hydrides that was not observed, the confirmation of a conventional high-temperature superconductivity in these compounds or the possibility to recover at ambient pressure polyhydrides with a large hydrogen content. However, this thesis has shown that the study of hydrides under pressure is a promising theme of research:

- Experimental techniques to synthesize and characterize new hydrides have been developed;
- The predictability of the DFT calculations has made it into a powerful tool to guide experimentalists in their search of new materials;
- Heuristic laws have been demonstrated;
- A conventional superconductivity in H_3S has recently been discovered.

All ingredients are now available to engineer new materials with important impacts. The main effort should now be to explore further this domain in order to get a better understanding about the complexity of these hydrogen-rich systems and to obtain a form of poly-hydride recoverable at ambient conditions.

Bibliography

- [1] R. J. Hemley. Effects of high pressure on molecules. *Annu. Rev. Phys. Chem.*, 51:763, 2000.
- [2] M. Nicol, K. R. Hirsch, and W. B. Holzapfel. Oxygen phase equilibria near 298 K. *Chem. Phys. Lett.*, 68:49–52, 1979.
- [3] S. Desgreniers, Y. K. Vohra, and A. L. Ruoff. Optical response of very high density solid oxygen to 132 GPa. *J. Phys. Chem.*, 94:1117–1122, 1990.
- [4] K. A. Goettel, J. H. Eggert, I. F. Silvera, and W. C. Moss. Optical evidence for the metallization of xenon at 132(5) GPa. *Phys. Rev. Lett.*, 62:665, 1989.
- [5] Y. Ma, M. Eremets, A. R. Oganov, Y. Xie, I. Trojan, S. Medvedev, A. O. Lyakhov, M. Valle, and V. B. Prakapenka. Transparent dense sodium. *Nature*, 458:182, 2009.
- [6] T. Matsuoka and K. Shimizu. Direct observation of a pressure-induced metal-to-semiconductor transition in lithium. *Nature*, 458:186, 2009.
- [7] C. J. Pickard and R. J. Needs. Aluminum at terapascal pressures. *Nature Materials*, 9:624, 2010.
- [8] W. Zhang, A. R. Oganov, A. F. Goncharov, Q. Zhu, S. E. Boulfelfel, A. O. Lyakhov, E. Stravou, M. Sommayazulu, V. B. Prakapenka, and Z. Konôpkova. Unexpected stable stoichiometries of sodium chlorides. *Science*, 342:1502, 2013.
- [9] P. Loubeyre, M. Jean-Louis, R. LeToullec, and J. P. Pinceaux. High pressure measurements of the He-Ne binary phase diagram at 296 k: evidence for the stability of a stoichiometric Ne(He)₂ solid. *Phys. Rev. Lett.*, 70:178, 1993.
- [10] P. Loubeyre, R. LeToullec, and J. P. Pinceaux. Compression of Ar(H₂)₂ up to 175 GPa: a new path for the dissociation of molecular hydrogen? *Phys. Rev. Lett.*, 72:1360, 1994.
- [11] T. Plisson, G. Weck, and P. Loubeyre. (N₂)₆Ne₇: a high pressure van der Waals insertion compound. *Phys. Rev. Lett.*, 113:025702, 2014.
- [12] E. Wigner and H. B. Huntington. On the possibility of a metallic modification of hydrogen. *J. Chem. Phys.*, 3:764–770, 1935.
- [13] P. Loubeyre, F. Occelli, and R. LeToullec. Optical studies of solid hydrogen to 320 gpa and evidence for black hydrogen. *Nature*, 416:613, 2002.
- [14] E. Babaev, A. Sudbø, and N. W. Ashcroft. A superconductor to superfluid phase transition in liquid metallic hydrogen. *Nature*, 431:666, 2004.

-
- [15] J. Bardeen, L. N. Cooper, and J. R. Schrieffer. Theory of superconductivity. *Phys. Rev.*, 108:1175, 1957.
- [16] P. B. Allen and R. C. Dynes. Transition temperature of strong-coupled superconductors reanalyzed. *Phys. Rev. B*, 12:905, 1975.
- [17] N. W. Ashcroft. Metallic hydrogen: A high-temperature superconductor? *Phys. Rev. Lett.*, 21:1748, 1968.
- [18] I. F. Silvera and J. W. Cole. Metallic hydrogen: The most powerful rocket fuel yet to exist. *J. of Physics: Conf. Series*, 25:012194, 2010.
- [19] L. Dubrovinsky, N. Dubrovinskaia, V. B. Prakapenka, and A. M. Abakumov. Implementation of microball nanodiamond anvils for high-pressure studies above 6 Mbar. *Nat. Comm.*, 3:1163, 2012.
- [20] P. Loubeyre, R. LeToullec, D. Hausermann, M. Hanfland, R.J. Hemley, H.K. Mao, and L.W. Finger. X-ray diffraction and equation of state of hydrogen at megabar pressures. *Nature*, 383:702–704, 1996.
- [21] Y. Kong, O. V. Dolgov, O. Jepsen, and O. K. Andersen. Electron-phonon interaction in the normal and superconducting states of MgB₂. *Phys. Rev. B*, 64:020501, 2001.
- [22] P. Cudazzo, G. Profeta, A. Sanna, A. Floris, A. Continenza, S. Massidda, and E. K. U. Gross. Ab initio description of high-temperature superconductivity in dense molecular hydrogen. *Phys. Rev. Lett.*, 100:257001, 2008.
- [23] J. M. McMahon and D. M. Ceperley. High-temperature superconductivity in atomic metallic hydrogen. *Phys. Rev. Lett.*, 106:165302, 2011.
- [24] A. K. M. A. Islam, M. M. Ali, and M. L. Ali. AlH₃ between 65 and 110 GPa: implications of electronic band and phonon structures. *Physica C*, 470:403–406, 2010.
- [25] H. Wang, J. S. Tse, K. Tanaka, T. Iitaka, and Y. Ma. Superconductive sodalite-like clathrate calcium hydride at high pressure. *PNAS*, 109:6463–6466, 2012.
- [26] N. W. Ashcroft. Hydrogen dominant metallic alloys: High temperature superconductors? *Phys. Rev. Lett.*, 92:187002, 2004.
- [27] E. Zurek, R. Hoffmann, N.W. Ashcroft, A.R. Oganov, and A.O. Lyakhov. A little bit of lithium does a lot for hydrogen. *PNAS*, 106:17640–17643, 2009.
- [28] S. Yu, Q. Zeng, A. R. Oganov, C. Hu, G. Frapper, and L. Zhang. Exploration of the crystal structures and superconductivity properties of beryllium hydrides via first-principles evolutionary calculations. *AIP Advances*, 4:107118, 2014.
- [29] Z. Wang, Y. Yao, L. Zhu, T. Iitaka, H. Wang, and Y. Ma. Metallization and superconductivity of BeH₂ under pressure. *J. Chem. Phys.*, 140:124707, 2014.
- [30] P. Baettig and E. Zurek. Pressure-stabilized sodium polyhydrides: NaH_n (n>1). *Phys. Rev. Lett.*, 106:237002, 2011.

-
- [31] D. C. Lonie, J. Hooper, B. Altintas, and E. Zurek. Metallization of magnesium polyhydrides under pressure. *Phys. Rev. B*, 87:054107, 2013.
- [32] J. Hooper, B. Altintas, A. Shamp, and E. Zurek. High pressure potassium polyhydrides: A chemical perspective. *J. Phys. Chem. C*, 117:2982, 2012.
- [33] D. Zhou, X. Jin, X. Meng, G. Bao, Y. Ma, B. Liu, and T. Cui. *Ab Initio* study revealing a layered structure in hydrogen-rich KH_6 under high pressure. *Phys. Rev. B*, 86:014118, 2012.
- [34] C. M. Pépin, A. Dewaele, G. Geneste, P. Loubeyre, and M. Mezouar. New iron hydrides under pressure. *Phys. Rev. Lett.*, 113:265504, 2014.
- [35] Z.G. Bazhanova, A.R. Oganov, and O. Gianola. Fe-C and Fe-H systems at pressures of the Earth's inner core. *Phys. Usp.*, 55:489–497, 2012.
- [36] M. I. Eremets, I. A. Trojan, S. A. Medvedev, J. S. Tse, and Y. Yao. Superconductivity in hydrogen dominant materials: Silane. *Science*, 319:1506, 2008.
- [37] T. A. Strobel, M. Sommayazulu, and R. J. Hemley. Novel pressure-induced interactions in silane-hydrogen. *Phys. Rev. Lett.*, 103:065701, 2009.
- [38] K. Abe and N. W. Ashcroft. Quantum disproportionation: the high hydrides at elevated pressures. *Phys. Rev. B*, 88:174110, 2013.
- [39] S. Zhang, Y. Wang, H. Liu, G. Yang, L. Zhang, and Y. Ma. Phase diagram and high-temperature superconductivity of selenium hydrides at high pressures. *arXiv*, 1502.026072, 2015.
- [40] K. Abe and N. W. Ashcroft. Crystalline diborane at high pressure. *Phys. Rev. B*, 84:104118, 2011.
- [41] G. Gao, A. R. Oganov, A. Bergara, M. Martinez-Canales, T. Cui, T. Iitaka, Y. Ma, and G. Zou. Superconducting high pressure phase of germane. *Phys. Rev. Lett.*, 101:107002, 2008.
- [42] Y. Li, G. Gao, Y. Xie, Y. Ma, T. Cui, and G. Zou. Superconductivity at ~ 100 K in dense $\text{SiH}_4(\text{H}_2)_2$ predicted by first principles. *PNAS*, 107:15708–15711, 2010.
- [43] J. S. Tse, Y. Yao, and K. Tanaka. Novel superconductivity in metallic SnH_4 under high pressure. *Phys. Rev. Lett.*, 98:117004, 2007.
- [44] C. Zhang, X-J. chen, Y-L. Li, V. K. Struzhkin, R. J. Hemley, H-K. Mao, R-Q. Zhang, and H-Q. Lin. Superconductivity in hydrogen-rich material: GeH_4 . *J. Supercond. Nov. Magn.*, 23:717–719, 2010.
- [45] C-H. Hu, A. R. Oganov, Q. Zhu, G-R. Qian, G. Frapper, A. O. Lyakhov, and H-Y. Zhou. Pressure-induced stabilization and insulator-superconductor transition of BH. *Phys. Rev. Lett.*, 110:165504, 2013.
- [46] Y. Fukai. *The metal-hydrogen system: Basic Bulk Properties*. edited by Springer, Berlin, 2005.
- [47] B. Li, Y. Ding, D. Y. Kim, R. Ahuja, G. Zou, and H. K. Mao. Rhodium dihydride (RhH_2) with high volumetric hydrogen density. *PNAS*, 108:18618, 2011.
- [48] J. Hooper, B. Altintas, A. Shamp, and E. Zurek. Polyhydrides of the alkaline earth metals: a look at the extremes under pressure. *J. Phys. Chem. C*, 117:2982–2992, 2013.

- [49] J. Hooper, T. Terpstra, A. Shamp, and E. Zurek. Composition and constitution of compressed strontium polyhydrides. *J. Phys. Chem. C*, 118:6433–6447, 2014.
- [50] J. Hooper and E. Zurek. Rubidium polyhydrides under pressure: emergence of the linear H_3^- species. *Chem. Eur. J.*, 18:5013–5021, 2012.
- [51] A. Shamp, J. Hooper, and E. Zurek. Compressed cesium polyhydrides: Cs^+ sublattices and H_3^- three-connected nets. *Inorg. Chem.*, 51:9333–9342, 2012.
- [52] T. Scheler, M. Marques, Z. Konopkova, C. L. Guillaume, R. T. Howie, and E. Gregoryanz. High-pressure synthesis and characterization of iridium trihydride. *Phys. Rev. Lett.*, 111:215503, 2013.
- [53] C. E. Weir, E. R. Lippincott, A. Van Valkenburg, and E. N. Bunting. Infrared studies in the 1- to 15-micron region to 30,000 atmospheres. *Journal of Research of the National Bureau of Standards*, 63: , 1959.
- [54] W. A. Basset. Diamond anvil cell, 50th birthday. *High Pressure Research*, 29:163–186, 2009.
- [55] H. K. Mao and P. M. Bell. Design of a diamond windowed high-pressure cell for hydrostatic pressure in the range 1 bar to 0.5 Mbar. *Carnegie Institute Washington Year Book*, 74:402, 1974.
- [56] L. Merrill and W. A. Bassett. Miniature diamond anvil pressure cell for single crystal x-ray diffraction studies. *Rev. Sc. Instr.*, 45:290, 1974.
- [57] R. LeToullec, J. P. Pinceaux, and P. Loubeyre. The membrane diamond anvil cell: a new device for generating continuous pressure and temperature variations. *High Press. Res.*, 1:77–90, 1988.
- [58] R. Boehler and K. De Hantsetters. New anvil design in diamond-cells. *High Press. Res.*, 24:391–396, 2004.
- [59] T. Scheler, O. Degtyareva, and E. Gregoryanz. On the effects of high temperature and high pressure on the hydrogen solubility in rhenium. *J. Chem. Phys.*, 135:214501, 2011.
- [60] J. C. Jamieson, J. N. Fritz, and M. H. Manghnani. *High Pressure Research in Geophysics*. edited by S. Akimoto and M. H. Manghnani, Center for Academic Publications, Tokyo, 1982.
- [61] P. I. Dorogokupets and A. Dewaele. Equations of state of MgO, Au, Pt, NaCl-B1 and NaCl-B2: internally consistent high-temperature pressure scales. *High Pressure Research*, 27:431–446, 2007.
- [62] K. Takemura and A. Dewaele. Isothermal equation of state for gold with a He-pressure medium. *Phys. Rev. B*, 78:104119, 2008.
- [63] C. Donnerer, T. Scheler, and E. Gregoryanz. High-pressure synthesis of noble metal hydrides. *J. Chem. Phys.*, 138:134507, 2013.
- [64] V. F. Degtyareva. Crystal structure of gold hydride. *arXiv*, 1412.5293, 2014.
- [65] R. A. Forman, S. Block, and J. D. Barnett. Pressure measurement made by utilization of ruby sharp-line luminescence. *Science*, 176:284–285, 1972.
- [66] H. K. Mao, J. Xu, and P.M. Bell. Calibration of the ruby pressure gauge to 800 kbar under quasi-hydrostatic conditions. *J. Geophys. Res.*, 91(B5):4673–4676, 1986.

-
- [67] A. Dewale, P. Loubeyre, and M. Mezouar. Equations of state of six metals above 94 GPa. *Phys. Rev. B*, 70:094112, 2004.
- [68] P. I. Dorogokupets and A. R. Oganov. Ruby, metals and MgO as alternative pressure scales: a semiempirical description of shock-wave, ultrasonic, x-ray and thermochemical data at high temperature and pressures. *Phys. Rev. B*, 75:024115–024130, 2007.
- [69] F. Datchi, R. LeToullec, and P. Loubeyre. Improved calibration of the $\text{SrB}_4\text{O}_7\text{:Sm}^{2+}$ optical pressure gauge: advantages at very high pressures and high temperatures. *J. Appl. Phys.*, 81:3333–3339, 1997.
- [70] P. Loubeyre, F. Occelli, and P. Dumas. Hydrogen phase IV revisited via synchrotron infrared measurements in H_2 and D_2 up to 209 GPa at 296 K. *Phys. Rev. B*, 87:134101, 2013.
- [71] Y. Akahama and H. Kawamura. Pressure calibration of diamond anvil raman gauge to 410 GPa. *J. Phys.: Conf. Ser.*, 215:012195–012199, 2010.
- [72] Z. Geballe and R. Jeanloz. Origin of temperature plateaus in laser-heated diamond anvil cell experiments. *J. Appl. Phys.*, 111:123518, 2012.
- [73] D. W. Bennett. *Understanding single-crystal x-ray crystallography*. edited by Wiley-VCH, 2010.
- [74] A. P. Hammersley, S. O. Svensson, M. Hanfland, and A. N. Fitch D. Häusermann. Two dimensional detector software: from real detector to idealised image or two-theta scan. *High Pressure Research*, 14:235, 1996.
- [75] H. M. Rietveld. A profile refinement method for nuclear and magnetic structures. *Acta Crystallogr.*, 2:65, 1969.
- [76] O. Stecher and E. Wiberg. Über einen nichtflüchtigen, polymeren aluminiumwasserstoff $(\text{AlH}_3)_x$ und einige flüchtige verbindungen des monomeren AlH_3 . *Ber. Dtsch. Chem. Ges.*, 75:2003–2012, 1942.
- [77] A. E. Finholt, A. C. Bond, and H. I. Schlesinger. Lithium aluminium hydride, aluminium hydride and lithium gallium hydride, and some of their applications in organic and inorganic chemistry. *J. Am. Chem. Soc.*, 69:1199–1203, 1947.
- [78] G. Chizinsky. Non-solvated aluminium hydride. *J. Am. Chem. Soc.*, 77:3164–3165, 1955.
- [79] F. M. Brower, N. E. Matzek, P. F. Reigler, H. W. Rinn, C. B. Roberts, D. L. Schmidt, J. A. Snover, and K. Terada. Preparation and properties of aluminium hydride. *J. Am. Chem. Soc.*, 98:2450–2453, 1976.
- [80] J. W. Turley and H. W. Rinn. Crystal structure of aluminium hydride. *Inorg. Chem.*, 8:18–22, 1969.
- [81] I. Goncharenko, M. I. Erements, M. Hanfland, J. S. Tse, M. Amboage, Y. Yao, and I. A. Trojan. Pressure-induced hydrogen-dominant metallic state in aluminum hydride. *Phys. Rev. Lett.*, 100:045504, 2008.
- [82] C. J. Pickard and R. J. Needs. Metallization of aluminum hydride at high pressures: A first-principles study. *Phys. Rev. B*, 76:144114, 2007.

- [83] B. Rousseau and A. Bergara. Giant anharmonicity suppresses superconductivity in AlH_3 under pressure. *Phys. Rev. B*, 82:104504, 2010.
- [84] M. Tkacz, T. Palasyuk, J. Graetz, and S. Saxena. High-pressure raman spectroscopy study of α and γ polymorphs of AlH_3 . *J. Raman Spectrosc.*, 39:922–927, 2008.
- [85] N. Shimura, T. Takeichi, T. Kume, S. Sasaki, H. Shimizu, A. Ohmura, K. Ikeda, Y. Nakamori, and S. Orimo. High-pressure raman and visible absorption study of AlH_3 . *J. Phys.: Conf. Ser.*, 215:012047, 2010.
- [86] P. Vajeeston, P. Ravindran, and H. Fjellvag. Novel high pressure phases of β - AlH_3 : A density-functional study. *Chem. Mater.*, 20:5997–6002, 2008.
- [87] D. Y. Kim, R. H. Scheider, and R. Ahuja. Dynamical stability of the cubic metallic phase of AlH_3 at ambient pressure: Density functional calculations. *Phys. Rev. B*, 78:100102, 2008.
- [88] I. G. Gurtabay, B. Rousseau, and A. Bergara. Undamped low-energy plasmon in AlH_3 at high pressure. *Phys. Rev. B*, 82:085115, 2010.
- [89] E. Pietsch. Bildung von Metallhydriden durch atomaren Wasserstoff. *Z. Elektrochem.*, 39:577–586, 1933.
- [90] H. I. Schlesinger and A. E. Finholt. The preparation of the hydrides of zinc, cadmium, beryllium, magnesium and lithium by the use of lithium aluminum hydride. *J. Amer. Chem. Soc.*, 73:4585–4590, 1951.
- [91] R. W. Baker, G. J. Brendel, B. R. Lowrance, J. R. Mangham, E. M. Marlett, and L. H. Shepherd. Preparation of beryllium hydride by an improved pyrolysis technique. *J. Organomet. Chem.*, 159:123, 1978.
- [92] M. D. Senin, V. V. Akhachinskii, Y. E. Markushkin, N. A. Chirin, L. M. Kopytin, I. P. Mikhaleiko, N. M. Ermolaev, and A. V. Zabrodin. The production, structure and properties of beryllium hydride. *Inorg. Mat.*, 29:1416, 1993.
- [93] S. Sampath, K. M. Lantzky, C. J. Benmore, J. Neufeind, J. E. Siewenie, P. A. Egelstaff, and J. L. Yarger. Structural quantum isotope effects in amorphous beryllium hydride. *J. Chem. Phys.*, 119:12499, 2003.
- [94] G. J. Brendel, E. M. Marlett, and L. M. Niebylski. Crystalline beryllium hydride. *Inorg. Chem.*, 17:3589, 1978.
- [95] S. K. Konovalov and B. M. Bulychev. High pressures in the chemistry of beryllium and aluminium hydrides. *Russian J. of Inorg. Chem.*, 37:1361, 1992.
- [96] G. S. Smith, Q. C. Johnson, D. K. Smith, D. E. Cox, R. L. Snyder, R-S. Zhou, and A. Zalkin. The crystal and molecular structure of beryllium hydride. *Solid State Comm.*, 67:491–494, 1988.
- [97] A. D. Zdetsis, M. M. Sigalas, and E. N. Koukaras. *Ab initio* theoretical investigation of beryllium and beryllium hydride nanoparticles and nanocrystals with implications for the corresponding infinite systems. *Phys. Chem. Chem. Phys.*, 16:14172, 2014.

-
- [98] S. V. Marchenko, V. F. Petrunin, Y. E. Markushin, M. D. Senin, and N. A. Chirin. Neutron diffraction study of amorphous beryllium hydride. *Sov. Phys. Solid State*, 24:1308, 1982.
- [99] R. Baer and D. Neuhauser. Molecular electronic structure using auxiliary field Monte-Carlo, plane-waves and pseudopotentials. *J. Chem. Phys.*, 112:1679, 2000.
- [100] U. Hantsch, B. Winkler, and V. Milman. The isotypism of BeH₂ and SiO₂: an ab initio study. *Chem. Phys. Lett.*, 378:343–348, 2003.
- [101] J. Haines, C. Chateau, J. M. Léger, A. Le Sauze, N. Diot, R. Marchand, and S. Hull. Crystal structure of moganite-type phosphorous oxynitride: relationship to other twinned-quartz-based structures. *Acta Cryst.*, B55:677–682, 1999.
- [102] P. Vajeeston, P. Ravindran, A. Kjekshus, and H. Fjellag. Structural stability of BeH₂ at high pressures. *Appl. Phys. Lett.*, 84:34, 2004.
- [103] L. George and S. K. Saxena. Structural stability of metal hydrides, alanates and borohydrides of alkali and alkali-earth elements: a review. *Int. J. Hydrogen Energy*, 35:5454–5470, 2003.
- [104] F. H. Welch. Lithium hydride: a space age shielding material. *Nuclear Engineering and Design*, 26:444–460, 1974.
- [105] P. Loubeyre, R. LeToullec, M. Hanfland, L. Ulivi, F. Datchi, and D. Hausermann. Equation of state of ⁷LiH and ⁷LiD from x-ray diffraction to 94 GPa. *Phys. Rev. B*, 57:10403, 1998.
- [106] Y. Kondo and K. Asaumi. Effect of pressure on the direct band gap of LiH. *J. Phys. Soc. Jpn.*, 57:367, 1988.
- [107] J. Hama, K. Suito, and N. Kawakami. First-principles calculation of the shock-wave equation of state of isotopic lithium hydride. *Phys. Rev. B*, 39:3351, 1989.
- [108] J. L. Martins. Equation of state of alkali hydrides at high pressures. *Phys. Rev. B*, 41:7883, 1990.
- [109] G. Roma, C. M. Bertoni, and S. Baroni. The phonon spectra of lih and lid from density-functional perturbation theory. *Solid State Commun.*, 98:203, 1996.
- [110] S. Lebègue, M. Alouani, B. Arnaud, and W. E. Pickett. Pressure-induced simultaneous metal-insulator and phase-transitions in LiH: a quasiparticle study. *Europhys. Lett.*, 63:562–568, 2003.
- [111] A. Lazicki, A. Dewaele, P. Loubeyre, and M. Mezouar. *Phys. Rev. B*, 86:174118, 2012.
- [112] J. Zhang, L. Zhang, T. Cui, Y. Li, Z. He, Y. Ma, and G. Zhou. Phonon and elastic instabilities in rocksalt alkali hydrides under pressure: First-principles study. *Phys. Rev. B*, 75:104115, 2007.
- [113] Y. Xie, Q. Li, A. R. Oganov, and H. Wang. Superconductivity of lithium-doped hydrogen under high pressure. *Acta Cryst. C*, 70:104–111, 2014.
- [114] R. T. Howie, O. Narygina, C. L. Guillaume, S. Evans, and E. Gregoryanz. *Phys. Rev. B*, 86:064108, 2012.
- [115] K. Kuno et al. Heating of Li in hydrogen: possible synthesis of LiH_x. *High Pressure Research*, 35:16–21, 2015.

- [116] D. M. Adams and J. Haines. A study of the high-pressure phase transition in lithium hydroxide by infrared and raman spectroscopy. *J. Phys. Chem.*, 95:7064–7067, 1991.
- [117] A. Dewaele, P. Loubeyre, F. Occelli, M. Mezouar, P. I. Dorogokupets, and M. Torrent. Quasihydrostatic equation of state of iron above 2 Mbar. *Phys. Rev. Lett.*, 97:215504, 2006.
- [118] J-P. Poirier. Light elements in the Earth’s outer core: A critical review. *Phys. Earth Plan. Inter.*, 85:319–337, 1994.
- [119] T. Yagi and T. Hishinuma. Iron hydride formed by the reaction of iron, silicate and water - implications for the light-element of the Earth’s core. *Geophys. Res. Lett.*, 22:1933–1936, 1995.
- [120] K. Sakamaki, E. Takahashi, Y. Nakajima, Y. Nishihara, K. Funakoshi, K. Suzuki, and Y. Fukai. Melting phase relation of FeH_x up to 20 GPa: implication for the temperature of the Earth’s core. *Phys. Earth Plan. Inter.*, 174:192–201, 2009.
- [121] V.E. Antonov, E. Cornell, V.K. Fedotov, A.I. Kolesnikov, E.G. Ponyatovsky, V.I. Shiryayev, and H. Wipf. Neutron diffraction investigation of the dhcp and hcp iron hydrides and deuterides. *J. Alloys Comp.*, 264:214–222, 1998.
- [122] V. Antonov, I. Belash, V. Degtyareva, E. Ponyatovsky, and V. Shiryayev. *Sov. Phys. Dokl.*, 25:490, 1980.
- [123] J. V. Badding, R. Hemley, and H.K. Mao. High-pressure chemistry of hydrogen in metals: In situ study of iron hydride. *Science*, 253:421–424, 1991.
- [124] C. Elsässer, J. Zhu, S.G. Louie, B. Meyer, M. Fähnle, and C.T. Chan. Ab initio study of iron and iron hydride: structural and magnetic properties of close-packed Fe and FeH. *J. Phys. Condens. Matter.*, 10:5113–5129, 1998.
- [125] T. Tsumuraya, Y. Matsuura, T. Shishidou, and T. Oguchi. First-principles study on the structural and magnetic properties of iron hydride. *J. Phys. Soc. Jpn.*, 81:064707, 2012.
- [126] W.L. Mao, W. Sturhahn, D.L. Heinz, H.K. Mao, J. Shu, and R.J. Hemley. Nuclear resonant x-ray scattering of iron hydride at high pressure. *Geophys. Res. Lett.*, 31:L15618, 2004.
- [127] N. Ishimatsu, T. Shichijo, Y. Matsushima, H. Maruyama, Y. Matsuura, T. Tsumuraya, T. Shishidou, T. Oguchi, N. Kawamura, M. Mizumaki, T. Matsuoka, and K. Takemura. Hydrogen-induced modification of the electronic structure and magnetic states in fe, co, and ni monohydrides. *Phys. Rev. B*, 85:104430, 2012.
- [128] O. Narygina, L.S. Dubrovinsky, C.A. McCammon, A. Kurnosov, I.Y. Kantor, V.B. Prakapenka, and N.A. Dubrovinskaia. X-ray diffraction and mossbauer spectroscopy study of fcc iron hydride FeH at high pressures and implications for the composition of the Earth’s core. *Earth Planet. Sci. Lett.*, 307:409–414, 2011.
- [129] S. Anzellini, A. Dewaele, M. Mezouar, P. Loubeyre, and G. Morard. Melting of iron at Earth’s inner core boundary based on fast x-ray diffraction. *Science*, 340:464–466, 2013.
- [130] E.I. Isaev, S.V. Skorodumova, R. Ahija, Y.K Velikov, and B. Johanson. Dynamical stability of Fe-H in the Earth’s mantle and core regions. *PNAS*, 104:9168–9171, 2007.

-
- [131] M. Ahart, J. L. Yarger, K. M. Lantzky, S. Nakano, H. K. Mao, and R. J. Hemley. High-pressure Brillouin scattering of amorphous BeH₂. *J. Chem. Phys.*, 124:014502, 2006.
- [132] B. Baranowski, S. Majchrzak, and T. B. Flanagan. The volume increase of fcc metals and alloys due to interstitial hydrogen over a wide range of hydrogen content. *J. Phys. F*, 1:258, 1971.
- [133] Y. Fukai. Site preference of interstitial hydrogen in metals. *J. Less-Comm. Metals*, 101:1–16, 1984.
- [134] I. Errea, M. Calandra, and F. Mauri. First-principles theory of anharmonicity and the inverse isotope effect in superconducting palladium-hydride compounds. *Phys. Rev. Lett.*, 111:177002, 2013.
- [135] G. R. Stewart. Superconductivity in iron compounds. *Rev. Mod. Phys.*, 83:1589, 2011.
- [136] G. Geneste. *Private communication*.
- [137] I. G. Gurtubay, B. Rousseau, and A. Bergara. Undamped low-energy plasmon in cubic AlH₃. *Phys. Rev. B*, 82:085113, 2010.
- [138] Z. Tang, Y. Tan, X. Chen, L. ouyang, M. Zhu, D. Sun, and X. Yu. Immobilization of aluminum borohydride hexammoniate in a nanoporous polymer stabilizer for enhanced chemical hydrogen storage. *Angew. Chem. Int. Ed.*, 52:12659–12663, 2013.
- [139] A. Vaillionis, E. G. Gamaly, V. Mizeikis, W. Yang, A. V. Rode, and S. Juodkazis. Evidence of superdense aluminium synthesized by ultrafast microexplosion. *Nature Comm.*, 2:445, 2011.

Abstract

Over the past 5 years numerous calculations have unveiled a novel view on the chemical combination of hydrogen with metals under pressure. Three remarkable trends can be identified: (i) Hydrogen stoichiometry should drastically increase under pressure in metals, (ii) Polyhydrides with non-traditional stoichiometries should be stable under pressure, (iii) These hydrogen-dominant systems may become metallic at much lower pressure than for pure hydrogen and could exhibit a high-temperature of superconductivity.

A systematic experimental study of different hydrides of low Z-elements has been undertaken in this thesis. First, a new synthesis method of high-quality and high-purity samples has been developed: a metallic foil is heated at high pressure in hydrogen medium using a YAG-laser. Using this method hydrides of aluminium (AlH_3), beryllium (BeH_2) and iron (FeH_x) were synthesized at high pressure in a diamond anvil cell. These compounds were characterized *in situ* by means of Raman spectroscopy in our laboratory, infra-red spectroscopy and X-ray diffraction using synchrotron radiation light sources. Our results evidence that the properties of the hydrides are strongly influenced by the properties of the hydrogen sublattice and confirm the existence of a strong analogy between hydrides with a high hydrogen content and pure hydrogen. Moreover we confirmed the stability of new polyhydrides with non-traditional stoichiometries under high pressure through the synthesis of new iron hydrides FeH_2 and FeH_3 and the formation of LiH_2 and LiH_6 when compressing pure lithium hydride LiH .

Keywords: hydrides, hydrogen, high pressure

Résumé

Ces 5 dernières années de nombreux travaux théoriques ont révélé l'existence d'une nouvelle chimie entre l'hydrogène et les métaux sous pression. De ces prédictions il est possible d'identifier trois tendances principales : (i) La stœchiométrie en hydrogène dans les métaux devrait drastiquement augmenter sous pression, (ii) De nouveaux polyhydrides présentant des stœchiométries inhabituelles devraient être stable à haute pression, (iii) De tels systèmes à fortes concentrations d'hydrogène pourraient devenir métalliques à des pressions bien plus basses que celles nécessaires pour l'hydrogène et pourraient présenter une supraconductivité à haute-température.

Cette thèse présente une étude expérimentale systématique réalisée sur différents hydrides d'éléments légers. Dans un premier temps une nouvelle méthode de synthèse d'échantillons d'excellente qualité et haute pureté a été développée : une feuille métallique est chauffée à haute pression en présence d'hydrogène à l'aide d'un laser YAG. En utilisant cette méthode les hydrides d'aluminium (AlH_3), de béryllium (BeH_2) et de fer (FeH_x) ont été synthétisés à haute pression dans une cellule à enclumes de diamant. Ces composés ont été caractérisés *in situ* dans notre laboratoire par spectroscopie Raman et à l'aide de sources de lumière synchrotron par spectroscopie infra-rouge et diffraction des rayons X. Nos résultats mettent en évidence l'influence du sous-réseau d'hydrogène sur les propriétés physiques des hydrides et confirment l'existence d'une forte analogie entre l'hydrogène pure et les hydrides à forte concentration d'hydrogène. De plus la stabilité à haute pression de nouveaux polyhydrides présentant des stœchiométries inhabituelles a été confirmée par le biais de la synthèse de nouveaux hydrides de fer, FeH_2 et FeH_3 , et par la formation de nouveaux hydrides de lithium, LiH_2 et LiH_6 , lors de la compression de LiH pur.

Mots clés : hydrides, hydrogène, haute pression